The University Of Sheffield.

The Feasibility of Bio-lubricants in Marine Stern Tubes and their Tribological Performance

Sam Harry Davison

A thesis submitted in partial fulfilment of the requirements for the degree of

Doctor of Philosophy

The University of Sheffield

Faculty of Engineering

Department of Mechanical Engineering

Submission Date

March 2023

Acknowledgements

I would like to express my gratitude to my supervisors Professor Tom Slatter, Professor Rob Dwyer-Joyce and Dr Julia Carrell for their support and mentoring throughout my time as a PhD student.

Thank you to the technical staff in the department for always being ready to help and provide advice, especially David Butcher, who was incredibly knowledgeable and helpful in designing and building the DiMITRI rig.

Also my fellow PhD students and friends who were always there for moral (and sometimes technical!) support.

A special thank you to Tace who has provided bottomless moral support and patience when I was finding it tough.

I would also like to thank The Douglas Bomford Trust for providing the finance for the purchase of parts for the DiMITRI rig and the Peter Jost Travel Fund whose financial support allowed me to attend an international conference which was invaluable in disseminating my research and opening up collaboration opportunities.

Abstract

Bio-lubricants are an important part of modern tribology. Their potential to replace toxic mineral oil lubricants is being realised in applications from metal working fluids and hydraulics, to forestry machinery and power generation and more recently in the propellor shaft bearings of marine vessels (stern tube bearings). These bio-lubricants are often referred to as EALs (environmentally acceptable lubricants). This thesis was completed because research into marine bio-lubricants was lacking given the relative size of the market compared to other applications and the environmental impact which these can lubricants have.

The aim was to assess the feasibility of bio-lubricants in marine stern tube applications in terms of their tribological properties. Four EAL candidates were assessed and compared to a mineral oil equivalent stern tube lubricant using two bespoke journal bearing test rigs. One of these test rigs, DiMITRI, was designed specifically for this work. The design and development of DiMITRI is described in this thesis.

Initially two hypothesis were tested. The first was that EAL performance at least matches that of mineral oil based lubricants in terms of their frictional properties and film thickness and the second was that there would be a trade-off between EAL stability and lubricity. These were tested using experiments on the Baxter journal bearing rig which compared the film thickness and friction generated with each lubricant under realistic stern tube shear rates. The initial experiments revealed that for the first hypothesis, that EAL performance would at least match that of mineral oil based lubricants in terms of their frictional properties and film thickness, was answered in the hydrodynamic lubrication regime and highlighted limitations with the test rig in the mixed lubrication regime. The second, that there would be a trade-off between EAL stability and lubricity also required significant modifications to the test rig. Hence a novel test rig, DiMITRI was developed.

The development of DiMITRI aimed to remove limitations found in the initial experiments. It was designed to match the Sommerfeld number of a real marine stern tube bearing. This took into account load, speed, temperature and bearing dimensions into a single non-dimensional number. DiMITRI was designed so that it could operate at low Sommerfeld numbers in the range 0.004-0.01 (lower than all other journal bearing test rigs) which would replicate the most extreme conditions found in a real stern tube bearing. A low lubricant volume is required (50ml) to allow experimental lubricant samples produced on a laboratory scale to be tested. Stribeck curves which spanned across the mixed and hydrodynamic regimes were generated for the lubricants and the point at which the transition occurred could be identified and compared between lubricants.

The use of the Sommerfeld number enabled the results obtained on DiMITRI to be put into context of a scaled up marine stern tube bearing in a novel way and predictions about EAL performance in the field were made. It was found that the EALs had equivalent performance to the mineral oil under operating conditions in real vessels.

The effect on the tribology of the lubricants with ageing through oxidation has been investigated and assessed using DiMITRI. The lubricants were oxidised in the presence of a copper catalyst and with a novel method using a tin catalyst. Both metals can be found in stern tube bearings. It was found that the aged sample performance was inferior to the fresh samples (increased Sommerfeld number at the inflection point) for all lubricants and generally displayed higher friction in the mixed lubrication regime of up to a 69% increase in the mixed lubrication regime.

Comparison between the mineral oil and EALs showed no notable difference in either the friction or the transition between the mixed and hydrodynamic lubrication regimes. The presence of tin as an oxidation catalyst suggested that the EALs may be more sensitive to this metal as a catalyst than mineral oil which would need further investigation.

Overall it was found that EALs have equivalent performance in both fresh and oxidised forms with their mineral oil counterparts in terms of their friction performance and ability to form a lubricant film for a Sommerfeld number range of 0.004-0.01. Given this and their superior biodegradability

and lower toxicity to mineral oils they should be more widely adopted. This thesis finds that bio-lubricants are indeed feasible for use in marine vessel stern tubes.

Contents

1 Introduction **1**

1.1 The field of bio-lubricants 1

1.2 Scope of work 3

1.3 Aim and objectives 4

1.4 Structure of thesis 5

2 Lubricant properties and principles **6**

2.1 Lubricant properties 6

2.1.1 Viscosity 6

2.1.2 Viscosity temperature relationship 7

2.1.3 Pressure-viscosity coefficient 7

2.1.4 Viscosity shear rate relationship 8

2.2 Types of lubricant 9

2.2.1 Mineral base fluids 9

2.2.2 Synthetic base fluids 10

2.2.3 Synthetic esters 11

2.2.4 Vegetable base fluids 11

2.3 Lubricant degradation 11

2.3.1 Oxidation 12

2.3.2 Testing techniques 13

2.3.3 Hydrolysis 14
2.3.4 Acidity 15
2.3.5 Additives 15
2.3.6 Solvency 15
2.4 Lubrication regimes 16
2.5 Lubricant properties and principles conclusion 17

3 Bio-lubricant applications **19**
3.1 Current research 19
3.2 Marine lubricant applications 23
3.2.1 Thruster lubricants 23
3.2.2 Stabiliser lubricants 24
3.2.3 Greases 24
3.2.4 CPP fluids 25
3.2.5 Stern tube lubricants 25
3.2.6 Current legislation 26
3.2.7 Marine applications conclusion 27

4 Literature review **28**
4.1 EALs properties 28
4.2 Stern tube critical properties 30
4.3 Stern tube bearing operating conditions and parameters 33
4.4 Journal bearing test rigs 35
4.5 Literature review discussion 38

5 Initial experiments **40**

5.1 Test Equipment 40

5.1.1 Oil viscosity measurement 40

5.1.2 Baxter journal bearing test rig 41

5.1.3 Film thickness measurement 43

5.1.4 Friction measurement 46

5.2 Initial experiments method 49

5.2.1 Test parameters 51

5.2.2 Design of experiments 51

5.3 Results 53

5.3.1 Viscosity-temperature tests 53

5.3.2 Oil film thickness comparison 53

5.3.3 Oil film friction comparison 55

5.3.4 Stribeck curves 57

5.4 Initial experiments discussion 59

5.5 Initial experiments conclusions 59

6 Test rig design - DiMITRI **61**

6.1 Design brief 62

6.2 Concept development 63

6.3 Motor and drive system 65

6.4 Bearing selection 66

6.5 Sommerfeld number led design 67

6.6 Housing design 70

6.7 Shaft design 73

6.8 Rig Assembly 76

6.8.1 Alignment 77
6.8.2 Misalignment measurement of the test bearing shaft 79
6.8.3 Clearance measurement 81
6.9 Cartridge heater installation 82
6.10 Test rig design conclusions 83

7 Experimental methodology **84**
7.1 Understanding the temperature viscosity relationship 84
7.2 Design of experiments (DOE) 88
7.2.1 Load parameters 88
7.2.2 Bearing shell wear 90
7.2.3 Heater control 92
7.2.4 Ancillary Bearing Friction 93
7.2.5 Test matrix 97
7.3 Pressure-viscosity effect modelling 97
7.4 Data processing methodology 100
7.4.1 Error plotting 105
7.5 Measuring Wear 106
7.6 Oxidation of oils 107
7.6.1 RPVOT method 107
7.6.2 Using a tin catalyst in the RPVOT 110

8 Results and analysis **112**
8.1 Hypothesis 1 - Fresh oil Stribeck curves 113
8.1.1 Hypothesis 1 conclusion 117
8.2 Hypothesis 2 - Stability trade-off 117
8.2.1 Hypothesis 2 conclusion 120

8.3 Hypothesis 3 - Oxidised compared to fresh lubricant samples 120
8.3.1 Hypothesis 3 conclusion 125
8.4 Effect of the results in a marine stern tube context 125
8.5 Catalysts for oxidation 128
8.6 Shaft wear 129
8.7 Bearing shell wear 131

9 Conclusions **135**
9.1 Review of the objectives 135
9.1.1 Objective 1 135
9.1.2 Objective 2 135
9.1.3 Objective 3 136
9.1.4 Objective 4 136
9.2 Main findings 137
9.2.1 Novelty 138
9.2.2 Advice to industry 138
9.2.3 Limitations and future work 139
9.2.4 Improvements to DiMITRI 140
9.3 Publications arising 142

Bibliography **143**

Appendices **152**

Appendix A DiMITRI product design specification **153**

Appendix B DiMITRI assembly drawing **159**

List of Figures

2.1 Types of crude oil structures 10

2.2 Triglyceride structure 12

2.3 A basic hydrocarbon chain molecule - Butane 12

2.4 Oxidation of an alkane 13

2.5 Stribeck curve adapted from [11] 17

3.1 Initial pass mind map of the bio-lubricants research field 21

3.2 U.S. lubricants market by application 22

3.3 Lubricated areas in a large ship 23

3.4 Typical stern tube and bearing arrangement 26

4.1 "Wiped" and "polished" aft stern tube bearing image 35

4.2 University of Sheffield "Baxter" Journal bearing test rig image 36

5.1 Baxter (journal bearing rig) schematic 41

5.2 Baxter shaft instrumentation 43

5.3 Speed of sound test rig image 45

5.4 Plot of the speed of sound for DE11417 at different temperatures. . . 45

5.5 Phase change graph 46

5.6 Modified Baxter rig with newly installed torque meter and couplings . 47

5.7 Journal bearing cross section showing parameters for friction force calculations 47

5.8 Viscosity temperature relationship for lubricants tested in the Baxter rig 53

5.9 Minimum oil film thickness at 100rpm. 54

5.10 Minimum oil film thickness at 200rpm. 55

5.11 Bearing coefficient of friction measured at 200rpm under a range of loads 56

5.12 Bearing stribeck curve under 20kN load and 40°C 58

6.1 Four concepts for the design of DiMITRI mounted onto the Schenck 250 servo-hydraulic machine 64

6.2 Overview of the DiMITRI set-up 66

6.3 TD60 bearing shell image 67

6.4 Model of Sommerfeld number at 80°C with DE11419 with three different bearing clearance values 69

6.5 Comparison of Sommerfeld number at 80°C with DE11419 with two different bearing clearance values 70

6.6 Exploded view of the bearing housing and component assembly . . . 71

6.7 Annotated view of the bearing housing 72

6.8 Cross-section of a journal bearing with exaggerated clearance for clarity 73

6.9 Shaft design showing loaded and supported areas with mesh 74

6.10 Predicted shaft displacement and stress generated using SOLIDWORKS Simulation FEA tool 75

6.11 Exploded view of DiMITRI assembly 77

6.12 Dial gauge shown at approximately the 45°position on DiMITRI during alignment checks 78

6.13 Laser displacement sensor set-up used to measure the change in height of the shaft end when under load 80

6.14 Measurement from laser displacement sensor at different loads 81

6.15 Red mark on bottom bearing shell left by the clearance gauge 82

7.1 Comparison of viscosity model accuracy 86

7.2 Viscosity temperature graph for all lubricants 87
7.3 Viscosity temperature graph for all oxidised lubricants 87
7.4 Sommerfeld number at different loads for DiMITRI 89
7.5 DiMITRI bearing shell 1 and 2 91
7.6 Photo of heater controller 92
7.7 DiMITRI support bearing friction coefficient for all loads and speeds 94
7.8 DiMITRI support bearing friction torque for all loads and speeds . . 95
7.9 Schaeffler rod-end bearing friction 96
7.10 Effect of pressure-viscosity coefficient under stern tube conditions . . 98
7.11 Effect of pressure-viscosity coefficient under stern tube conditions for a higher pressure range 99
7.12 Example of tdms file data after each test. 100
7.13 Stribeck curve generator process flow using MATLAB 102
7.14 Example of temperature measurements after being processed with the MATLAB program in Figure 7.13 103
7.15 Example of torque measurements after being processed with the MATLAB program in Figure 7.13 103
7.16 Example of load measurements after being processed with the MATLAB program in Figure 7.13 104
7.17 Example of speed measurements after being processed with the MATLAB program in Figure 7.13 104
7.18 Example of Stribeck measurements after being processed with the MATLAB program in Figure 7.13 105
7.19 Photo of portable profilometer and set-up method 106
7.20 Photo of Alicona lens and set-up method 107
7.21 Rapid Pressure Vessel Oxidation Tester schematic 108
7.22 Image of copper coil submerged in lubricant ready to be inserted into the RPVOT chamber 109

7.23 Rapid Pressure Vessel Oxidation Tester image 109

7.24 Example of RPVOT measurement trace from ASTM [85] 110

8.1 Fitted Stribeck curves collected during run down test for each lubricant, separate graph for each load 113

8.2 Direct comparison of mineral oil based lubricant and EAL Stribeck curves collected during run down test for each lubricant 115

8.3 Direct comparison of mineral oil based lubricant and EAL Stribeck curves collected during run down test for each lubricant 116

8.4 Oxidation induction time using the RPVOT 118

8.5 Correlation of OIT with friction in mixed lubrication regime 119

8.6 Direct comparison of Stribeck curves for fresh and oxidised lubricant under the same conditons at 1kN 121

8.7 Direct comparison of Stribeck curves for fresh and oxidised lubricant under the same conditons at 5kN 124

8.8 Inflection point of fresh samples with the equivalent marine stern tube rpm 126

8.9 Inflection point of oxidised samples with the equivalent marine stern tube rpm 127

8.10 Oxidation induction time of mineral oil based lubricant compared to an EAL 128

8.11 Roughness of shaft before each lubricant test set in the radial direction 130

8.12 Roughness of shaft before each lubricant test set in the axial direction 130

8.13 Appearance of shaft after a test with an oxidised lubricant (left) and with a fresh lubricant (right) 131

8.14 Worn and unworn bearing shells 133

8.15 Individual worn bearing shell 134

9.1 Rod-end with roller spherical bearing as opposed to a plain spherical bearing from [94]. 141

Nomenclature

α	Pressure-viscosity coefficient (Pa^{-1})
η	Dynamic viscosity (Pas)
ω	Angular frequency $(rads^{-1})$
Φ	Phase shift $(radians)$
ρ	Density (kgm^{-3})
θ	Attitude angle $(^{\circ})$
ε	Eccentricity ratio $(-)$
C	Speed of sound (ms^{-1})
c	Radial clearance (m)
D	Diameter (m)
e	Eccentricity (m)
F	Friction force (N)
f	Frequency (Hz)
h	Film thickness (m)
h_0	Minimum film thickness (m)
k	Stiffness (Nm^{-1})
L	Length (m)
N	Rotation Speed (Hz)
P	Load per unit of projected bearing area (Nm^{-2})
p	Pressure (Pa)
R	Applied load (N)
r	Radius (m)
S	Sommerfeld number $(-)$
T	Torque (Nm)
t	temperature $(^{\circ}C)$
v	Kinematic viscosity (mm^2s^{-1})
z	Acoustic impedance $(Rayl)$

Chapter 1

Introduction

Lubricants are everywhere. From the joints in your knees to the bearings in your car. Their fundamental use is to provide separation between two surfaces which are moving relative to each other. Crucially, they prevent wear between the surfaces, reduce friction and can carry energy to and from the region in which they are used. Their application is critical to the efficiency and longevity of mechanical systems, so the mastery of their properties and performance is an key part of engineering research within the field of tribology.

The vast majority of present day machinery lubricants are made from mineral oil sources [1, 2], which are non-renewable, toxic to the environment and prone to massive price fluctuations depending on world politics. It is widely accepted that the reliance of the modern world on mineral oils is not sustainable in the long term. Therefore, future lubricant demand must be met using renewable and more diverse raw material sources to produce a less toxic, more secure and more biodegradable, end product. Bio-lubricant is the term most commonly used to describe lubricants with some, or all, of these properties. The adoption of bio-lubricants to replace mineral oil based lubricants creates new challenges, such as early lubricant degradation and research in the field of bio-lubricants is highly important.

1.1 The field of bio-lubricants

Most lubricants that were used before the end of the 19th century, were vegetable oils, which would today be called bio-lubricants. The beginning of mineral oil production and refinement at the turn of the 19th century brought with it new lubricant products, which lasted longer than what was previously available. For example, their viscosity

would be more consistent after a period of use and they were less likely to form sludge through reactions with oxygen and other substances. The mineral oil based lubricants were not necessarily superior in terms of their lubricating properties, but they realised their potential as a solvent for a wide range of additives. This allowed chemists and engineers to design lubricants that were as effective as ever, but with superior stability and longevity. As recently as 2016, over 98% of the global lubricants market was still dominated by mineral-oil based products [1, 3]. The other 2% are bio-lubricants. A large proportion of the 2% are vegetable oils and are not dissimilar to pre 19th century lubricants. Due to modern environmental awareness, potentially superior lubricity and viscosity-temperature stability, it is the bio-lubricants sector that is expected to be the fastest growing segment of the global lubricant market. As society weens itself off of mineral oil, perhaps bio-lubricants will one day be mainstream again. It is possible that this is why the word bio-lubricant is so ambiguous, because while the term is relatively new, a lot of the raw materials are not. Indeed, even the spelling of the word is ambiguous. The hyphenated spelling used in this thesis, bio-lubricant, has been chosen according to the British Standards Institute (BSI) publication PD CEN/TR 16227:2011 [4].

A lubricant may be referred to as a bio-lubricant because it is bio-based (derived from a biological source), bio-degradable (degrades to specified amount in a specific time-frame when released into the environment) or renewable (does not rely on petroleum sources) or any combination of the three. Consequently the definition of the size of the bio-lubricants market is also variable and estimates range from 1.5 to 2.4 billion at the time of writing [3, 5, 6]. Further to this, within the bio-lubricant category there are a range of terms which are used to indicate the effect that a lubricant has on the environment, which is usually preceded by the word environmentally. These include environmentally: friendly, acceptable, aware, adapted and neutral lubricants, to name but a few. These are often names that refer to a specific product line of lubricants or are aimed at meeting a certain piece of legislation but the terms are not always well defined and can be easily misconstrued, especially if trying to compare products designed for different uses or from different companies. The only thing that is certain about any lubricant described as a bio-lubricant is that its an alternative to a purely mineral oil derived lubricant.

Future growth in the bio-lubricants sector is driven in part by superior properties and environmental credentials, but is greatly accelerated by legislation which mandates their use. The most high profile example of this in recent times is the introduction

of the vessel general permit (VGP) legislation which was introduced in 2013 by the United States Environmental Protection Agency (EPA). It enforces the use of environmentally acceptable lubricants (EALs) in ships that enter North American waters. The international nature of the shipping industry means that this legislation has a global effect. It was estimated in 2013 that 12,430 foreign flagged vessels would need to be VGP compliant when visiting US waters and 94% of these were merchant freight and tanker ships [7]. This equates to a share of around 25% of an an estimated 45,179 non-United States owned merchant freight and tanker ships globally in 2013 [8]. A key motivation for this legislation was the discovery that over 80 million litres of oil leaks into the sea every year from normal vessel operational discharges [9]. The marine industry is the largest end user of bio-lubricants and the VGP is thought to be the main driver for this [3, 5, 6].

1.2 Scope of work

This project aimed to increase understanding of bio-lubricant tribology and to assess the feasibility of their use in marine machine contacts. The following constraints to the work have been identified to achieve this aim.

1. Environmetally acceptable lubricants (EALs) designed to meet the 2013 Vessel General Permit (VGP) legislation for marine lubricants were characterised. Given the huge range of bio-lubricants available it was appropriate to limit the lubricant formulations that were studied. Focusing on EALs suitable for the VGP ensures that the work will be relevant and should be valuable.

2. Lubricants were characterised experimentally, but were not be limited to specimen level testing as there is lack of more complex and realistic tests in the current research.

3. Experimental parameters that replicate conditions as closely as possible with potential applications for the EALs were used.

1.3 Aim and objectives

The work presented in this thesis aimed to assess the feasibility of bio-lubricants in marine stern tube applications in terms of their tribological qualities. The following objectives were set in order to meet this aim:

1. Review the field of bio-lubricant tribology and identify an application where research and understanding is lacking.

   The bio-lubricants market is expected to grow from around USD 2.0billion to USD 2.4billion between 2020 and 2025 [5]. Bio-lubricants are an increasingly relevant technology, due to their potential environmental benefits, such as biodegradability, renewability and energy efficiency of the machines that they are applied in. Furthermore, they have shown great potential as viable replacements for mineral oil lubricants because they have demonstrated superior performance in terms of their low friction properties and viscosity stability.

2. Conduct learning experiments to assess the performance characteristics of the different lubricants that are available for marine stern tubes.

   Industry confidence in EAL lubricant performance is lower than in the mineral oil based lubricants which they have replaced. However the evidence to support this is largely anecdotal. There is also a range of EAL products available on the market, which have different formulations and structures that mean some may perform better than others.

3. Design a test rig to investigate the performance of EALs under extreme operating conditions.

   Literature shows that the level of experimental testing with bio-lubricants is low, with most tests being conducted at a specimen level ie. basic tests with limited similarities to real conditions. At the component level (more complex, slightly more realistic conditions with specimens that have more realistic geometries) there is relatively little work.

4. Use the test rig to make comparisons at a range of different lubrication regimes from boundary/mixed to full hydrodynamic level.

   Research into existing test rigs shows that few have the capability to explore the mixed lubrication regime and have limited sensitivity and temperature control.

1.4 Structure of thesis

Chapter 2 summarises some fundamental knowledge pertaining to lubricants and their applications and the laws governing the development and use of bio-lubricants.

Chapter 3 explains the rationale behind the focus of the thesis on marine bio-lubricants by explaining the initial research into the field of bio-lubricants and moving on to explaining marine specific bio-lubricant applications.

Chapter 4 reviews the literature surrounding synthetic esters (a type of bio-lubricant) and marine stern tube EAL research and the experimental rigs used in the literature. Here, specific gaps in experimental characterisation of EALs are outlined.

Chapter 5 explains the initial learning experiments conducted and the methodologies for these.

Chapter 6 is concerned with the design of a novel journal bearing test rig design.

Chapter 7 provides information regarding the experimental methods used with the new test rig in order to characterise the rig and the lubricants. It also explains the method used to age the lubricants.

Chapter 8 presents the results from the experiments with the novel test rig regarding three hypotheses.

Chapter 9 contains the conclusions of this thesis, its main findings and advice to industry and a discussion about its limitations and future work.

Chapter 2

Lubricant properties and principles

This chapter introduces the properties and principles that are necessary to understand to enable a comparison of different lubricants and their tribological performance. It starts by introducing the basic building blocks of lubricants and how lubricants can be categorised into three main types: mineral based, synthetic and bio-based. Common parameters that are used to describe lubricant properties are explained, followed by some mechanisms by which lubricants can degrade over time and the effect of this on such properties. Additives and their role in lubricant performance is also discussed. Lastly the different lubrication regimes which are used to distinguish 3 distinct levels of lubrication are explained. Many relevant fully formulated lubricants that are considered bio-lubricants will contain some mineral oil elements. Consequently, some of these constituents are also discussed.

2.1 Lubricant properties

Lubricants are applied in a huge variety of applications, from the hinges on a door to the solar array erection mechanism on a space satellite [10]. Consequently there is an array of specific properties which describe the ability of lubricants to function under certain conditions and demands. These properties are defined in the following section.

2.1.1 Viscosity

The most important of these properties is the viscosity of the lubricant, because it must be considered in any lubricant application. Viscosity is a measure of the resistance to flow of a lubricant. The thicker a lubricant, the more viscous it is. When

applied in a bearing, more viscous lubricants can support higher loads before damage occurs to the bearing. Energy losses in components using more viscous oil will also be higher, hence, when selecting a lubricant, there is normally a trade-off between load carrying capacity and energy loss due to internal friction in the lubricant. This energy loss is sometimes referred to as viscous loss. The viscosity of a lubricant can change depending on conditions such as the temperature, pressure and shear rate. Viscosity is given in two ways. Dynamic viscosity (absolute viscosity) is the ratio of force over area of a flat plate moving over a thickness of fluid (fluid film), with the velocity gradient of the fluid film. Viscosity that includes the influence of gravity is called the kinematic viscosity and is most commonly quoted by lubricant manufacturers as it is easier to measure. Its usually determined by measuring the time it takes for fluid to flow through a vessel and is equivalent to the dynamic viscosity divided by the fluid density.

2.1.2 Viscosity temperature relationship

The temperature of a lubricant has a significant effect on the viscosity. For instance, heating some lubricants up by 25°C can result in an 80% drop in viscosity [11]. Viscosity is inversely related to temperature. An increase in temperature, causes a decrease in viscosity. The relationship can be described by viscosity temperature equations, or displayed on charts. The most commonly used method of obtaining the viscosity temperature (VT) relationship is the viscosity index method (VI) in accordance with the American Society for Testing of Materials (ASTM) standard D2270 [12]. Using this method gives the researcher the largest database for comparison of oils. A high VI indicates that a lubricant is less sensitive to changes in viscosity due to temperature than a lubricant with a low VI. The VI method compares the kinematic viscosities of a lubricant measured at 40°C and 100°C with a 0 and 100 VI standard oil. ASTM D2270 is used to find a hypothetical reference oil with a matching 100°C viscosity to the lubricant in question and obtain the VI [13].

2.1.3 Pressure-viscosity coefficient

Pressure-viscosity coefficient is often represented by α and is used to describe the degree to which the viscosity of a lubricant increases with its pressure. Pressure-viscosity coefficient increases with viscosity, but decreases with temperature. It can be found by measuring the viscosity of a lubricant at a range of different pressures at constant temperature, usually through the use of a pressurised viscometer either

a capillary tube type or falling ball viscometer. The Barus equation equation is most commonly used to describe the relationship between viscosity-pressure coefficient, temperature and viscosity, however this is usually only suitable up to pressures of 500MPa.

$$\eta_p = \eta_0 e^{\alpha p} \tag{2.1}$$

where:

η_p is viscosity at pressure p (Pas)

η_0 is viscosity at atmospheric pressure (Pas)

α is pressure-viscosity coefficient m^2/N

p is pressure of interest (N/m^2)

2.1.4 Viscosity shear rate relationship

Viscosity of a lubricant can also vary with shear rate. Shear rate is the velocity gradient normal to the shear stress on a lubricant. Described by the following equation:

$$\lambda = u/h \tag{2.2}$$

where:

u is the surface velocity (ms^{-1})

h is the film thickness (m)

λ is the shear rate (ms^{-1})

Shear rate is a useful parameter because it links the velocity of two bearing surfaces in relative motion to each other, to the film thicknesses that are generated.

A Newtonian fluid will have a viscosity which is proportional to the shear rate. Most mineral oil base fluids are Newtonian up to a shear rate of $10^6 s^{-1}$. Some lubricants are known to exhibit shear thinning behaviour. These are usually multi-grade oils where a mixture of fluids, each with different viscosities, are mixed together to form one lubricant. One mechanism of shear thinning in occurs when the longer fluid molecules in a fluid align themselves causing a reduction in viscosity. This form of shear thinning is referred to as psuedoplastic behaviour. Thixotropic behaviour is another form of shear thinning which occurs after a sustained period of high shear and

is time dependent, hence it is often referred to as shear duration thinning. Dilatant fluids are those which thicken with an increase in shear.

2.2 Types of lubricant

Lubricants are made up of base fluids and additives. The base fluid is the main constituent, within which additives are dissolved, typically 1-25 % of a lubricant [12]. Bulk properties of the lubricant such as viscosity and density are primarily determined by the base fluid. Lubricant base stocks are commonly characterised into five groups according to standards designed for the automotive industry [14]. However, this grouping system does not consider biodegradability. For this work, it is more useful to categorise the lubricant base stocks into three categories, mineral base fluids, synthetic base fluids and vegetable base fluids. Furthermore, the base stocks used for all of the lubricants currently available for use in marine stern tubes can be divided into these categories.

2.2.1 Mineral base fluids

Mineral base fluids are derived from crude oil and are by far the most commonly used and widely available base fluids. They are some of the cheapest to buy and can produce lubricants with a variety of properties depending on their source and the type of refinement that has been applied to the raw crude oil. However, they are fundamentally floored because of the diminishing and finite supply of crude oil and the toxicity to the environment and low-biodegradability of the finished lubricant product. Mineral base fluids contain blends of different compounds which can be split into three main categories based on their content of certain hydrocarbon structures: paraffinic, naphthenic and aromatic (Figure 2.1). Many other organic molecules and residuum are found are contained within petroleum, but these hydrocarbons are the main constituent.

Paraffinic base crude oils are those with composition above 40% paraffins, if the paraffins and naphthenes together make up more than 50%. These molecules have a linear or branched structure, which are saturated (no carbon-carbon double bonds) and attributes to the best oxidation stability of the three types. They also benefit from higher VI, however suffer from poorer solvency (ability to dissolve additives) and pour point (will become too thick to pour at operational temperature). These are

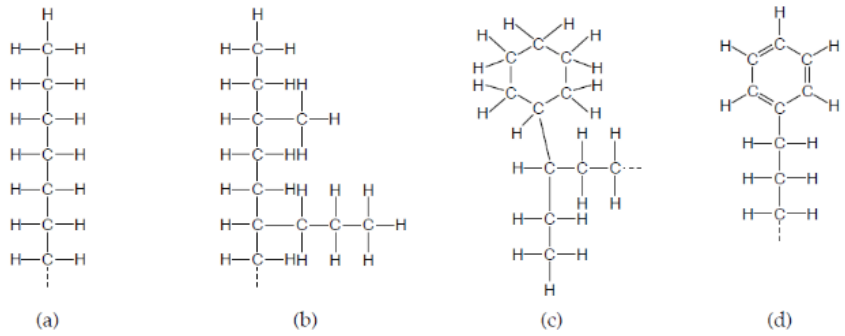

Figure 2.1: a) straight parrafin b) branched paraffin c) naphthene d) aromatic [11]

primarily used as engine oils, transmission fluids and gear oils due to their superior VI and oxidation stability.

Naphthenic base crude oils are those with a composition above 40% naphthenes, where paraffins and naphthenes are already over 50% of the composition. These oils have a lower VI compared to paraffinic oils, but benefit from greater solubility so the degradation products of these structures can dissolve into the oil, resulting in a reduced likelihood of deposits and sludge formation when they are applied in machinery. They are saturated hydrocarbons, but also contain cyclic rings made up of 5 or 6 carbon atoms.

Aromatic structures are cyclic and unsaturated, with alternating double to single bonds carbon bonds around the rings. Aromatic crude oils are those with more than 50% aromatic content. Their structures are most commonly 6 membered benzene rings [12].

Mineral oils refers to API (American Petroleum Institute) groups I to III [15], synthetic base fluids refers to API groups IV and above.

2.2.2 Synthetic base fluids

Synthetic base fluids were first used on an industrial scale to meet the performance requirements for applications for which mineral based fluids were inadequate, particularly in aircraft engines in the 1930s [16]. Synthetic lubricants can be designed to meet certain criteria because their molecular structures are more definite than the structure of mineral oils, which are a mix of many different compounds. Synthetic lubricants can offer advantages over mineral oil based stocks in terms of their viscosity index, oxidation stability, hydrolytic stability and biodegradability. The downside is

that in general, synthetic base fluids are at least two to three times more expensive to produce than synthetic base fluids [1, 17].

The bio-degradibiltiy of synthetic lubricants varies and depends somewhat on the source of the raw materials. Synthetics base fluids that are derived from oleochemical sources (vegetable oils or animal fats), are likely to be the most readily biodegradable. This includes many synthetic esters (SEs). However, some synthetic base fluids from petrochemical sources can also be classed as biodegradable like polyalkylene glycols (PAGs) and some low viscosity poly-α-olefins (PAOs).

2.2.3 Synthetic esters

An ester is an organic compound which is formed when an acid, usually carboxylic acid, is reacted (by esterification) with an alcohol. The hydrogen in the -COOH group in the acid is replaced by a hydrocarbon group (an alcohol). These reactions can form hydrocarbon esters of varying length. Animal fats and oils are examples of natural esters, but esters with specific properties can be synthesised to create lubricant base fluids. These lubricants are often referred to as synthetic esters.

2.2.4 Vegetable base fluids

Naturally occurring oils are often referred to as vegetable oils. They are most commonly extracted by mechanical means. For example rapeseed oil is extracted by cold pressing the seeds, so that the oil is squeezed out without the use of high temperatures. Rapeseed oil and most other vegetable oils are referred to as triglycerides, shortened from the technical name of triacyl glycerol, because they consist of three fatty acid chains which are joined together by a glycerol molecule, Figure 2.2.

Other varieties of vegetable base fluids include, but are not limited to: Canola oil, Castor oil, Jatropha oil, Jojoba oil, Linseed oil, Palm oil, Soybean oil, Sunflower oil, and Tallow oil.

2.3 Lubricant degradation

Lubricant degradation can can occur as a result of the presence of oxygen (oxidation), water (hydrolysis) and with the application of heat (thermal degradation) as well as biological degradation and through the depletion of additives (such as antioxidants). Degradation can result in an increase in viscosity, formation of deposits (sludge), acid formation and discolouration of the lubricant. Furthermore, the suspension of

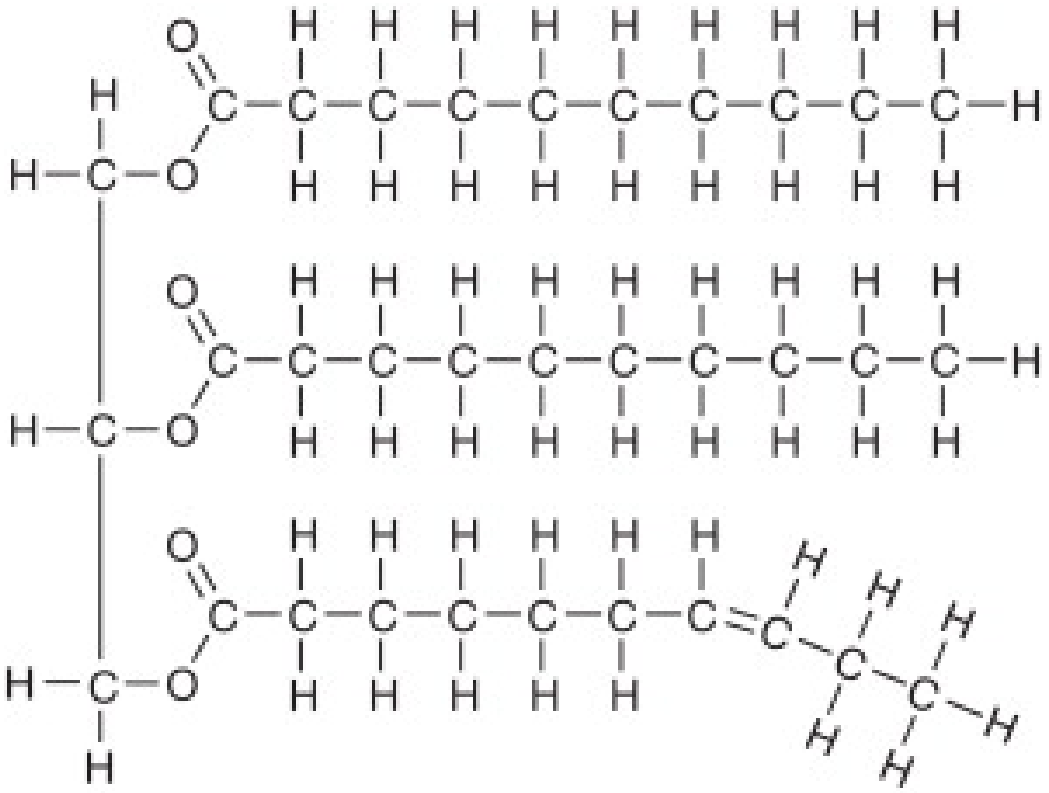

Figure 2.2: Triglyceride structure [18]

metal debris can cause damage to machinery and can act as a catalyst for oxidation mechanisms.

2.3.1 Oxidation

In the presence of large amounts of energy, for instance in combustion, hydrocarbons react with oxygen, to produce compounds such as water and carbon dioxide. Lubricants have functional groups and other additions to the basic hydrocarbon chain, which means that oxidation reactions can occur with much less energy, resulting in the formation of carboxylic acid and other impurities. An example of a basic hydrocarbon chain is illustrated in Figure 2.3.

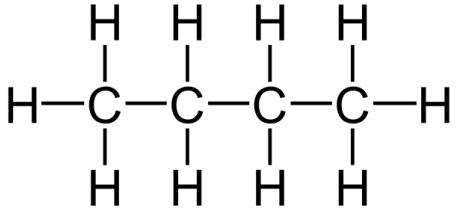

Figure 2.3: A basic hydrocarbon chain molecule

Oxidation causes the hydrocarbon chains to break, such as in Figure 2.4, into smaller sections which alter the physical properties of the bulk lubricant such as the viscosity. An oxygen free lubricant base oil will be made up of multiple chains that can easily move around each other, since they are physically similar. However, oxidation products can interrupt the structure of the lubricant and prohibit free movement. The viscosity of the oxidised oil is generally larger since the lubricant will be more resistant to flow. The formation of carboxylic acid and other organic acids are detectable as an increase in the total acid number (TAN). The base number (BN) can be used to indicate the amount of base fluid that has been used up by these reactions.

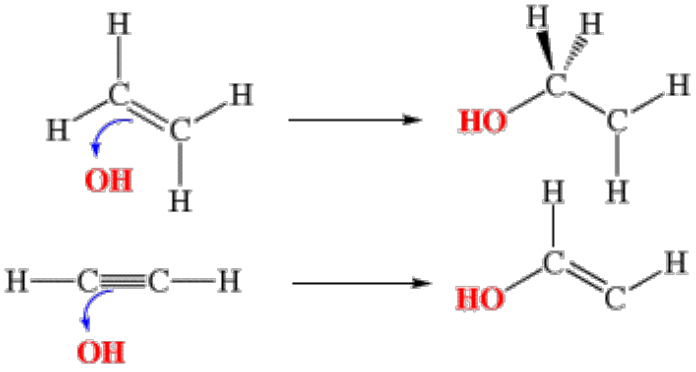

Figure 2.4: Oxidation of an alkane

The structure of hydrocarbon chains can influence their susceptibility to oxidation. Unsaturated hydrocarbons (Alkanes) contain at least one carbon to carbon double bond (C=C) and saturated hydrocarbons contain only single carbon to carbon bond (C-C) (Alkenes). Unsaturated hydrocarbons are more susceptible to oxidation since one of the bonds in the double bond pair is weaker and requires significantly less energy to break.

2.3.2 Testing techniques

In industry the oxidation characteristics of different lubricants are usually measured using standard test equipment under specific conditions, so the results are comparable with competitors. ASTM standards such as: the Universal Oxidation Test (D6514, D5846), Pressure Differential Scanning Calorimetry (D6186) and the RPVOT (D2272) are all tests which aim to accelerate the oxidation of a lubricant formulation using standard laboratory equipment into a practical timeline for its effects to be studied during lubricant development. The various techniques are summarised below:

Pressure differential scanning calimetry (PSDC) – The lubricant sample is held at a constant pressure and temperature and temperature probes measure the heat flow from the sample. Eventually decomposition (oxidation) will occur which results in an exothermic heat flow which is detected by the apparatus. The time taken for decomposition to initiate is used to compare different lubricants for oxidation resistance. This is called Oxidation induction time (OIT).

Universal Oxidation Test (D6514, D5846) – Oil is heated to 135°C with a copper or iron catalyst, then the acid number is monitored until it reaches a threshold above the original acid number, or when insoluble solids appear from a drop released onto filter paper. If this test is practically too slow or insufficient, standard D6514 is adopted. This involves a higher temperature of 155°C held for 96 hours. The quantity of insoluble particles is measured by using a vacuum filter. In both thests the viscosity and acid number compared to the pre-test state. Furthermore, residual deposits in each sample cell can be compared.

RPVOT – Test oil is pressurised to 6.2 bar then mixed with water and a copper catalyst. The vessel is rotated at 100rpm in a 150°C oil bath or dry block. The number of minutes required to reach a specific drop in gauge pressure (25psi) is used as a measure to represent the oxidation stability of oil sample. Usually a gradual pressure drop can be observed before an induction type pressure drop occurs. A standard drop threshold 175kPa is sufficient to stop the test, or 100 minutes at temperature is usually enough to see an induction type drop. RPVOT is used for lubricants where water presence is likely in the intended application. Commercially this test is usually used for batch control of lubricant oxidation specifications and not for comparison of new oils of different compositions.

RSSOT Rapid small scale oxidation test (RapidOxy) – The test oil is enclosed in a pressure vessel with a 700kPa oxygen charge. Its heated to 140°or 160°C. The net change in pressure observed results from consumption of oxygen and the gain in pressure occurs due to formulation of volatile oxidation by-products. This test is not designed for lubricant stability indications and is usually more appropriate for batch comparison of the same oil product.

2.3.3 Hydrolysis

Lubricant base oils can also degrade as a result of the presence of water, referred to as hydrolysis. Mineral oil based lubricants and PAOs are not susceptible to hydrolysis

but synthetic ester lubricants are, when in the presence of an acid catalyst [12].

2.3.4 Acidity

Lubricants become more acidic as they degrade through oxidation. Unused lubricants can have an inherent acidity level, due to the additives dissolved within them, such as sulphur based additives. Acidic lubricants can corrode metals found in machinery and bearings. Corroded surfaces are easily separated from the substrate material through normal operation of bearings and other rubbing surfaces, exposing fresh material to the acidic lubricant. This corrosive wear causes oxidised wear debris to be suspended in a lubricant, which can catalyse further oxidation reactions and result in a positive feedback loop of ever increasing acidity and wear. The level of acidity of a lubricant is defined using the TAN measured in KOH mg/g (milligrams of potassium hydroxide per gram of lubricant) required to neutralise the lubricant.

2.3.5 Additives

Additives are so called because they are added to a lubricant base oil to modify certain characteristics of the lubricant, depending on the application and operating conditions. When additives are included in a base oil it is often then referred to as a fully formulated lubricant. The vast majority of additives fit into three categories, which are: Performance enhancing, surface active and lubricant protective additives. [19]. Some examples are shown in Table 2.1.

2.3.6 Solvency

The solvency of a lubricant is linked to both the lubricity and the elastomer compatibility. Solvency is determined primarily by the polarity of its constituent molecules. The greater the polarity, the more readily that the lubricant will adsorb to highly polar metal surfaces, resulting in the formation of protective layer . If a mix of polar and non-polar molecules are present, this will lead to greater lubricity. Examples of base oils with non-polar molecules are PAOs and paraffinics. However, esters have much higher solvent power [1]. Elastomer compatibility is improved when the base stock has sufficient solvency to embed into the elastomer and cause it to swell sufficiently to provide good contact between the seal and surface.

Additive Class	Function
Surface active additives	
Anti-wear agents	Reduce wear of loaded contact surfaces
Extreme pressure agents	Prevent microwelding
Friction modifiers	Reduce frictional forces
Rust inhibitors	Prevent corrosion of ferrous materials
Corrosion inhibitors	Protect against chemical attack
Detergents	Keep metal surfaces clean
Dispersants	Disperse particulate matter (debris)
Tackiness agents	Increase surface adhesiveness
Performance-enhancing additives	
Viscosity index improvers	Improve V-T relation
Pour point depressants	Affect fluidity by controlling crystal formation
Emulsifiers	Disperse water in base oil
Deposit control additives	Control deposits
Thickeners	Convert oil into solid or semi-solid lube
Lubricant protective additives	
Antioxidants	Improve oxidation resistance
Foam inhibitors	Prevent foaming
Antileak agents	Prevent leakage; seal conditioning
Biocides	Regulate microbial activity

Table 2.1: Table of additives adapted from [1]

2.4 Lubrication regimes

The lubrication regime describes the degree of contact between a pair of lubricated materials with relative motion to each other (a tribopair). Total separation of a tribopair by an intermediate lubricant is described as the hydrodynamic regime. A tribopair that moves with a mixture of separation and contact is referred to as operating in the mixed regime. Minimal separation between the tribopair in the presence of a lubricant is known as the boundary lubrication regime.

The difference between the regimes is often visualised using an annotated stribeck curve, see Figure 2.5. Once total separation is apparent, the friction increases because of increasing viscous losses from the lubricant.

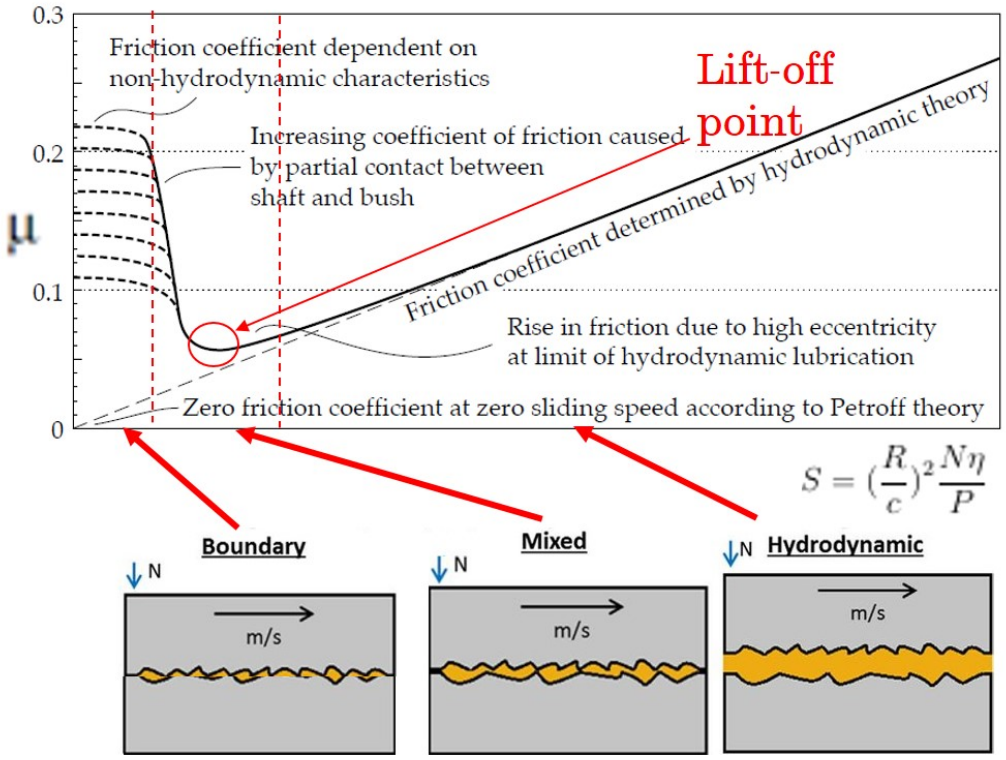

Figure 2.5: Stribeck curve adapted from [11]. Three seperate lubrication regime areas are indicated by the dashed vertical lines

This is represented on the stribeck curve as the increase in friction after the inflection point due to an increase in relative velocity of the tribopair or an increase in viscosity. A common method of representing the stribeck curve is by plotting friction against Sommerfeld number for a journal bearing, see Figure 2.5. The Sommerfeld number is dependent on the viscosity (which is primarily effected by temperature), velocity of the relative motion, the load normal to the contact area and the clearance ratio of the bearing. The stribeck curve shown uses μ to represent the friction coefficient. The equation for Sommerfeld number is as follows:

$$S = (\frac{R}{c})^2 \frac{N\eta}{P} \tag{2.3}$$

2.5 Lubricant properties and principles conclusion

Lubricant formulations can be complex and comparison of the performance of the different EALs used in Chapter 5 onwards relies on an understanding of the knowledge in this chapter. The variation in performance between lubricants is be dependent on viscosity effects and the type of lubricant. For journal bearing applications it was

essential to understand the different lubrication regimes and the variables which effect this so that experiments which represent realistic conditions for the lubricants could be designed.

Aged lubricants are examined in the following chapters and different ageing techniques are used to generate the lubricant samples so an understanding of the ageing methods and effects was also essential to this work.

Chapter 3

Bio-lubricant applications

In the following chapter the initial searches into the field of bio-lubricants which were conducted are outlined, which leads to a focus on marine lubricants. A variety of potential bio-lubricant applications are identified on a single marine vessel and the remaining part of the chapter takes the reader on a journey around the main lubricated parts of a marine vessel where bio-lubricants can be used. It finishes by discussing recent legislation and hones in on EALs for use in stern tube bearings as the main focus for the proceeding literature review.

3.1 Current research

As part of Objective 1, an overview of current research in the bio-lubricant field in general was conducted to gain background knowledge and to break the field down into smaller research topics and areas of interest. Research and journal databases, such as Science Direct, Scopus and Web of Science were used to search for published work systematically. The keyword search terms used on each site were:

- Bio-lubricant and Tribology
- Bio-lubricant and Tribological
- Bio-Lubricant and Wear

The number of results returned for a search using the term "biolubricant" was an order of magnitude smaller than when the hyphenated version was used. Hence the term bio-lubricant was used for the searches which fits with BSI standard CEN/TR 13227:2011 [4]. Each of these search terms were separately input into each site and

Machinery Field Tests	Testing of actual tribomachinery under practical operating conditions
Machinery Bench Tests	Testing of actual tribomachinery under practical-orientated (simplified, simulated or accelerated) operating conditions
Systems Bench Tests	Testing of specific tribosystems under practice-orientated operating conditions
Component Bench Tests	Testing of specific tribocomponents under practice-oriented operating conditions
Specimen Tests	Testing of arbitrary test specimens under practice-oriented or laboratory operating conditions

Table 3.1: Explanation of experimental categories

a cross-section of the papers that came up were read and summarised in a database. It was apparent that the papers seemed to fit into 3 main categories:

- General characterisation
- Lubricant Additive Based research
- Application Based research

Each of these categories makes up a primary branch of the spider diagram in Figure 3.1. It was important to comprehend the practical aspects of the research that has been conducted in order to identify the appropriate resources needed to make a valid research contribution. Consequently, the sources of the lubricants and the level of experimental testing that had been done were added as two further categories on Figure 3.1. It was found that most of the work done was experimentally based so this was split into 5 categories. This helped to identify the extent of the experimental work done and potential for expansive work. The 5 categories are explained in Table 3.1.

A total of 36 papers were summarised from the various sources and categorised to build a mind map of the Bio-Lubricants Field of research, Figure 3.1. This exercise was useful to an understanding of the field in general and to identify potential research gaps.

A lack of experimental testing of bio-lubricants at a component level complexity and above became clear; aside from a few full-scale machinery tests. This exercise also highlighted the scale of bio-lubricants as a field and the difficulty in summarising the field of research in a using the general term of bio-lubricant. As mentioned in Section

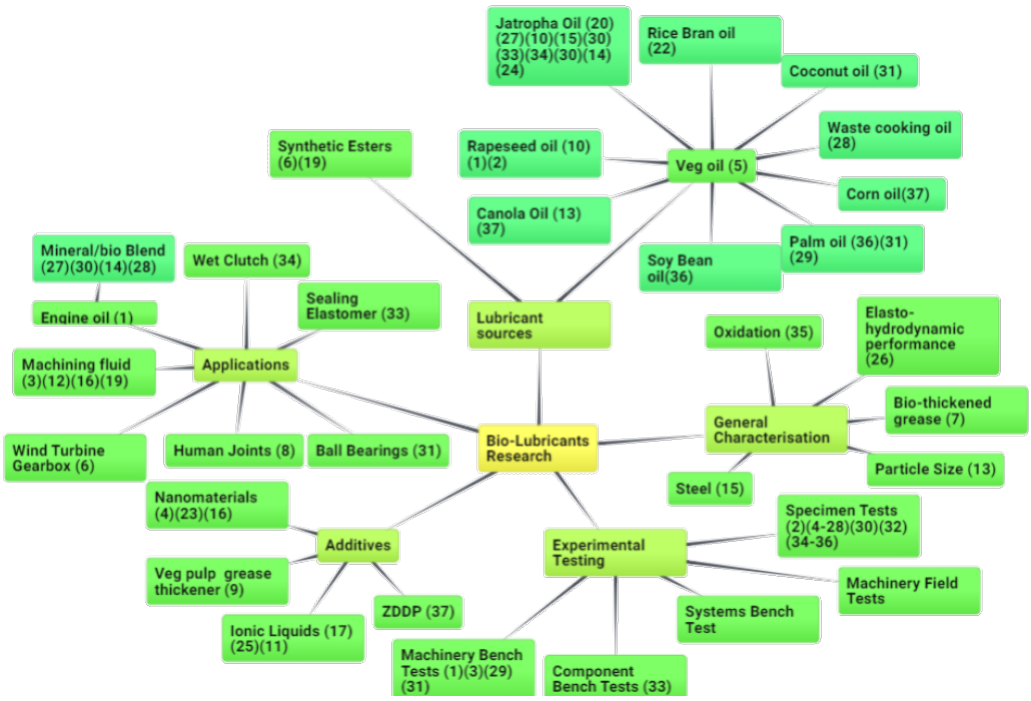

Figure 3.1: Initial pass mind map of the bio-lubricants research field

1.1 there is no universal definition for a bio-lubricant, although they are generally more biodegradable than mineral oil-based lubricants they are not necessarily derived from a renewable source and vice-versa [1]. This is demonstrated on Figure 3.1 by the high number of second-tier categories which emerged.

Industrial context was important to increase the impact of the research therefore an understanding of the wider lubricant market was sought to help focus the search for a gap. The lubricants market is often split into four main sectors, industrial, automotive, marine and aerospace, each with a share of approximately 38%, 55% 6% and 1% in the U.S.A. in 2015 from Figure 3.2.

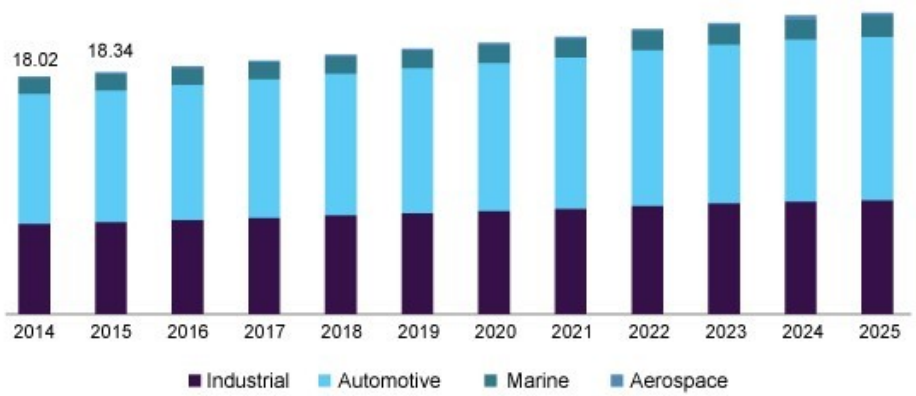

Figure 3.2: U.S. lubricants market by application [20]

It seems that the most under-represented industry relative to the size of the proportion of the lubricants market that it holds is the marine industry, with no research appearing in the initial searches. This small percentage of the market still equates to a value of approximately $1.1 billion for the marine lubricants industry in the US alone. Furthermore, the research papers that were relevant to engine oil, which could be considered relevant to the marine industry, were all investigating bio-lubricants for automotive applications. The apparent lack of research seems disproportionate given that around 21% of the annual (average) worldwide input of oil into the oceans is from vessel operational discharges [21], most of which are lubricants [22]. This is perhaps because the legislation governing these fluids (and emissions) lags behind other sectors such as the automotive sector. These figures were estimated in 2003, and is the most recent information available. Furthermore, lubricants are a significant source of toxins such as Polycyclic Aromatic Hydrocarbons (PAH) which are harmful to the health of all living organisms and are carcinogens which can be ingested by consumption of seafood [23].

3.2 Marine lubricant applications

There are a range of applications where lubricants may become exposed to the marine environment, such as in hydroelectric turbines, water pumps and sewage treatment machinery. Perhaps the largest variety of different lubricant applications in one place in the marine environment is in the variety of machinery found on a marine vessel, such as that shown in Section 3.3. The greases found on cranes, ropes and anchor chains are total loss lubricants so are almost certain to end up as contaminants in marine environments. Hydraulic fluids are used in on deck cranes, davits and capstans and also in below deck machinery such as thruster, stabiliser, controllable pitch propeller (CPP), rudder lubricants and stern tube lubricants. Hydraulic fluids are not usually total loss lubricants, but leaks are known to occur continuously and are normally classed as operational discharges [24].

While engine oils are a significant portion of marine lubricant usage, the motivation to use bio-lubricants within them is minimal due to the lack of a sea-water to oil interface. However, the use of engine oils in stern tubes is still common despite the introduction of the 2013 VGP (legislation discussed further in Section 3.2.6). Engine oils used in stern tubes are toxic to the environment due to the additives and non-biodegradable base oils used in their formulations.

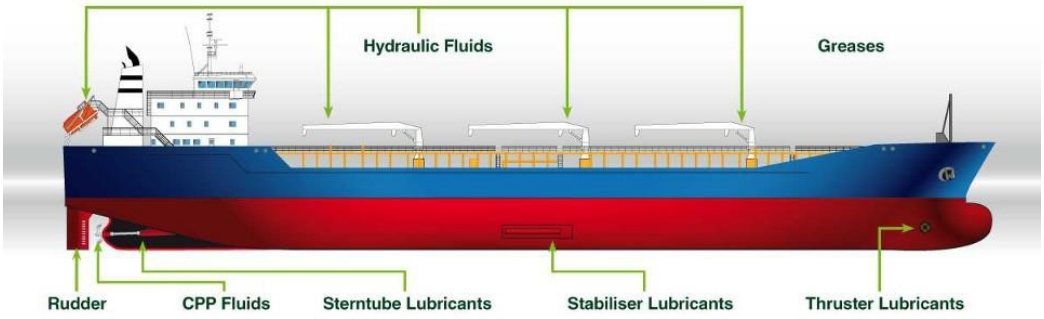

Figure 3.3: Lubricated areas in a large ship

3.2.1 Thruster lubricants

Thrusters are used for manoeuvres which might ordinarily have been fulfilled using tug boats. Three main types of thruster are the tunnel thruster, azimuth thruster and jet thrusters. Tunnel thrusters are usually impellors which are mounted in a tunnel that spans laterally across the bottom of a ship hull, usually at the narrow

stern. When manoeuvring in port these thrusters are usually employed to rotate the ship in a tighter circle that the rudder alone would allow.

Azimuth and jet thrusters can both be used for propulsion and/or manoeuvring depending on how they are utilised in overall propulsion arrangement of a vessel. Azimuth thrusters are so called because they allow thrust to be directed at any angle in the horizontal plane (azimuth angle). Jet thrusters draw water from an inlet duct and eject it out of a nozzle at high speed and can be mounted so that they rotate and can be pointed in at any angle as with an azimuth thruster.

With each type, there is potential for lubricant leak from both the bearings which support the rotating impeller or propeller and from high pressure hydraulic fluid when hydraulically powered motors are employed. Furthermore, azimuth and jet thrusters have additional lubricated bearing mechanisms so they can be pointed in different directions. While the lubricants used are not total loss, all thruster types are fully submerged and have direct oil to sea interfaces. Stern thruster oil is the main area for concern for lubricant leakage from thrusters because they are replaced at the highest rate in port according [24].

3.2.2 Stabiliser lubricants

Stabilisers are the machinery used to stabilise a ship against roll and motion due to waves. These are employed for comfort and safety, to keep the deck level and prevent injury. Active stabilisers normally consist of a fin which is rotated so that they resist the rolling motion of the ship. The lubricants in this machinery can be similar to those used stern tube oils in terms of their performance requirements and potential for water ingress to interfere with their operation. This is demonstrated by the fact that some manufacturers recommend the same oil for both stern tubes and stabilisers depending on the design [25].

3.2.3 Greases

Greases are applied on deck exposed machinery such as on wire ropes, chains and bushes. Under the water line the rudder bearings (stave bearings) are grease lubricated. An estimate for the grease loss from a typical rudder stave bearing before a typical two week service interval is 5% [26]. This means that the original as-new quantity of rudder stave grease can be considered a total loss to the environment after a single year of operation. Above deck greases can also be considered total-loss

lubricants and the rate of loss depends heavily on the operational environment and weather conditions.

3.2.4 CPP fluids

Controllable pitch propellers (CPP) have an extra degree of freedom which allows the blades to be rotated about their base where they are mounted to the hub. This adjustment is known as the pitch of the blades and can be optimised to reduce drag and increase efficiency depending on the flow velocity. Controllable pitch propellers are not present on all vessels and can often use the same lubricants designed for stern tubes or stabilisers. The sea-water to oil interface present makes them prone to hydrolysis. Therefore they are supplied in emulsify-able and non-emulsify-able forms depending on whether a sea-water drain off system is present.

3.2.5 Stern tube lubricants

Of the machinery shown in Section 3.3, the worst offender for lubricant transfer into the marine environment is the stern tube. It has been estimated that stern tube lubricants are discharged into the sea under normal operation on most ocean-going ships, at a collective volume of around 80 million litres per year [9].

The interface between the propeller shaft and seal to prevent water ingress into a ship is lubricated with a 'Stern tube lubricant', which is fundamentally a journal bearing lubricant. Stern tube lubricants are used at the interface between the propeller shaft and its supporting stern tube bearings in ocean going vessels. Figure 3.4 shows the location of a stern tube in a large ship and the arrangement of these components.

It is accepted in the marine industry that stern tube bearing failures have been increasing in recent years, which could be due to several factors [27]. A common modification to ocean going vessels to improve fuel efficiency is to replace the original propeller with a larger design. This increases the loading on the propeller shaft and stern tube bearings, which are often left unmodified, increasing the likelihood of failure. The effect is enhanced in single bearing stern tube designs. More severe operational conditions such an increase in the number of vessels that must travel long distances in shallow waters, are also a factor [27]. In this situation propellers are not as heavily submerged and therefore the stern tubes are more susceptible to heating up above the maximum operating parameters for the lubricant. However, a large proportion of failures occur under transient conditions, such as at slow speed during

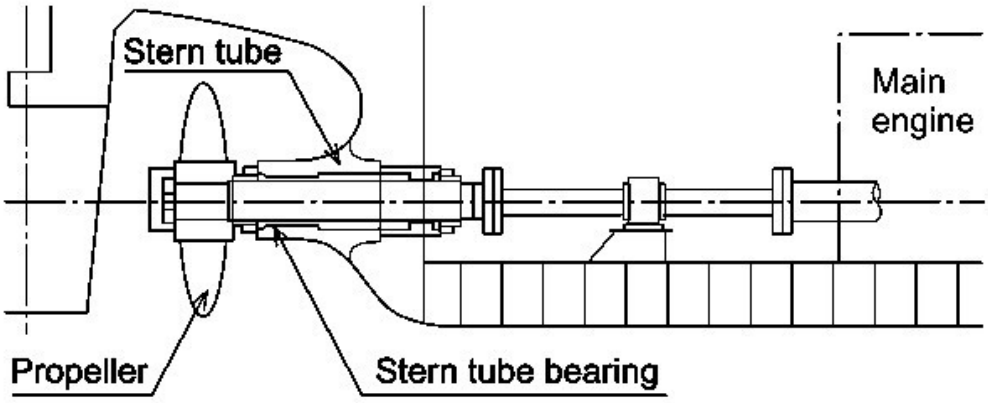

Figure 3.4: Typical stern tube and bearing arrangement

mooring trials (shakedown testing of new ships) where hard turns are conducted while lubricating oil is at low temperature or under high speed high load turns [28].

Another factor is a change in the lubricant for a bio-lubricant in recent years. The introduction of the strict regulations in 2013 has coincided with the increase in failures, suggesting that the new EALs are also responsible for some of the failures. It is reported that around 50 % of ship operators who use EALs in stern tubes experience problems outside of the norm [29]. Other problems with stern tube lubricants include reports that some EALs decompose early, resulting in more frequent oil changes and damaged seals and components.

3.2.6 Current legislation

In general, the motivation to adopt bio-lubricants as a replacement for mineral oils has been predominantly driven by legislation which outlaws the use of mineral based lubricants in some applications. For instance, in Germany, Austria and Switzerland, the use of mineral oil-based lubricants is illegal around inland waterways and in forest areas. In the UK, all chainsaws and harvesters working on Forestry Commission land use biodegradable oils [1]. Perhaps the most prolific regulations in force are those of the Registration, Evaluation, Authorisation and Restriction of Chemicals (REACH), which is a regulation of the European Union. These regulations require chemical producers to report information regarding toxicity, use and measures of exposure to which they are accountable. The social and financial burden of this encourages the use of alternative, less environmentally harmful chemicals. REACH regulations effect

all lubricants and their components imported and manufactured in the EU.

The most consequential legislation governing marine lubricants is the Vessel General Permit (VGP) which is enforced by the Environmental Protection Agency (EPA), of the United States of America, to enforce its National Pollutant Discharge Elimination System regulations [30]. It sets out requirements and limitations for the waste that is generated by ships in USA waters. In 2013, the VGP was updated and now mandates the use of environmentally acceptable lubricants (EALs) for certain applications while in USA waters. Consequently, lubricant manufacturers have developed a range of EALs to replace the lubricants which were used in marine applications prior to 2013.

3.2.7 Marine applications conclusion

It is apparent that the greatest impact from the application of bio-lubricants in the marine industry has been from the introduction of EALs used in the stern tube. It is a critical component for the propulsion of any ship and its performance can effect the fuel consumption of a ship, its sea-worthiness and the environmental impact of its operation. Therefore the the following work has focused on issues with the performance of EALs that are applied in stern tubes.

Chapter 4

Literature review

The literature review begins with common characteristics of synthetic esters which make up most stern tube EALs and how these are linked to their molecular structure and also reviews the work which highlights specific areas of concern with stern tube EALs. It also summarises literature which explains the typical operating conditions of marine stern tubes and proceeds to review experimental work and looks at test rigs that are relevant to this.

4.1 EALs properties

The majority of EALs use synthetic ester (SE) base stocks, but some are polyalphaolefin (PAO) or polyalkyleneglycol (PAG) types. A common way to categorise the lubricants which are available on the market is using the ISO 6743-4 classification of biodegradable hydraulic fluids [31]. From this, EALs with potential for use in stern tubes can be split into the following categories: hydraulic oil ester synthetic (HEES), hydraulic environmental polyalkylene glycol (HEPG), hydraulic environmental PAO and related products (HEPR) and hydraulic environmental triglycerides (HETG). Water is another EAL which is used in specifically designed bearings with polymer bushings [32, 33] however the recent trend in bearing failures is not linked to this type of bearing. Hence this review will focus on oil lubricated bearings.

While HETG oils are potential candidates for stern tube lubricants the author has not found any examples of them being sold as such. They are often referred to as triglycerides or vegetable oils, see Section 2.2.4. Their relative scarceness as stern tube lubricants is due to short service life [34] and the fact that the viscosity of most raw vegetable oils cannot be as easily designed or selected. It is generally lower than

ISO100 viscosity oils that are specified by stern tube manufacturers, apart from a few exceptions such as castor oil [35] which is much thicker.

HEPR base stocks are made up of PAOs which are produced from petrochemical resources [36] so are not bio-based. However, they are biodegradable in low viscosities (<8cSt) [37]. Bio-degradable HEPR lubricants are formulated by blending low viscosity PAOs with higher viscosity esters. PAOs are primarily employed for their high oxidative stability and good low temperature properties and because they crystallise at a lower temperature than other EALs. They are also cheaper than SEs of the equivalent oxidative stability. The addition of esters improves the additive solubility of the formulation, because PAOs tend to be non-polar whereas esters can be more polar (depending on their constituent level of alcohol and carboxylic acid).

HEPG lubricants demonstrate good friction control, high VI and good low temperature properties [1]. Their main disadvantage is poor seal compatibility and poor miscibility with other lubricating oils. [34, 38]. Their use as stern tube EALs has not been reported in public to date.

HEES lubricants are formulated by esterification of acids with alcohols. There are many combinations of acids and alcohols that will form an ester and consequently the esters can be designed and tailored to suit the intended application. Sources can be both petro-chemical and bio-based for both the acid and the alcohol [36]. These are the most common types of EAL used in stern tubes as they can be tailored to provide specific performance benefits (due to their wide variation in chemical structure) and their biodegradability.

While many comprehensive summaries which compare the properties of different types of lubricants can be found, the range of different products that are available that fit into each category makes generalisations about their properties potentially misleading. For example, the elastomer compatibility of HEES's are less favourable than HEPR according to Table 4.1 which has been adapted from a text book. Pettersson [17] explains that the low polarity of PAOs can lead to seal shrinkage and loss of elasticity. Synthetic esters have a much lower non-polarity index of around 50 (a higher polarity) compared to up to and over 300 non-polarity index (lower polarity) for PAOs [17].

It would follow that their seal compatibility would be preferable to that of PAOs, which is contradictory. Seal material compatibility depends on both the base oil and additive package in addition to the potential of causing a seal to swell [39]. It is

Parameter	HETG	HEES	Mineral Oil	HEPG	HEPR
Renewability content	High	Variable	Not	Not	Not
Readily biodegradable	Good	Good	Not	Variable	Not
Water solubility	Low	Low	Low	Variable	Low
Low-temperature performance	Weak	Variable	Weak	Good	Good
Oxidation resistance	Weak	Good	Variable	Good	Good
Hydrolytic stability	Low	Medium	Good	Good	Good
Seal material compatibility	Good	Limited	Good	Limited	Good
Paint and varnish compatibility	Good	Limited	Good	Limited	Good
Additive solubility	Good	Good	Variable	Good	Limited
Lubricity of base oil	Good	Good	Limited	Good	Limited
Corrosion resistance	Poor	Limited	Good	Limited	Good

Table 4.1: General properties of EAL types [36]

probable that the comparison in Table 4.1 considers other factors, but does not explain what "seal compatibility" refers to. Here lies the issue with generalised statements about properties of different EALs. In practice, the use of flouroelastomer (FKM) material for the stern tube seals ensures universal compatibility with the HEES and HEPR type EALs.

4.2 Stern tube critical properties

Despite the fact that Figure 4.1 considers eleven general properties to compare EALs, in the context of stern tube EALs there are still more factors to consider. The pressure-viscosity, shear-viscosity, temperature-viscosity thermal properties and viscosity index have all been put under scrutiny in recent studies into EALs [40–42].

Yano et al. [42] has suggested that the lower viscosity pressure coefficient of some EALs compared to the equivalent mineral oil based lubricants results in the collapse of the oil film in stern tube bearings at lower pressures than ship operators have been used to. Whilst the study finds EALs have lower pressure-viscosity coefficents than non-EALs, it stops short of quantifying the effect that this has on the lubricant viscosity in the context of real temperatures and pressures in a stern tube. Pettersson [17, 43] studied the thermal properties of SEs and how these performed well in EHL because they are more effective at removing heat from the contact and absorbing heat before the viscosity reduces. Bayat et al. also approves the use of EALs in EHL and comments on the improved thermal conductivity working to their advantage

when compared to mineral oil lubricants [44]. Borras et al. [40] measured the shear viscosity of EALs and found that 3 of the 5 EALs tested exhibited shear thinning, with the PAO products being the most susceptible to thinning. One of the three shear thinning EALs was an SE type which thinned at a slower rate than the PAOs but at a lower threshold. It was also confirmed that the SE was permanently thinned and damaged after the test.

Viscosity index, see Section 2.1.2, is also fundamental to the understanding of how EALs in stern tubes will perform because it governs the viscosity which is fundamental to its load carrying capacity (Section 2.1.1) and film forming capability. Table 4.2 compares the VI of EAL types used in stern tubes with HEES and HEPR having higher potential VIs.

Cost is another consideration which will influence the type of lubricant used in stern tube bearings. It is estimated that 20-30% of a ship running cost is down to lubricant costs [45].

Table 4.2 summarises the properties discussed in the literature along with the VI and cost. HEES, HEPR and mineral oil (API groups I-III) based lubricants have been compared but HETG and HEPG types have been omitted because of their limited use in stern tubes.

EAL type	**Shear thinning resistance**[46]	**Heat transfer coefficient**[47]	**Pressure-viscosity coefficient** [48]	**Viscosity Index** [48]	**Relative cost**[49]
HEES	High	9.91	5.3 - 21.1	up to 170	2-10
HEPR	High	9.14	10.5-12.6	up to 150	2-5
Mineral oil	Low	7.33	18.0-36.0	up to 120	1

Table 4.2: EAL properties for stern tube applications

The heat transfer coefficient is highest for HEPR and HEES, demonstrating that EAL base oils both have superior heat transfer over mineral oil according to Table 4.2. It is reported that higher heat transfer coefficient is an advantage because it allows the lubricant to carry heat generated by friction away from bearing more efficiently, which means that a higher viscosity can be maintained [47] and this agrees with the conclusions of Pettersson et al. [43] [17]. The pressure-viscosity coefficient is generally higher for mineral oils with a small amount of overlap with SE's. This fits

with what Yano et al. [42] described when comparing three EALs with a mineral oil based equivalent. However, the work of Yano et al. and Borras et al. [42][40] both suggest that some EALs have lower shear thinning resistance than mineral oil based lubricants which contradicts the finding of Lord et al. [46].

Lord et al. tested and compared the performance of a VG150 naphthenic mineral oil, VG68 PAO (HEPR) and a VG46 trimethylolpropane ester (HEES) by measuring the film thickness and traction force generated under severe operating conditons in a ball and disc interferometer. All of the results were non-dimensionalised and fitted well with Hamrock-Dowson model predictions for pure rolling. Under greater sliding the HEES generated thicker films than both the HEPR and mineral oil and exhibited consistently low friction while the HEPR and mineral oil friction rose with increased sliding. Non-Newtionian effects were observed in the mineral oil and the non-dimensionalisation was shown to be imperfect, with the authors suggesting that the absence of factors such as the Eyring stress, heat capacity and thermal expansivity should be investigated to help explain this. This work concludes that the film forming capability of the HEES lubricant is superior to that of the PAO, which is itself superior to the mineral oil in extreme operating conditions.

The lubricants tested in the study by Lord et al. [46] had no additives present and were base oil only, which is a significant difference between this work and the work of Borras et al. and Yano et al. who both tested fully formulated lubricants. Viscosity index improvers were present in both of the synthetic esters in the work of Yano et al. and this information was not specified in the work of Borras et al. so its possible that VI improvers were present in these formulations also. Given that esters are more polar and compete with additives to adhere to the metal surfaces [48], the additive packages are likely to be less effective in the HEES lubricants and HEPR lubricants because of their higher polarity than mineral oil. The lack of additives means that the additive packages in the mineral oil could have made the difference in the "friction rising point" (inflection point on the Stribeck Curve) which Yano et al. observed and the shear thinning which Borras et al. recorded. Neither author mentions the affects of the additive packages or what they consist of.

Castro et al. tested fully formulated hydraulic oils and compared HEES and HEPR types to a mineral oil based hydraulic lubricant. The authors quantify and compare the different additives present in each lubricant and test them in a pin on disk tribometer. They observe increased wear in the more biodegradable HEES and HEPR

lubricants and conclude that this due to a lack of anti-wear additives when compared to the mineral oil based lubricant [50].

4.3 Stern tube bearing operating conditions and parameters

In order to understand the issues surrounding EALs applied in stern tubes, literature that describes the stresses, requirements and operating conditions of the machinery was studied. The dimensions of the bearing varies depending on the size of ship and the number of propellers. The larger the propeller, both in terms of its mass and swept area, the larger and more concentrated the maximum loads on the stern tube bearing are. DNV registrar and classification society (DNV GL) have reported issues [27] which suggests that many recent stern tube failures are with large ships such as bulk carriers and container ships. Shaft diameters can reach as much as one metre so the projected pressure on the bearing is unexpectedly small when considering that the with the maximum loads are measured in hundreds of kilo-Newtons. Projected pressures tend to be less than one mega pascal even at maximum load. This means that they would be expected to operate in the hydrodynamic lubrication regime and not get close to the EHL regime.

According to the Riviera article, [27], there does not appear to be a specific set of conditions under which the failures have occurred. Some were during sea trials, others were a few months into operation but the problems are not limited to these conditions. During sea trials, when the maximum load on the shaft might be expected to occur, the speed is set at 85% MCR (maximum continuous rating speed) for turning tests [51]. Maximum speed is typically around 100rpm for large ships, but one would expect there to be a thick hydrodynamic film at that speed because the bearing would be optimised to generate a supporting lubricant film and therefore be operating in the hydrodynamic lubrication regime at a lower speeds than this. Therefore maximum speed should theoretically would be the optimum conditions for supporting a high load. Large and slower rotating propellers is another factor which is considered [52]. The trend for slow steaming could also be a problematic operating condition for the reliability of stern tube bearings because of the lower entrainment velocity of the lubricant which would reduce the film thickness and chance of full film formation. A summary of typical operating conditions can be found in Table 4.3. Maximum loads have been included and it is assumed that any conditions up to this maximum would

also be possible in operation. The minimum Sommerfeld number has been calculated assuming a minimum propeller shaft rpm of 22 (from an appropriate minimum speed of a large marine diesel engine found in [53]) at maximum load and using this to solve Equation 2.3. The viscosity used was 0.036 Pa.s, which is based on a worst case assumption of 60°C operating temperature using a standard stern tube lubricant Shell Melina S30.

Source	**Diameter (m)**	**Clearance (mm)**	**Length (m)**	**Max Load (kN)**	**Projected pressure (MPa)**	**Max rpm**	**Sommerfeld No.**
Komar 2013[54]	0.99	1.2	2.03	1325	0.5	109	0.007-0.03
Komar 2013[54]	0.47	0.8	0.95	225	0.3	123	0.005-0.03
He 2014[55]	0.52	0.9	1	290	0.32	89	0.01-0.1

Table 4.3: Stern tube bearing dimensions and operating conditions

WJ2 is a typical specification of tin based white metal material that is used. For the WJ2 material to be damaged a stress of at least 40MPa would need to inflicted [56]. The damage to a stern tube bearing is normally characterised by a "wiping" of the journal, which occurs when the propeller shaft comes into contact with the bearing and generates temperatures high enough to plastically deform the material, see Figure 4.1. It is not expected that stern tube bearing lubricant pressures reach above 5MPa, with the highest value seen in the literature suggesting a maximum value of 10MPa [40]. Therefore, the conditions for such damage to occur would require a break down of the lubricant film, or some significantly large (compared to the oil film thickness) debris. The "polished" stern tube bearing in Figure 4.1 would be classed as serviceable, but heavy scoring (duller in appearance) would be classed as advanced wear and not serviceable.

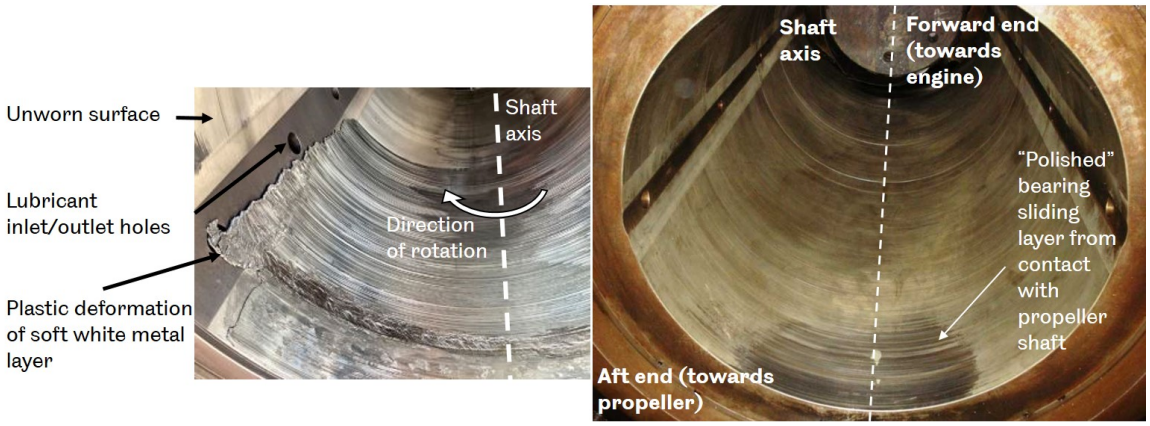

Figure 4.1: "Wiped" aft stern tube bearing (left) [57] and "polished" aft stern tube bearing (right) [58].

4.4 Journal bearing test rigs

There are several commercially available journal bearing rigs. For example the Pheonix Tribology TE39 with which the operator can measure the friction in a journal bearing whilst: controlling the speed up to 2000rpm, the normal load up to 5kN and an oscillating motion of the shaft rotation. The Lewis Research Inc LRI-8H also measures bearing friction and is similar in its size with a maximum load of 4.5kN and also features control of the inlet lubricant temperature. The latter was used by Lu et al. [59] to study the "lift off" (inflection point on a stribeck curve, see Section 2.4) speed under different loads and temperatures.

Bespoke test rigs can also be found in the literature. Cristea et al. [60] used the "Pprime" test rig which featured hydraulic loading on the shaft and oil bath temperature control and was fitted with several pressure probes at 10° intervals around the bearing circumference. Also measured was the electrical contact resistance which was used to indicate the amount of contact between the shaft and journal and the relative lubricant film thickness. Zhang et al. [61] investigated the seizure load of an aligned and misaligned air conditioning compressor journal bearing using a bespoke rig by measuring the bearing friction and adjusting the misalignment until the friction level started to rise.

The journal bearing rigs at The University of Sheffield can apply both static and dynamic loads whilst controlling the speed and temperature (to some degree) of a journal bearing whilst measuring friction and oil film thickness. The statically loaded rig, Baxter, was used in the study by Beamish et al. [62] is shown in Figure 4.2. It

was also used in studies with EALs, but this work has not been published. A dynamically loaded rig at The University of Sheffield, Betty, has the capability to introduce dynamic loads with different wave patterns (sine or square) onto its journal bearing through the use of a solenoid valve. The effect of dynamic loads at a rate of up to 2.5Hz on the bearing film thickness was investigated in [63]. Both the existing rigs at The University of Sheffield require large volumes of lubricant (5 litres or more) and realignment after each bearing replacement. Re-alignment after the test bearing replacement is time consuming and reduces experimental repeatability. Required lubricant volumes of more than 100ml means that the creation of a sufficient amount lubricant is not practical on a laboratory scale. Therefore the test rigs are limited to using commercially available lubricant products. Furthermore the minimum Sommerfeld number achievable for a typical stern tube EAL in either rig is around 0.03 which is an order of magnitude the minimum realistic value for a real stern tube bearing seen in Table 4.3.

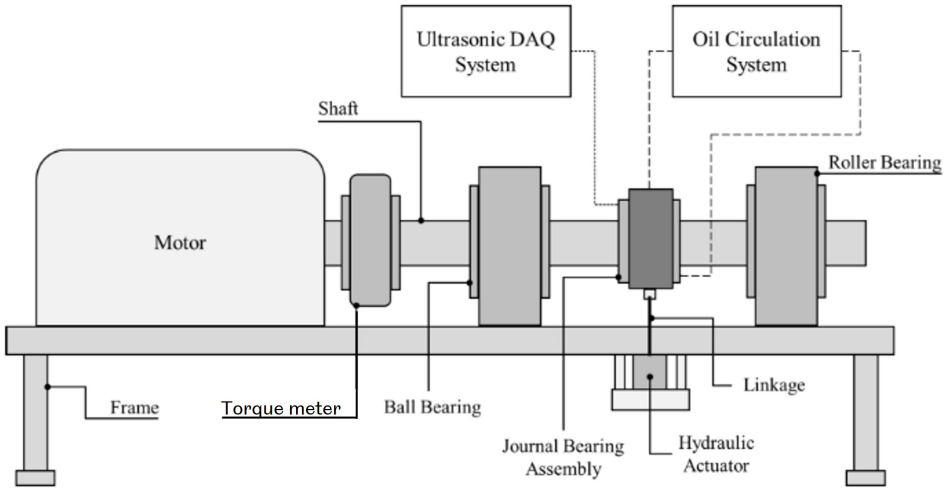

Figure 4.2: University of Sheffield "Baxter" Journal bearing test rig

The majority of rigs, including those mentioned at The University of Sheffield have been primarily designed to operate in the hydrodynamic regime. Test rigs of a component level of complexity (as opposed to material samples) which are specifically designed to operate the under severe conditions that are required to investigate the mixed and boundary regimes have not been found. Tachi et al. used a rig that was capable of operating in the mixed and boundary regimes, using a conformal block on a shaft. It was capable of speeds up to 600rpm and loads up to 30MPa to test different bearing bushing materials for their wear behaviour [56]. While this is more realistic

than a typical specimen level test because it replicates the geometry of a journal bearing, it is a partial replication only and could not be classed as a component level test.

Yano et al., [42] used a larger shaft diameter than in the machines aforementioned and the test rig in this work was specifically used to look at marine stern tube EALs. They studied the inflection point of the stribeck curve of a number of EALs and a mineral oil used as a benchmark. A bearing of 100mm in diameter was used and loads were applied which resulted in a projected pressure of up to 8MPa. As has been mentioned, their conclusion using this equipment was that EALs cause an earlier (farther to the right on the Stribeck curve) inflection point when compared to a mineral oil counterpart. The lubricant temperature was 25°C in all tests. The higher Sommerfeld number for the inflection point tests was attributed to lower pressure-viscosity coefficient for the mineral oil and shear thinning of one of the lubricants. The difference was seen in one of the three EALs and it was attributed to a lower pressure-viscosity coefficient and shear stability. However, its relevance to the application in stern tubes was unclear because the authors did not attempt to quantify the difference in performance between the lubricants in terms of the operating parameters of a real stern tube bearing. Furthermore there was no error information or quantification of the repeatability of the results given with the quoted Sommerfeld number so the significance of the results could not be verified. The authors suggested that the difference would be more obvious under the higher lubricant pressures seen under misaligned edge loading conditions, such as in a hard turn manoeuvrer, but no quantification of these conditions was given.

Litwin et al. has also conducted several studies using a journal bearing test rig which was designed for testing stern tube bearings. Several studies looked at water lubricated bearing performance using this rig [64–67]. More recently it has been used to study oil lubricated bearings and specifically the performance of EALs by Kowalski et al. [68]. However the rig is limited in not having the functionality to experimentally replicate the misalignment conditions seen in oil lubricated stern tube bearings. In reality misalignment is inevitable because the load from the propeller acts at the end of the shaft which is supported like a cantilever.

The work by Kowalski et al. suggested that industrial confidence in EALs is low because of their inferior performance when aged causing increased bearing wear. To address this they assessed the performance of EALs compared to mineral oil in a bench top test rig which replicates conditions in a marine stern tube of 100mm in

diameter. They used realistic pressures of up to 1.0MPa and speeds up to 660rpm and measured the friction generated and the pressure at various points around the bearing circumference. They chose to maintain a constant oil temperature in the bearing of 40°C. Bearing wear was also simulated by changing the bearing clearance by 0.1mm. No notable performance differences were found between the EALs and mineral oil for any of the conditions tested. Although this goes some way to comparing the effects of aged EALs compared to mineral oils in a worn bearing, which is perceived as a consequence of poorly aged EALs, it does not go as far as assessing the performance of EALs which are themselves aged. As far as the reader is informed, the lubricants used were all fresh. The test rig operates in the hydrodynamic regime and the scaling relative to real stern tube bearings is not addressed. Kowalski et al. also point out the limited amount of literature which assesses the performance of EALs in the context of a stern tube bearing and highlights the focus in the literature to date around water lubricated bearings.

4.5 Literature review discussion

The first problem which the review uncovered was the overgeneralisation of EAL properties. It was misleading because the varying range of products available makes generalised statements about a specific type of EAL's performance difficult to verify. This was highlighted in the work of Borras et al. [40] which shows how the because within the category of a HEES lubricant, there are significant variations shear stability.

A further gap in the work done is a lack of context in the analysis of EAL performance. For example, Yano et al. [42] does not quantify the effect that the pressure-viscosity coefficient has on the lubricant viscosity in the context of the temperatures and pressures in a stern tube.

The additives are crucial for boundary/mixed lubrication performance and this appears to have been overlooked in the literature, specifically with the experiments conducted on EALs. Only one example of the literature specified the lubricant by additives present or attempts to qualify their role in the context of EALs. The properties discussed in the literature are mainly bulk properties of the base oils in the lubricants.

A focus around water lubricated stern tube bearings is found, but research into the performance of oil lubricated bearings is comparatively much lower, despite the fact

that most large ships are in operation for upwards of 40 years and have no option to retrofit water lubricated bearings. Component level experimental work on stern tube bearing EALs is minimal relative to the size and value of the problem with two published studies which uses a bench-top level study. They are both arranged so that the shaft is supported either side of the test bearing. This is contrary to a real aft stern tube bearing which is the last support along the shaft before the main load applied at the end of the shaft by the propeller. In reality this causes significant bearing misalignment in the aft stern tube bearing.

The review also demonstrates the absence of work which characterises the performance of aged oils. Although Kowalski et al. [68] mentions that oil ageing could be an important factor in the performance of EALs, no aged oils are put to the test. Methods to age an oil are outlined in Section 2.3.2 all of which produce oil samples of less than 100ml and require significant laboratory time to produce. To experiment with any of the bench top rigs in the literature would require several litres of aged lubricant to be circulated which would be time consuming to produce and potentially damaging for pumping equipment. Hence a bespoke test rig would be required to use low oil volumes.

Lastly, all of these experiments are conducted at a small scale when compared to real stern tube bearing dimensions. The review has highlighted the need to contextualise the results of further experiments in a more comprehensive manner so that the results which are obtained can be related to real stern tube bearing performance. To do this, non-dimensionalisation of the bearing and lubricant parameters using the Sommerfeld number like in the work of Yano et al. [42] is appropriate, but an opportunity to use this to put the findings into context of a real stern tube bearing was missed.

Chapter 5

Initial experiments

As was apparent in the literature, experimental research on the performance of EALs designed for stern tubes was limited with inconclusive results. This chapter starts by explaining the equipment and tests used to conduct experiments to characterise the performance of a selection of EALs as per Objective 2 outlined in Chapter 1. It then moves on to explain the results from the film thickness, friction and temperature measurements.

5.1 Test Equipment

The viscosity of the EALs at different temperatures was measured using a Stabinger viscometer. This was necessary to be able to calculate the film thickness by the EALs when they were applied in a journal bearing. A journal bearing test rig, Baxter, was used for the initial experiments to characterise EALs. This was instrumented with ultrasound sensors which could be used to calculate the oil film thickness. It was adapted as part of the initial experiments to also measure friction in the journal bearing using a torque meter. The load applied, speed of the journal and temperature were controlled.

5.1.1 Oil viscosity measurement

The dynamic viscosity of each lubricant sample was measured using a Stabinger type viscometer (Model SVM 3001). This measured the dynamic viscosity using the Couette principle with a non-contact sensor. It also has a density measurement module which measures the density of the sample simultaneously. A kinematic viscosity-

temperature relationship can then be calculated from the measured dynamic viscosity divided by the density.

5.1.2 Baxter journal bearing test rig

The Baxter rig, Figure 5.1, was designed to replicate the conditions found in a stern tube bearing contact with scaled down bearing dimensions. It is a plain (non tilting-pad) journal bearing which is instrumented with film thickness sensors, a torque meter which measures the torque required to rotate the bearing (due to friction) and thermocouples around the oil circuit and on the bearing shells. The shaft rotational speed, the normal load on the shaft and the oil inlet temperature can be controlled. This rig allows bench top experiments with components and geometry similar to the full size machinery in a stern tube. The measured parameters of the modified Baxter rig are shown in Table 5.1. The bearing dimensions and material are shown in Table 5.2.

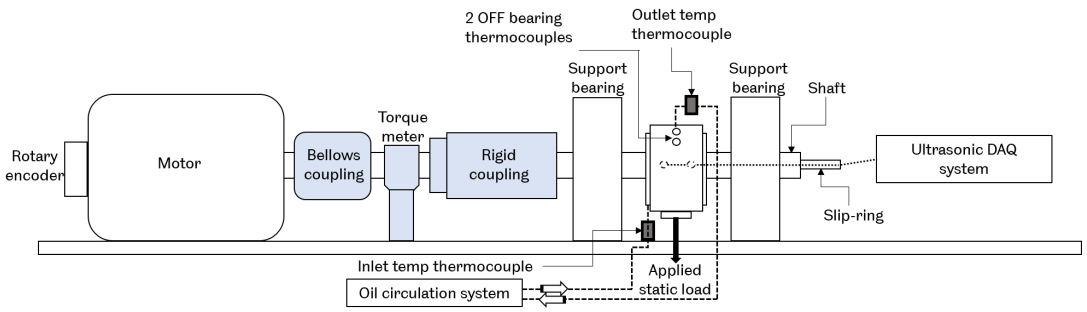

Figure 5.1: Baxter (journal bearing rig) schematic

Parameter	Range	Measurement device	Precision	Accuracy
Shaft rpm	1500	Rotary encoder	-	+/- 0.5°per rev
Normal load on shaft, kN	0-20	Load cell	+/-0.008	+/-0.25
Bearing shell temp, °C	0-100	K-type Thermocouple	+/-0.0005	+/-1.5
Oil inlet temp, °C	0-100	K-type Thermocouple	+/-0.0005	+/-1.5
Oil outlet temp, °C	0-100	K-type Thermocouple	+/-0.0005	+/-1.5
Film thickness along bearing length, μm	0.8 - 60 [69]	Ultrasound sensor	NA	NA
Bearing frictional torque, Nm	0-250	Non-contact rotary torque sensor	-	+/-0.5

Table 5.1: Rig instrumentation specification

Parameter	Specification
Bearing diameter, mm	112.0
Bearing length, mm	50.6
Radial clearance, μm	45
Projected pressure, MPa	0-3.5
Roughness radial, Ra	0.7 [69]
Material	Steel back with sintered lead-bronze alloy with galvanic bearing surface layer (3% copper)

Table 5.2: Baxter rig bearing details

5.1.3 Film thickness measurement

The film thickness in a journal bearing is a good indication of how close to the limit (boundary and mixed lubrication regimes) that the bearing is operating at. It is directly related to the lubrication regime that the bearing is operating within and the amount of wear that would be expected. A thicker film will offer greater load carrying capacity and protection against dynamic loads than a thinner film.

The Baxter rig is instrumented with ultrasound sensors which are embedded into the shaft surface, shown in Figure 5.2. This allows the measurement of the lubricant film thickness around the circumference of the bearing, the location of the minimum film and its magnitude to be determined.

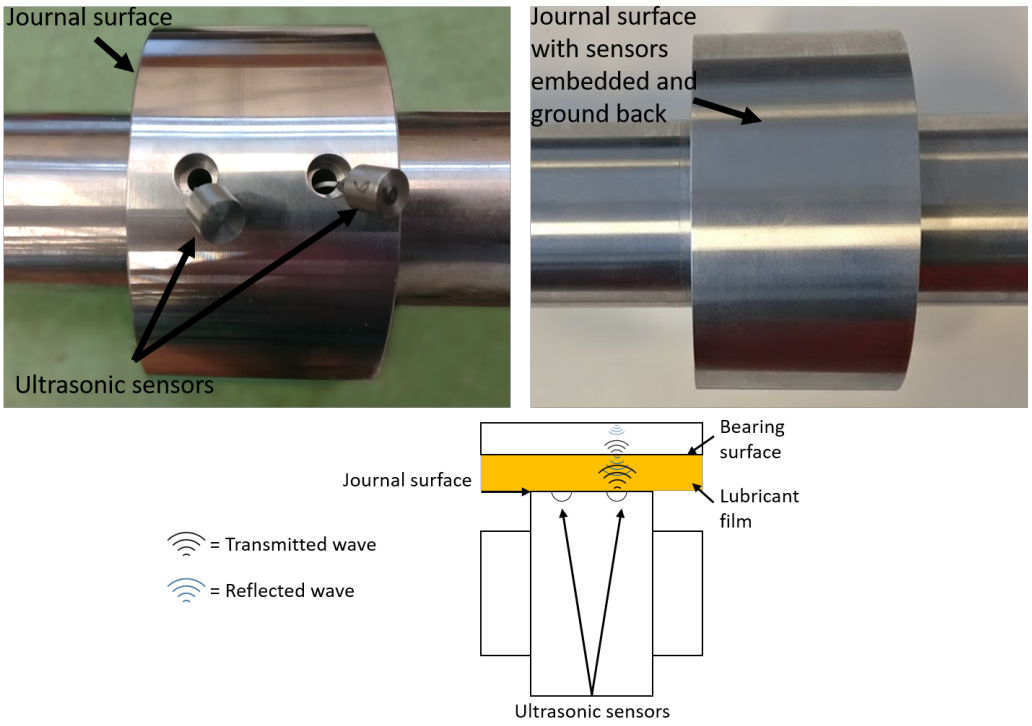

Figure 5.2: Baxter shaft instrumentation

An ultrasound wave transmitted by the transducers travels through the oil and a proportion of this wave is reflected when it reaches the oil-bearing shell interface. Using a quasi-static spring model to represent the oil film, its thickness can be determined by using the phase difference between the reference signal and measured response, shown in Equation 5.1 from [70].

$$h = \frac{\rho C^2 (tan\Phi_R)(z_1^2 - z_2^2)}{\omega z_1 z_2 \pm \sqrt{(\omega z_1 z_2^2)^2 - (tan\Phi_R)^2 (z_1^2 - z_2^2)(\omega z_1 z_2)^2}} \tag{5.1}$$

The acoustic impedance, z_1 and z_2 are known quantities for the two materials, in this case the bearing material and the lubricant. ω is the wave angular frequency, which corresponds to the sensor frequency (7MHz in this case). The density, ρ, of the lubricant and C is the speed of sound (SoS) in the lubricant. The acoustic impedance and angular frequency can be assumed to be constant under the temperature and pressure conditions which the Baxter rig operates [69]. The pressure and temperature affects the SoS in the lubricant and the lubricant density. Temperature effects on the SoS are the most significant of these. The higher the temperature, the slower the SoS. This inverse relationship is approximately proportional. In previous experiments with the Baxter rig, the temperature could reach a maximum of 100 °C and a minimum of 20°C. Given this range using Shell Melina lubricant, the SoS would vary from 1150 to 1500ms^{-1} (around 30%). For the purpose of the learning experiments, the pressure effects on the SoS and the pressure and temperature effects on the lubricant density were assumed to be negligible. Given the maximum projected pressure of 3.5MPa (Table 5.2) the SoS would change by around 1%. In terms of the density, the pressure and temperature range combined would affect the SoS by a maximum of 5% according to measurements taken by Beamish [69].

The relationship between SoS and temperature in each lubricant was measured using the speed of sound test rig, shown in Figure 5.3. It is constructed from Invar steel which has minimal expansion with temperature. To measure the speed of sound at different temperatures the rig was heated in a programmable oven and the time of flight of an ultrasound signal to be reflected from the lubricant to chamber boundary at the far end of the chamber was recorded. Since the distance (length of the chamber) could be assumed to be constant with temperature, the speed of sound in the lubricant at different set temperatures could be measured. The temperature of the lubricant was verified using a k-type thermocouple immersed into the lubricant. This test was conducted for each lubricant and an example is shown in Figure 5.4.

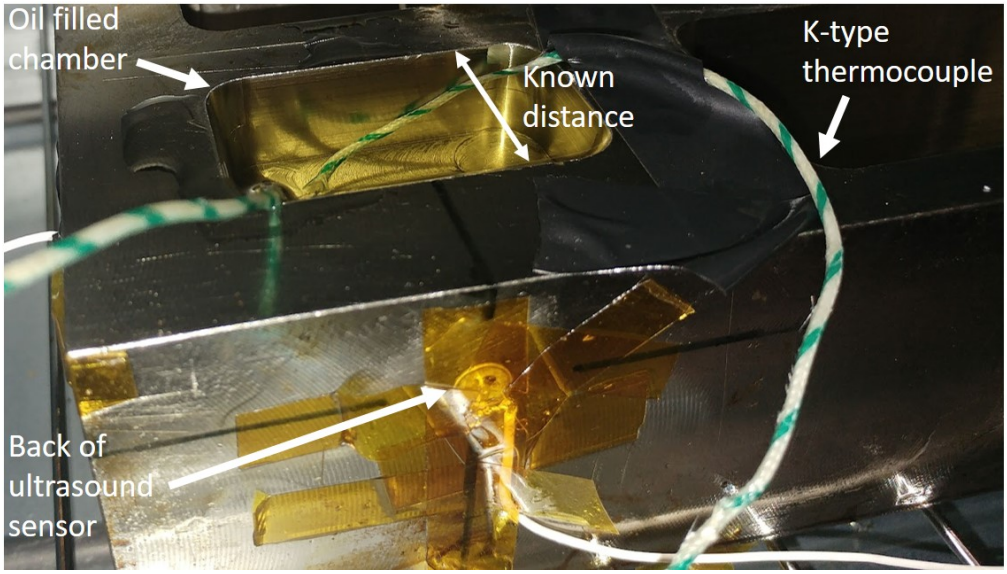

Figure 5.3: Speed of sound test rig

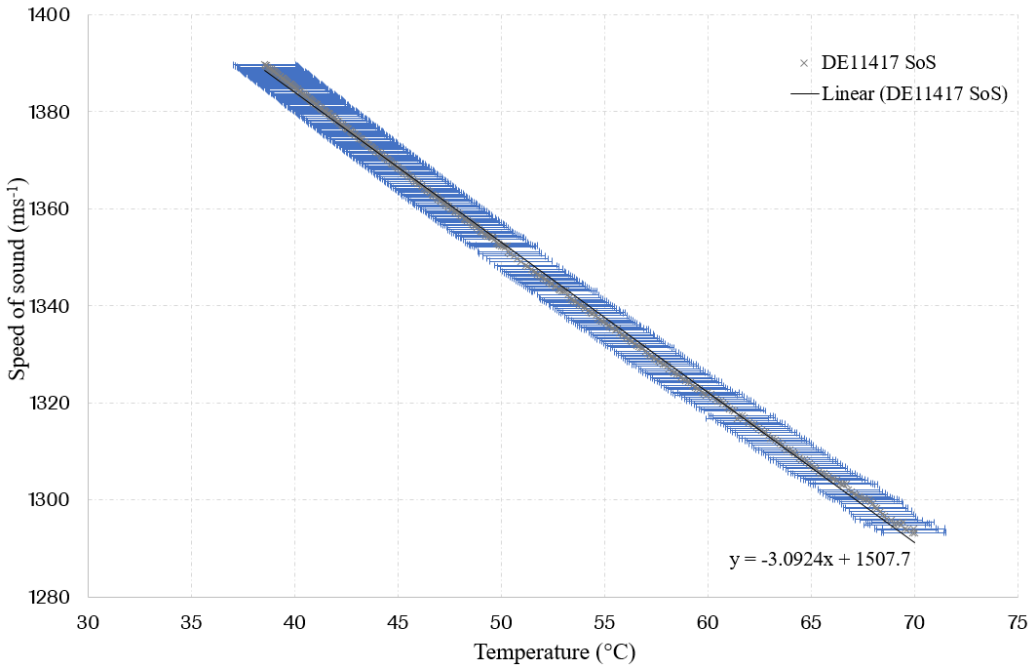

Figure 5.4: Speed of sound for DE11417 at different temperatures. The black line is a linear fit (equation shown), with blue error bars calculated from the thermocouple accuracy of +/-1.5°C

The shaft revolutions were measured using the rotary encoder fixed on the end of the motor which drives the rig, Figure 4.2. These measurements were cross-referenced with the raw data from the ultrasonic DAQ system to generate a profile of the phase

shift of the signal around for one rotation of the bearing. Data was recorded for a fixed period of time and a profile was generated for each revolution. The average of the profiles over the time period was plotted and the phase change on the mean average profile at the contact was input to Equation 5.1 to calculate the minimum film thickness. The phase change (Φ_R) at the minimum film point is the difference between the two blue lines on Figure 5.5. In this case the flat line is the reference point because the film is thick enough here that there is no difference in phase between this measurement and an infinitely thick film. This is referred to as the "infinite film" region because the phase change tends to zero [62].

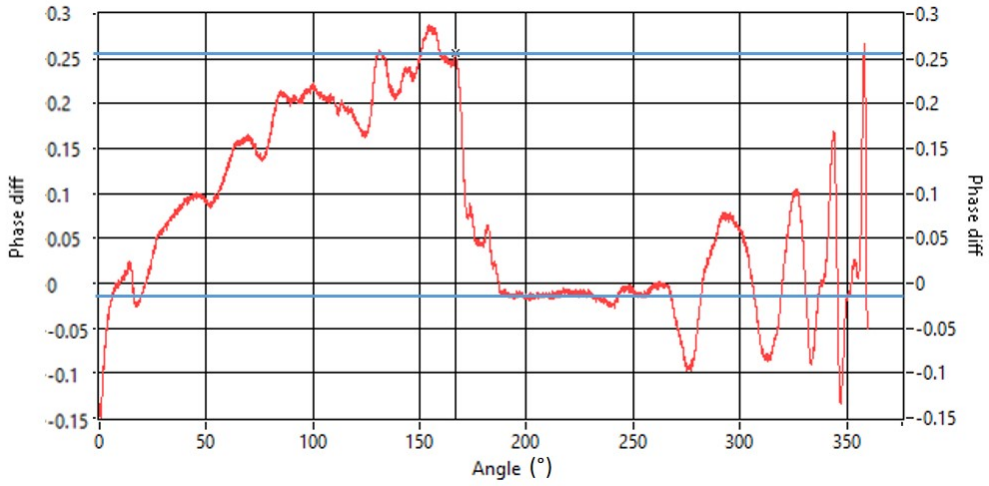

Figure 5.5: Phase change over 1 revolution

5.1.4 Friction measurement

To characterise the oils and further distinguish performance differences between the types of EALs, a torque meter was fitted to the rig, shown in Figure 5.6.

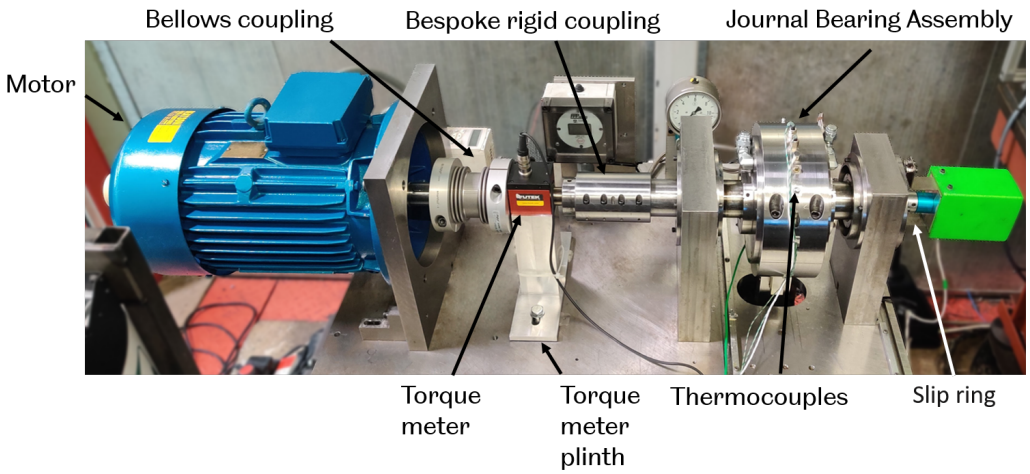

Figure 5.6: Modified Baxter rig with newly installed torque meter and couplings

This was designed to be directly mounted to the shaft of the Baxter rig to allow an accurate measurement of the torque, without backlash from a coupling. Consequently, a bespoke rigid coupling was designed to connect directly to the journal, labelled in Figure 5.6. The torque meter was calibrated from new, immediately before being installed on the rig.

The torque measurement taken is directly related to bearing friction using the relationship between forces acting on the journal in Figure 5.7 in Equation 5.3.

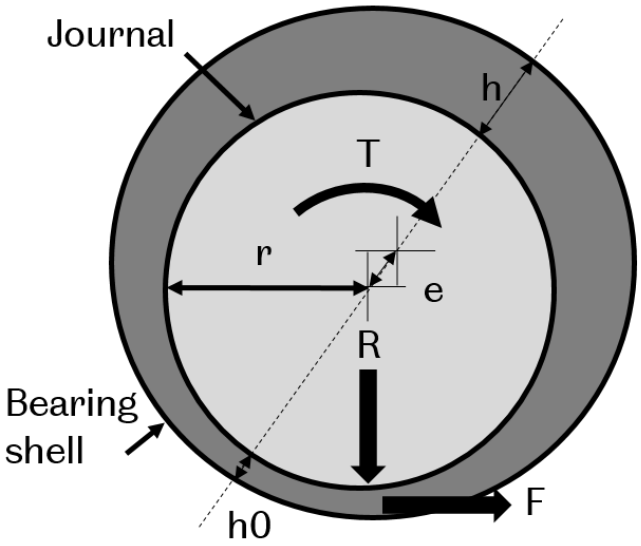

Figure 5.7: Journal bearing cross section showing parameters for friction force calculations. Scale of clearance is exaggerated for clarity

$$F = \mu R \tag{5.2}$$

$$T = Fr \tag{5.3}$$

Substituting Equation 5.2 into equation 5.3 results in:

$$\mu = \frac{T}{Rr} \tag{5.4}$$

The eccentricity value, e on Figure 5.7, can be calculated by subtracting the measured minimum film thickness, h_0, from the the maximum theoretical value for film thickness h: where the maximum theoretical value for film thickness is the difference between the shaft radius and the bush radius (i.e the radial clearance).

A theoretical method for evaluating torque and friction in a journal bearing is described by integrating the shear stress over the bearing area. This approximation is based on the Half-Sommerfeld approximation, therefore does not allow for any negative pressure or cavitation [11]. It also assumes that the bearing is infinitely short, meaning that the bearing length (in the axial direction on a shaft) is much less than the diameter and the change in pressure in the axial direction is considered negligible compared to the change in pressure of the circumferential direction. This can be used to approximate the friction expected from a journal bearing, dependent on its dimensions, lubricant viscosity, running speed and minimum film thickness using the following equation which is a modified version of the Petroff equation (Equation 5.5) from [11].

$$F = \frac{2\pi\eta ULr}{c} \frac{1}{(1-\varepsilon^2)^{0.5}} \tag{5.5}$$

5.2 Initial experiments method

Four fully formulated lubricants which were available on the market for stern tube applications were obtained and their performance was characterised in the Baxter rig. These were intended as learning experiments and the following hypotheses were tested:

1. EAL performance at least matches that of mineral oil based lubricants in terms of frictional properties and film thickness.
2. There will be a trade-off between EAL stability and lubricity.

The criteria that the EALs are theoretically required to to meet to be able to satisfy hypothesis number one are shown in Table 5.3.

Lubricant performance criteria	**Specification**
Viscosity	100cSt @40°C
Viscosity index	Less than 100
Film thickness	At least as high as the mineral oil under the most extreme speeds and loads delivered by the test rig
Energy efficiency	At least as high as mineral oil under all conditions, by comparing friction load on the motor.

Table 5.3: Stern tube lubricant performance criteria

The lubricants obtained for these experiments represent a cross-section of the types of lubricants available on the market for marine stern tube applications. Details of each formulations numbered one to four can be found in Table 5.4. The first three lubricants are all EALs, with the fourth being a mineral oil equivalent. A further EAL which was obtained at a later date and was not tested in the Baxter rig.

No.	Lubricant	Saturation	Class	Formulation	VI	Stability	Relative cost
1)	DE11417	Saturated	HEES	Product blend	139	Very High	12
2)	DE11418	Saturated	HEPR	Thin PAO and thicker ester	178	High	8
3)	DE11419	Unsaturated	HEES	Oleate based synthetic ester	170	Low	4
4)	Shell Melina S30	-	Mineral	Fully formulated	97	Medium	1 [49]
5)	Mobil SHC Aware ST [38]	Unknown	HEES	Fully formulated	188	Medium	4-12

Table 5.4: Lubricants compared in the experiments. Lubricant 5 was not tested in Baxter.

As can be seen in Table 5.4, there is a trade-off between hydrolytic and oxidative stability and cost for the EALs. Different levels of branching in the formulations is one reason for this, as the higher the levels of branching the higher the resistance to biodegradation [1]. Furthermore, the higher VIs in the cheaper lubricants are an attribute of their longer chains and lower levels of branching.

5.2.1 Test parameters

In the experiments which follow, the factors are the: speed, load, bearing temperature, lubricant type, friction of seals and ancillary components and the ambient temperature. The responses are the friction and wear. The intial analysis of the experimental factors is summarised in Table 5.5.

Factor	**Type (units)**	**Control/ Noise**	**Range**	**Levels**	**Interactions**	**Sensor**
Speed	Variable (rpm)	Control	100-200	2	Temperature, Friction	Rotary Encoder
Load	Variable (kN)	Control	2-20	10	Temperature, Friction	Pancake load cell
Lubricant type	Attribute	Control	N/A	5	Temperature, Friction	NA
Set temp	Variable (°C)	Control	40	1	Friction, Load, Speed, Lubricant (viscosity)	k-type thermocouple
Frictional torque of seals and support bearings	Variable (Nm)	Noise	Unknown	NA	Temperature, Load, Speed, Lubricant	Torque meter
Ambient temp	Variable (°C)	Noise	15-30	1/day	All variables	k-type thermocouple

Table 5.5: Experimental factors considered in the DOE

5.2.2 Design of experiments

DOE refers to the methodology used to investigate the influence of variable factors on the output response. A hypothesis is proposed based on the current understanding and theory and this hypothesis is tested with various DOE techniques. A common approach is to conduct learning experiments which test the extremes of each factor and measures the response. This gives the experimentalist an idea of which factors have the greatest effect on the output of the experiment and which ones are less important. This information is used to design experiments which maximise the knowledge gained but minimise the time and resources which are needed to conduct them.

According to the literature a stern tube bearing operating temperature is around 40°C [29, 71], with some designs operating up to 60°C [72]. Given this information it was decided that the bearing temperature would be kept at a constant 40+/-2 °C for the tests. It was found that the temperature of the lubricant in the bearing was very sensitive to changes in the speed and load. The main challenge was maintaining the bearing temperature at a constant value in order to take measurements. Furthermore, operating the rig below 100rpm was unrealistic because at speeds slower than this the control system and motor combination could not keep the rpm constant. At 100rpm the bearing temperature was steady at around 40°C depending on the load and lubricant. Above 200rpm steady temperature control at 40°C was not feasible. This is the reason that the speed is limited between 100 and 200rpm in the design of the experiments, Table 5.5.

Although lubricant type is technically a separate factor, each lubricant was in fact considered a separate set of experiments. This was because each oil change and clean up required half a day of lab time. The Baxter rig was available for a limited time so this was the main constraint to the testing. A complete set of tests on each lubricant was conducted on the same day. Considering the experiment in this way also allowed the elimination of significant variation in ambient temperature, since this did not tend to vary within the period of a day.

It was decided that each measurement would be taken over five seconds. This is because it would give a snapshot of the steady state performance of each lubricant with sufficient time to record the film thickness and torque of at least five full revolutions of the journal and the quantity of data captured was not too large to be impractical to analyse and process. Given two variable factors (l_1 and l_2) each with two and ten levels respectively, twenty experiments could be completed within a few minutes. Repeating the experiment three times for each of the four lubricants resulted in a total of 240 tests, see Equation 5.6. With five oil changes required, which each require half a day, a full factorial experimental design was practically possible for each lubricant within the remaining half day.

$$l_1 \times l_2 \times 3 \times 4 = 240 \tag{5.6}$$

5.3 Results

The results from the initial experiments are split into four sections. The first showing a comparison of the temperature viscosity relationship of the EALs. Then the oil film thickness generated by the EALs in the Baxter rig is compared and the third section shows a comparison of the friction generated. These were conducted at discrete loads and speeds and the data was recorded while the bearing was in a steady state at discrete loads and speeds. The final section presents Stribeck curves which were generated from experiments which the speed was varied continuously.

5.3.1 Viscosity-temperature tests

The shallower gradient of the lines representing the EALs on Figure 5.8 show that the viscosity of these lubricants is less sensitive to the temperature than with Shell Melina S30. Therefore the EALs all display a higher VI than Shell Melina as is in agreement with the information in Table 5.4 in Section5.2.

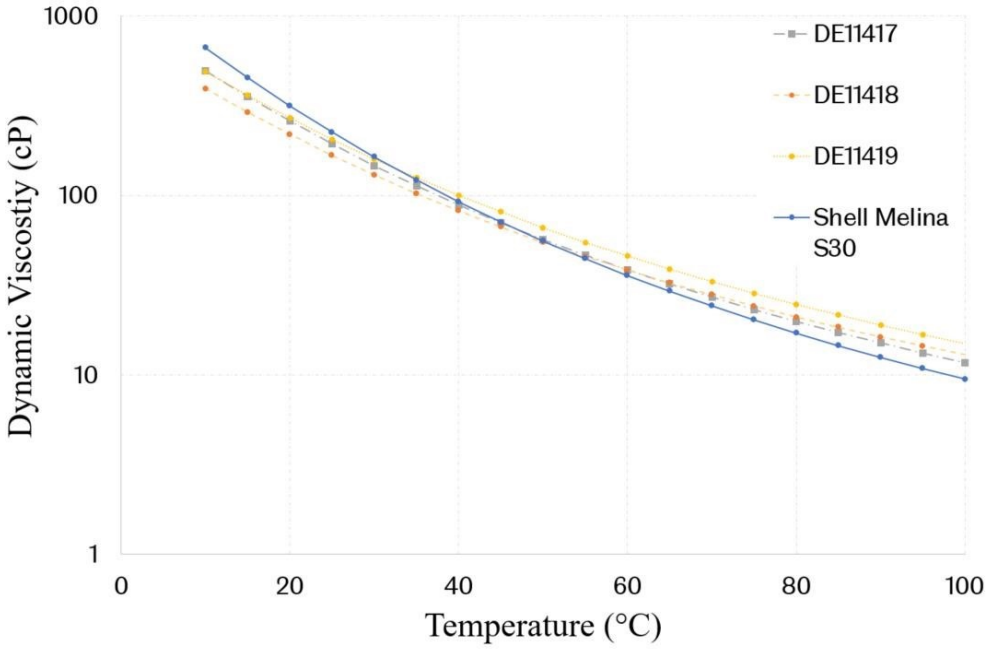

Figure 5.8: Viscosity temperature relationship for lubricants tested in the Baxter rig

5.3.2 Oil film thickness comparison

The minimum oil film thickness was measured using the phase change of the reflected ultrasound signal as described in Section 5.1.3. A dedicated LabVIEW software

(created by Li at the University of Sheffield [73]) was used to process the raw data into graphs such as that shown in Figure 5.5 so that the phase change could be recorded and converted into a value for the average film thickness for each recording. Each value is plotted against the load applied for both speeds tested, see Figures 5.9 and 5.10.

The error bars shown in Figures 5.9 and 5.10 result from the accuracy of the load cell shown in Table 5.1 and the error from measuring the speed of sound in the lubricant shown in Figure 5.4.

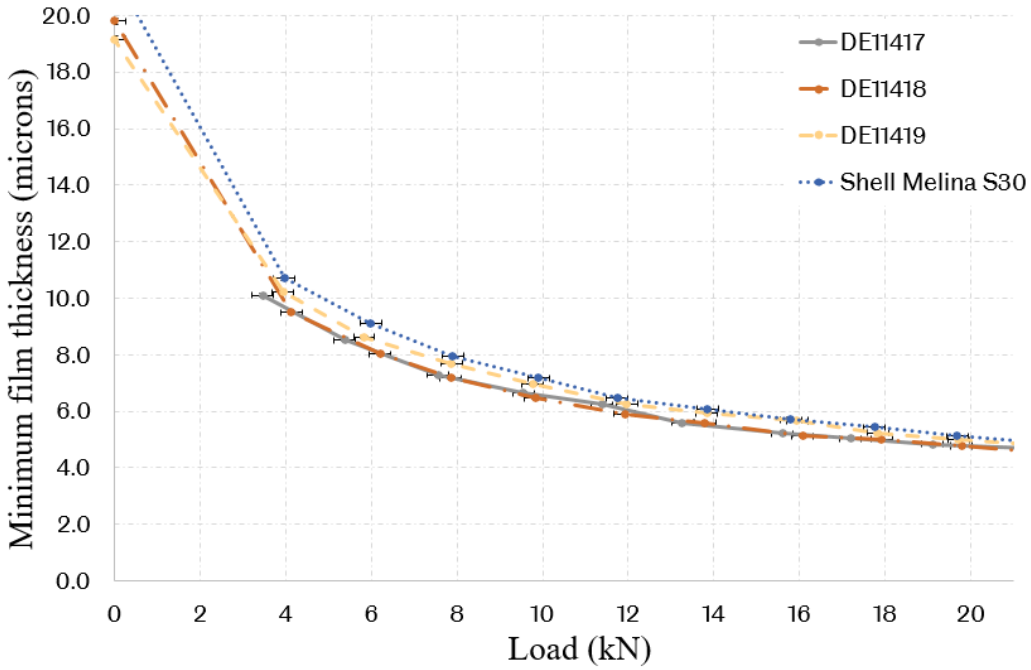

Figure 5.9: Minimum oil film thickness at 100rpm. Black error bars shown on each data point

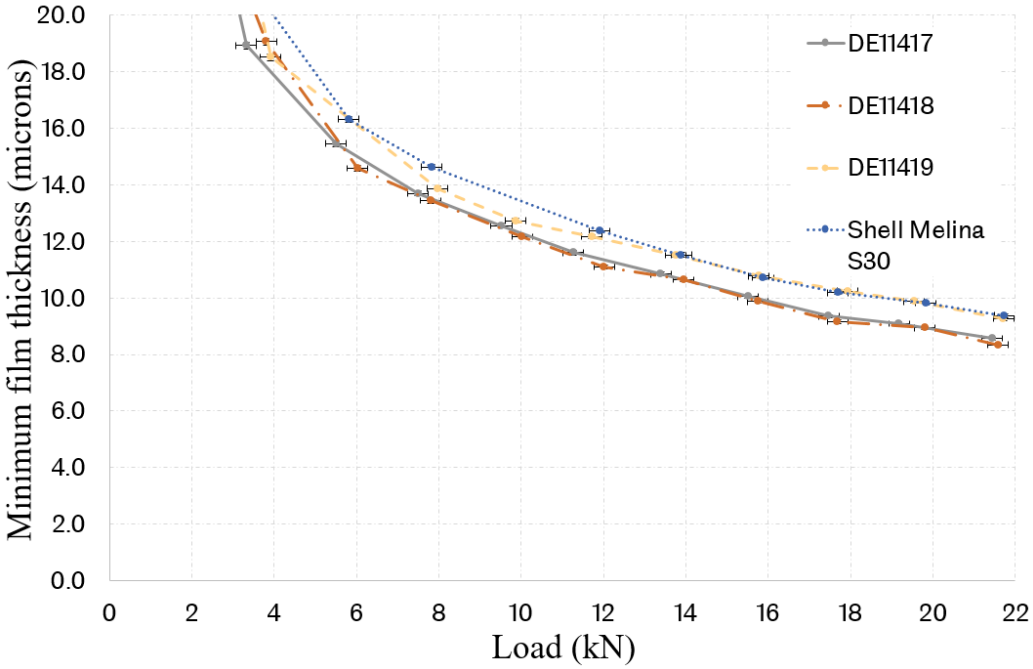

Figure 5.10: Minimum oil film thickness at 200rpm. Black error bars shown on each data point

Generally, in both Figure 5.9 and Figure 5.10, Shell Melina S30 generates the thickest films, followed by DE11419 and DE11417 with DE11418 generating the thinnest films. DE11419 generates a film that closely matches the thickness of the Shell Melina film under the higher loading conditions for both test speeds. In fact from 6kN-20kN at 100rpm and 10kN-20kN at 200rpm the difference between the film thickness of these two oils is barely distinguishable, considering the error in film thickness measurements of +/- 0.63% shown by the error bars. DE11417 generates consistently thinner films than DE11419 with the exception of the region between 6 and 8kN at 200rpm where the line representing DE11419 dips away from the Shell Melina line. This behaviour is somewhat repeated in Figure 5.9 at 100rpm.

5.3.3 Oil film friction comparison

The theoretical friction was compared to the measured friction in order to verify the measurements taken on the Baxter rig. The minimum film thicknesses measured in the experiments were input into Equation 5.5, because the eccentricity ratio, ε, was dependent on knowing the minimum film thickness. This then enabled a theoretical friction coefficient to be calculated for each test which is plotted on 5.11. The friction generated for each oil film was measured using the torque meter described shown

in 5.6 and was converted from torque to friction using Equation 5.4 where R is the measured applied load. This value of friction coefficient is compared to the theoretical friction coefficient.

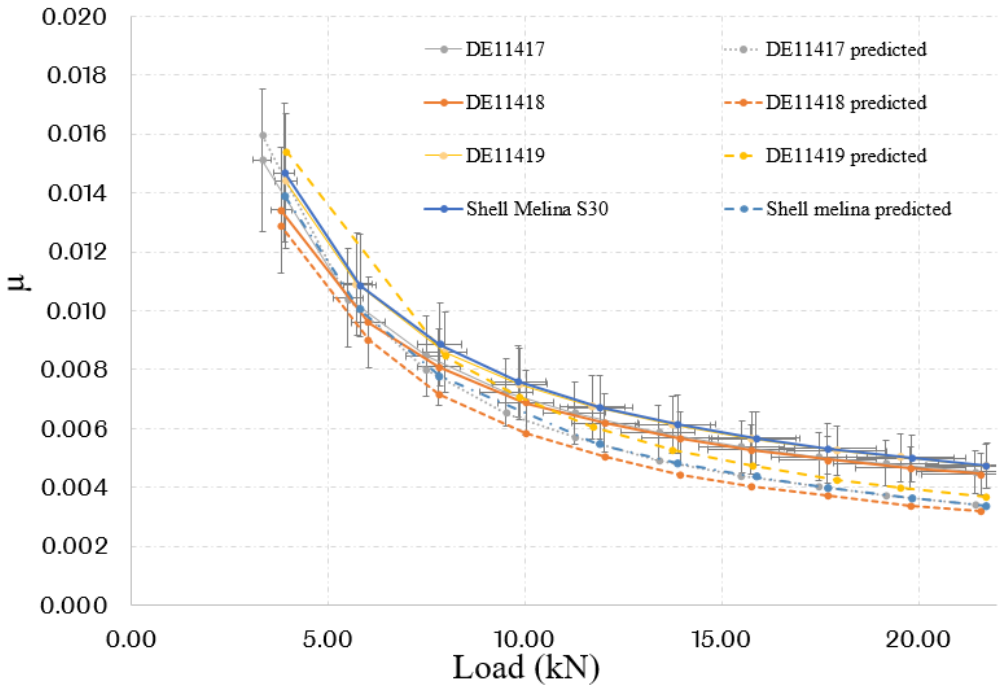

Figure 5.11: Bearing coefficient of friction measured at 200rpm under a range of loads

The error bars shown on Figure 5.11 result from the torque meter and load cell measurement uncertainties outlined in 5.1. They were calculated according to the methodology explained in [74].

DE11417 and DE11418 generate the lowest friction in the contact and they are very similar throughout the load range. DE11419 and Shell Melina S30, both develop higher friction. Hydrodynamic lubrication theory explains that the thicker the lubricant film, the higher the frictional losses are due to internal shearing of the lubricant. By observing Figure 5.10 the higher the load, the thinner the lubricant film at 200rpm. As Figure 5.11 shows, the friction increases as the load decreases, which would correspond to thicker lubricant films.

The magnitude of the predicted friction coefficient agrees well at low load values. Less agreement between theory and measurement as the load is increased could be caused by the fact that the theoretical calculation only takes into account friction generated between the journal and the shell, but on the real rig there are additional

components such as lip seals and shaft supporting bearings. The same would be the case for a real stern tube bearing. As a tool for validation of the measurements, the predicted torque was sufficient since it was of a similar magnitude. It also ranked the lubricants in the same order as the measurements in terms of their lubricity.

5.3.4 Stribeck curves

Additional experiments were conducted which were designed to characterise the lubricants outside of the hydrodynamic regime because the performance of the lubricants in the hydrodynamic regime was very similar.

The transition from the hydrodynamic to the boundary lubrication regime is characterised by a rise in bearing friction as the Sommerfeld number goes down (see Figure 2.5). For the following experiments, the temperature and therefore the viscosity of the lubricant was kept constant in the contact. Controlling this variable means that the Sommerfeld number would be controlled purely by the speed and load in the tests. The Stribeck curves were generated by running the bearing at 300rpm and gradually reducing the speed to 0rpm whilst measuring the torque and maintaining a constant 20kN load. The speed was reduced over time as opposed to increasing the load over time because the motor inverter could be utilised to control the deceleration accurately. In contrast, generating the Stribeck curve by reducing the load at a set rate relied on the operation of a hand operated valve which was less repeatable and less accurate due to the precise dexterity required.

The plots on Figure 5.12 were generated by taking a moving average of 100 readings of the torque and plotting these points. The points are merged such that they appear as a line. The rate at which the measurements were taken was 1000Hz and the deceleration rate of the motor was 1 revolution per minute per second. Each complete "run-down" took approximately 5 minutes.

The Stribeck curves generated suggest that the transition point between the mixed and hydrodynamic regimes was approximately 25rpm for all of the oils. This point was difficult to distinguish due to the poor performance of the motor at speeds below 100rpm. The capability of the rig to run under mixed lubrication conditions was unreliable as is demonstrated by the blue trace on 5.12 which does not show a transition because the motor stopped turning before the mixed lubrication regime was entered. It thought that it could be a characteristic of the Mobil SHC aware lubricant, however

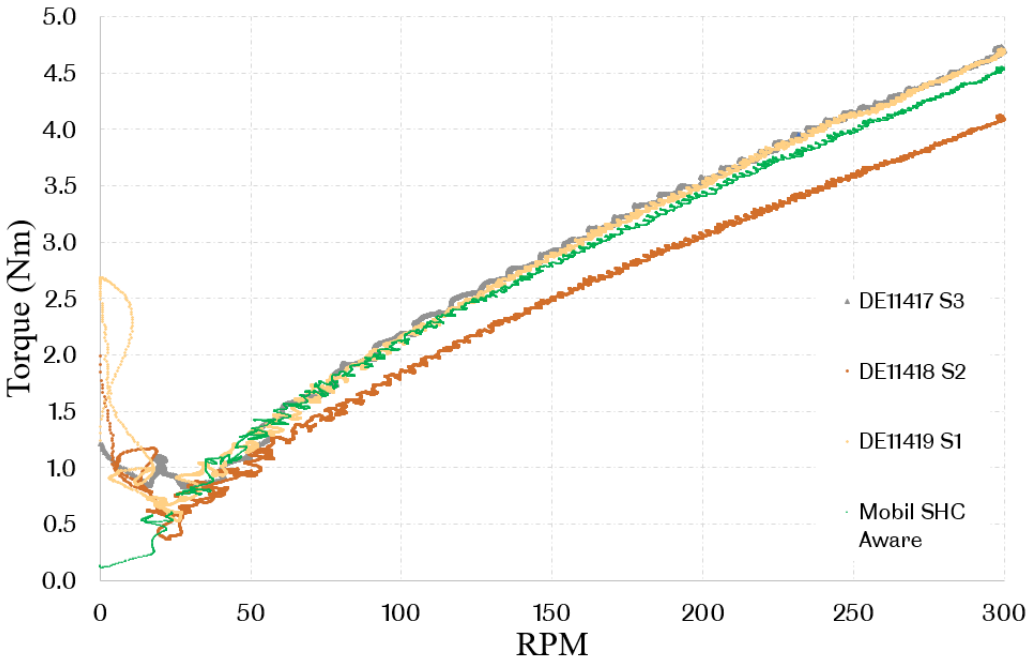

Figure 5.12: Bearing stribeck curve under 20kN load and 40°C

other repeats of the run down tests for DE11417, DE11418 and DE11419 were also unreliable as the rig sometimes failed to operate in the mixed lubrication regime.

5.4 Initial experiments discussion

The first hypothesis presented in Section 5.2 was that the EAL performance would match that of the mineral oil based lubricants in terms of the frictional properties and film thickness. The criteria was that the film thickness was at least as high as the mineral oil (Table 5.3). The results showed that the Shell Melina S30 mineral oil based lubricant generated the thickest films overall, this was closely matched by the DE11419 EAL and within the error allowed for the measurement equipment accuracy. The hierarchy of the thickest to the thinnest lubricant films generated as seen in Figures 5.9 and 5.10 is due to their relative viscosity. The viscosity measurements which were taken show that at 40°C the thickest lubricant would be the Shell Melina followed by the DE11419. In terms of the friction, DE11419 and Shell Melina were equally matched and it could be argued there was no difference in friction between any of the oils given the measurement uncertainty. Consequently hypothesis 1 has been met given that an EAL did indeed match a mineral oil lubricant's performance.

In terms of hypothesis 2, the trade-off between lubricant stability and lubricity, seems to hold true for the tests that have been conducted. Shell Melina and DE11419 generate the most friction and DE11417 and DE11418 the least. Given that DE11417 is the most hydrolytically and oxidatively stable, one might expect this to generate the lowest friction. Although they are very similar, the results suggest that DE11417 might be inferior to DE11418 in terms of its lubricity. However the higher frictional losses with DE11417 could be explained by the fact that it has a slightly thicker viscosity at 40°C than DE11418. Any differences in lubricity would be more obvious in the mixed and boundary lubrication regime. As has become apparent, the conditions which the learning experiments were conducted in could not reliably test the lubricants in the mixed and boundary regimes so although the hypothesis holds true, for conditions outside of the hydrodynamic regime, the test on this hypothesis is inconclusive.

5.5 Initial experiments conclusions

The friction and film thickness performance of all of the lubricants was very similar under the conditions tested. Hypothesis one was answered but only under hydrodynamic lubrication regimes. Hypothesis two was not satisfactorily answered and required further testing under more extreme conditions which would examine the lubricants in the mixed/hydrodynamic regime transition in order to investigate it further. It was apparent that further investigation and experiments at a component

level of realism, would require significant modifications to the Baxter rig or a different rig entirely. This was because it would need to operate with higher motor torque (requiring a new motor or gearbox) and alterations to the fabric of the other rig components to accommodate these modifications. Furthermore the space in which the Baxter rig was housed did not allow for expansion of the footprint of the rig.

The lessons from these experiments in terms of the rig design is explained in Section 6. The way in which future tests on the lubricants should be carried out along with the knowledge from the rigs which were evaluated in the literature review are combined and feed into the design of a new test rig in Chapter 6.

Chapter 6

Test rig design - DiMITRI

This chapter details the bespoke test rig which was designed and manufactured for this work by the author to satisfy Objectives 3 and 4 of this thesis. It explains the development of this rig from the initial concepts and more detailed design through to its manufacture, assembly and commissioning. The initial brief as per the Objective 3 was to design a test rig to investigate the performance of EALs under extreme operating conditions. To complete Objective 4 the rig was required to be capable of testing the lubricants in the mixed/boundary lubrication regime. The initial idea was to use a motor to spin the journal and a load would be applied on the end of the shaft with an existing servo hydraulic testing machine typically used for tension/compression and fatigue type testing (Schenck 250). This combination would allow dynamic loads up to 250kN to be applied to the shaft. The advantage of using an existing servo-hydraulic machine was that it was already an accurate and controllable way of applying and measuring the load because it features a built in load cell and complex control system. DiMITRI is a pseudo-acronym for "Davison Mixed Lubrication Test Rig" which is its name.

6.1 Design brief

To address the gaps found in the literature within the aim of this thesis further bench top experimental assessment of the performance of EALs is required. Hence Objective 2 of this thesis which was to: "Design a test rig to investigate the performance of EALs under extreme operating conditions", will be met by satisfying the following specifications:

1. Low oil volume of less than 100ml in total required to operate the test bearing so that aged oils may be characterised.
2. Scaled so that it can operate in conditions relevant to real stern tube lubricants, using non-dimensionalisation of test results. A Sommerfeld number range of 0.004 to 0.01 should be possible.
3. Be arranged so that the shaft is loaded as a cantilever to mimick the way that propellor shafts are primarily loaded. To achieve this the end of the shaft would have a load normal to its surface in the direction of gravity. Load magnitude would need to generate similar pressures in the bearing to those in a real stern tube bearing of at least 10MPa.
4. Allow disassembly and replacement of bearing parts so that the mixed and boundary lubrication regimes can be studied in more detail, without the need to realign the bearing as is the case with existing rigs at the University of Sheffield, to set up time.
5. Variable control of the rotational speed of the bearing from a speed which will generate hydrodynamic lubrication down to 0rpm. Variable control of the load applied on the bearing (to generate at least 0 to 10MPa projected pressure) and variable control of the temperature of the lubricant (room temperature to 100°C).

These design criteria are developed further in Chapter 6 and with the use of a product design specification (PDS) document which was updated as the design process was carried out and can be seen in Appendix A.

EALs will be used which represent a cross-section of the lubricants which are available on the market in terms of both the specification and cost. The performance of aged oils will also be assessed.

6.2 Concept development

Four concepts were devised which utilised the Schenck 250 to apply a load on a spinning journal bearing shown in Figure 6.1. These were developed using a product design specification (PDS) which is attached in Appendix A. The main design features in the PDS stated that the rig must be:

1. Capable of generating Sommerfeld numbers close to those of a real ship.
2. Modular in design to allow different bearings to be installed.
3. Designed with some form of temperature control – heating or cooling.
4. Easily disassembled with removable bearing shells that do not require movement of the shaft in order for them to be replaced.
5. Scaled to approximately half the size of the Baxter rig (see Section 4.2) to ensure that it was portable and would fit within the dimensions of the Schenck 250 test bed.
6. Compatible with solvents and degreasers. Surfaces need to be accessible to be wiped clean. Where access is not possible minimal dismantling of the rig will be required.
7. A misaligned bearing/loaded as a cantilever as per a real propeller shaft.
8. Small enough so that a low lubricant volume is required to run it of approximately 50ml.

All of the concepts shown in Figure 6.1 feature a step down gearbox because a high torque would be needed to drive the bearing in the mixed lubrication regime. High torque would reduce the maximum rpm available which was acceptable as hydrodynamic lubrication was not the area of interest. The gearbox is a right-angle bevel gearbox to reduce the overall length of the rig because lab space around the Schenck 250 was limited. Each concept also has a floating in-line torque meter with couplings either side of it to allow for friction measurement of the bearings and to compensate for misalignment between the shafts. The floating design was specified because it increased the tolerance to misalignment between the motor and test bearing shafts when compared to fixing it with a solid plinth like the design used in the Baxter rig. A higher misalignment tolerance has the advantage of reducing assembly time.

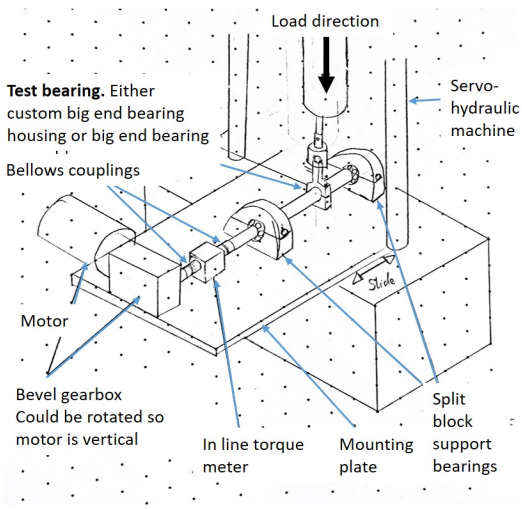

(a) Concept 1 sketch

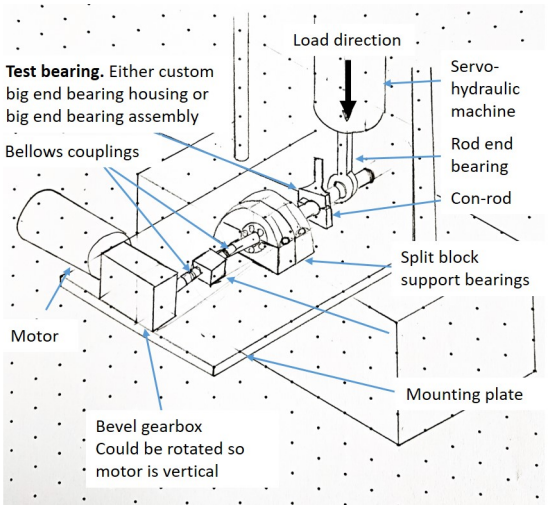

(b) Concept 2 sketch

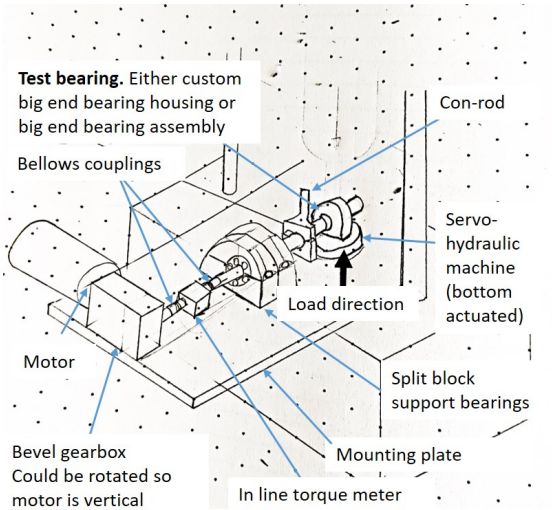

(c) Concept 3 sketch

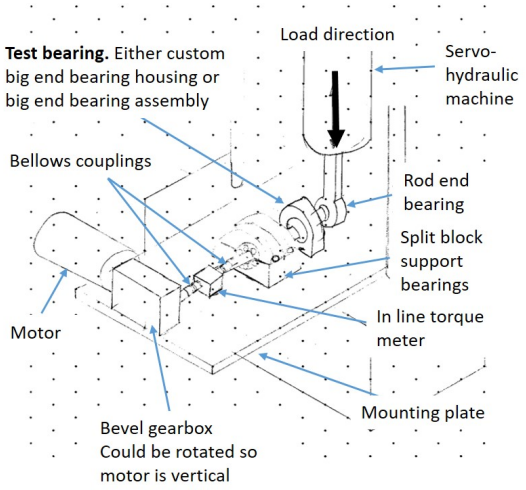

(d) Concept 4 sketch

Figure 6.1: Four concepts for the design of DiMITRI mounted onto the Schenck 250 servo-hydraulic machine

Concept 1 involved an automotive crankshaft bearing because this is a readily available journal bearing type. A suitable con-rod within which to house the bearing would also be an off-the-shelf component. Concept 2 was a development of this idea and featured a rod-end bearing on the end of the shaft to satisfy the need identified in the PDS to load the shaft as a cantilever to mimic the loading in a propeller shaft. Ultimately it was decided that the con-rod housing in Concepts 1 and 2 was not suitable because it would need to be modified for instrumentation and would therefore become a bespoke part, negative the advantage of using ready made components.

A bespoke test bearing housing would be more practical because it could be designed to house instrumentation such as thermocouples and heating or cooling circuits. Concept 3 features a bespoke test bearing housing which enabled the bearing to be loaded from the base of the Schenck 250 machine. In the final iteration Concept 4 was generated using a combination of the rod-end cantilever loading from Concept 2 and a bespoke bearing housing from Concept 3. Concept 4 (Figure 6.1d) was chosen as the optimum solution and this was confirmed when each Concept was evaluated as per an objective hierarchy in the PDS and it obtained the highest score.

6.3 Motor and drive system

The detailed design began with specifying the motor, drive system and gearbox. The torque required to drive a bearing of approximately 50mm in diameter (half the size of Baxter as per item 5 in Section 6.2) in the mixed lubrication regime was estimated by measuring the torque required to release the Baxter rig bearing from seizure at full load. This was done by loading the bearing and then applying a turning force on the shaft by hand and measuring the torque applied to turn the shaft. This was repeated and it was found that approximately 80Nm was required to release the Baxter rig bearing from seizure at a full load of 20kN. Therefore for DiMITRI, which would use a smaller bearing, 80Nm was the benchmark and deemed sufficient to drive the bearing in the mixed lubrication regime.

The mixed lubrication regime occurs at relatively low speed and high friction for a journal bearing. Therefore the drive system would need to rotate the bearing at slow speed but high torque whilst maintaining accurate control of the speed. A drive unit which was capable of vector control of the motor is the conventional option to provide stable speed control, quick response to sudden load changes as well as high torque at low speeds.

A 1.5kW AC induction motor connected to a worm gearbox with a ratio of 10:1 and a WEG CFW500 inverter drive was selected. This fitted with the budgetary constraints, torque requirement and preferred control system. An encoder was fitted on the motor to provide feedback to the inverter drive which would adjust the control parameters to maintain accurate control of the rotation speed. The components are visible in Figure 6.2. The final system was capable of delivering 89Nm of torque up to 165rpm at the bearing.

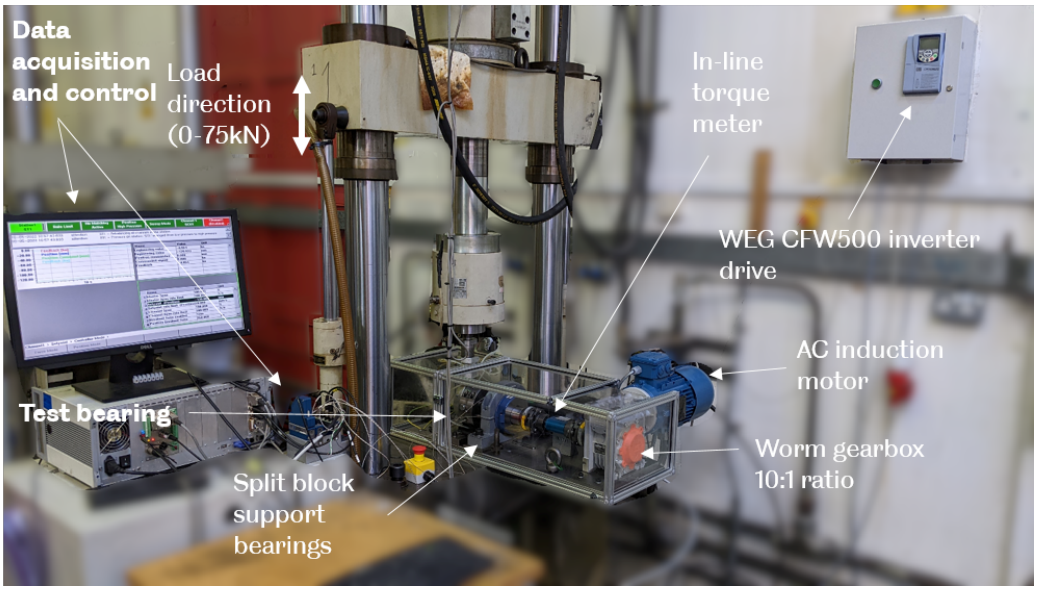

Figure 6.2: Overview of the DiMITRI set-up

6.4 Bearing selection

Automotive con-rod bearing shells were desired as stated in item 4 of the PDS (shown in Section 6.2) because they would be removable, readily available and cheap to replace. A bearing shell with a lubricant inlet hole was chosen because stern tube bearing designs feed lubricant into the bearing with holes in the side of the bearing. Most modern con-rod bearing shells of around 50mm diameter that were identified did not feature a lubricant inlet hole because modern crankshafts are hollow and provide a lubricant pathway from a hole in the shaft instead. As a result, bearing shells which are designed for a 1980's era Volvo TD60 engine were selected because they were still common, close to the desired diameter of 50mm (63mm actual diameter) and featured a lubricant inlet hole. The chosen bearing shells are shown in Figure 6.3.

The bearing shells are made with a steel back which have a three component structure

on top. The structure consists of a cast-on lead-bronze alloy (CuPb23Sn4) which is separated from a galvanic bearing surface layer (PbSn10Cu3) by a nickel dam.

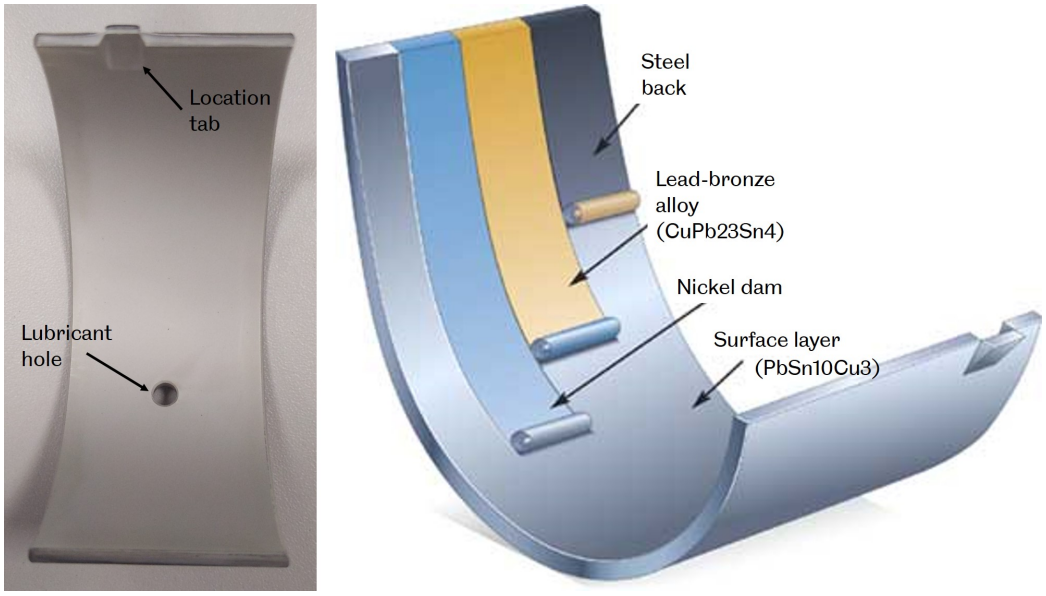

Figure 6.3: TD60 bearing shell. Diameter of 63.5mm and a length of 34mm. Part number: 77 138 600. Computer generated image was adapted from Machinery Lubrication magazine [75].

6.5 Sommerfeld number led design

A Sommerfeld number range of 0.004 to 0.01 was identified in Section **??**. Constraints on the maximum speed and diameter of the bearing were set with the selection of the drive system and bearing shell respectively. A maximum load was estimated given the maximum combustion pressure in the Volvo TD60 engine from which the bearing shell is sourced. This is around 200bar [76]. Given the piston diameter of 98mm, the maximum pressure results in a 150kN load on the 63mm diameter crank shaft which will be supported by the bearing. The shaft would be made with well understood materials (EN47 spring steel) operating under constant environmental conditions (laboratory) where the loads and stresses could be readily determined due to the fact that there would be a load cell on the actuator. Therefore a factor of safety of 2 was appropriate according to the definitions that can be found in engineering design reference books such as that by Pashneh-Tala et al. [77]. Therefore for the DiMITRI shaft an initial approximation of the appropriate maximum load was 75kN.

The effect of the clearance and viscosity over this speed and load range on the Sommerfield number of the bearing was investigated in order to identify the required shaft

diameter and the operating temperature of the rig.

The most repeatable and reliable experiments from the experiments in Chapter 5 which used the Baxter rig occurred when the bearing and lubricant where heated to a temperature above that which it would reach under steady state operation because it was much less complex and cheaper (in terms of the equipment required) to heat the bearing than to cool it. Controlling the temperature was important to increase the repeatability of the experiments and negate any effects from uncontrolled variables such as the thermal expansion on the bearing clearance. Although high temperatures are not necessarily found in normal stern tube bearing operation the difference would theoretically be accounted for by matching the Sommerfeld numbers between DiMITRI and real stern tube operating parameters. It was also useful to heat the lubricant because it would have the affect of decreasing the sensitivity of the Sommerfeld number to changes in load and speed which would increase the level of control over the Sommerfeld number that the bearing operates at. A temperature above 65°C in the Baxter rig was preferable from previous experiments with stern tube EALs.

Given that DiMITRI would operate under higher friction than the Baxter rig a temperature of 80°C was selected as the initial benchmark for DiMITRI. This was thought to be high enough to remove the need for bearing to be cooled, but low enough to prevent the generation of vapours from the lubricant. The sensitivity of the Sommerfeld number to changes in the test parameters in DiMITRI at this temperature was investigated and is shown in Figure 6.4. The viscosity of DE11419 lubricant at 80°C was used because this was the thickest lubricant at that temperature. This meant that if the minimum Sommerfeld could be reached with this lubricant then it would also be achievable with the other lubricants which would have an inherently lower Sommerfeld number because they are thinner under the same conditions.

The clearance specified by the bearing manufacturer for the TD60 engine was 38 microns of radial clearance. This is shown on Figure 6.4a by the blue surface. It shows a steep gradient over the Sommerfeld range of interest (0.004-0.01). Above 100rpm the Sommerfeld number would be above the desired range regardless of the load applied. Therefore a larger clearance would such as 50 or 100 microns would reduce the sensitivity of the Sommerfeld number to the speed and load allowing finer adjustment. This is shown by the comparatively shallower gradients of the yellow and white surfaces on Figures 6.4b and 6.4c.

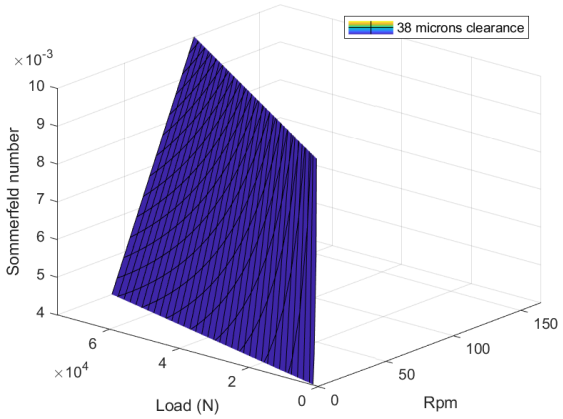

(a) Model of Sommerfeld number at 80°C with DE11419 and 38 micron clearance

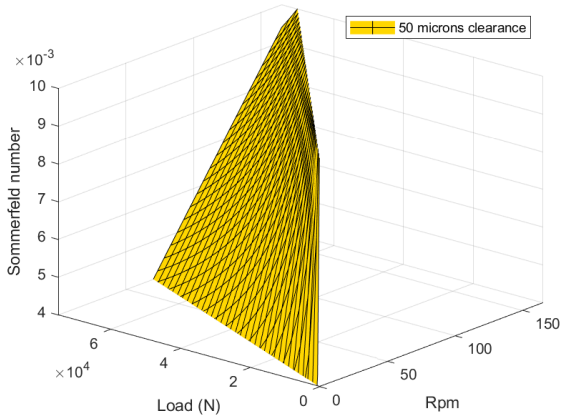

(b) Model of Sommerfeld number at 80°C with DE11419 and 50 micron clearance

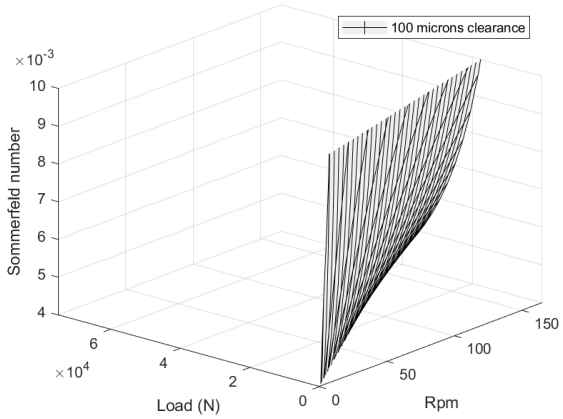

(c) Model of Sommerfeld number at 80°C with DE11419 and 100 micron clearance

Figure 6.4: Model of Sommerfeld number at 80°C with DE11419 with three different bearing clearance values

Since the standard bearing clearance was sub-optimal the effect of using a clearance of 50 microns and 100 microns was further compared using Figure 6.5. This is a two-dimensional view of the surface plots from Figure 6.4 and it shows that a clearance of 50 microns would enable the full range of operating parameters for DiMITRI were exploited to capture data in the desired Sommerfeld number range. The 50 micron desired bearing radial clearance (+/-10 microns) would be specified by controlling the diameter of the bespoke shaft used in DiMITRI.

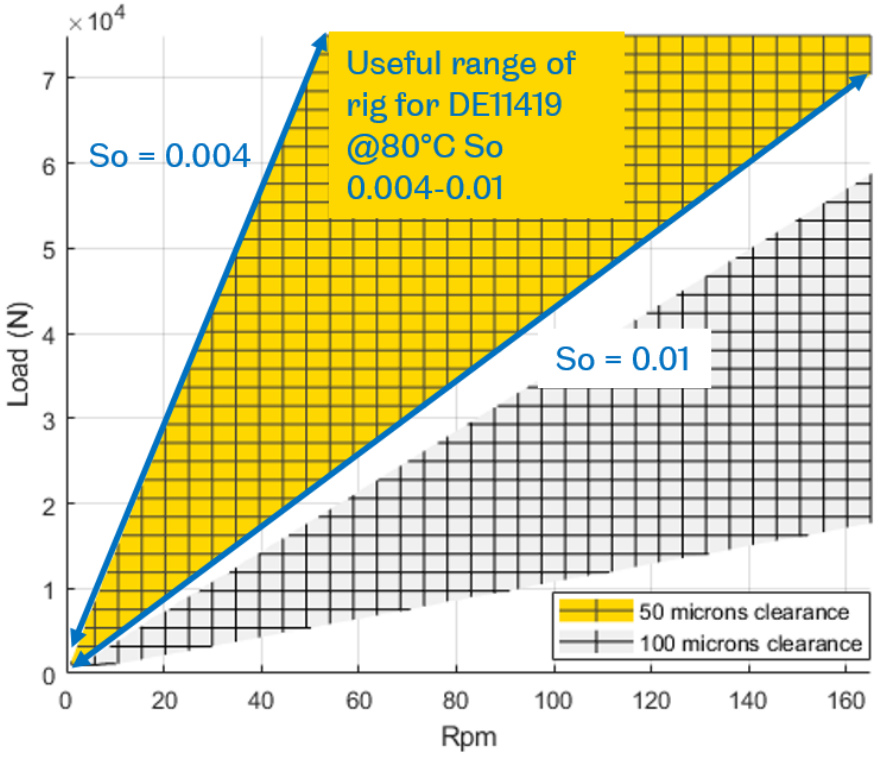

Figure 6.5: Comparison of Sommerfeld number at 80°C with DE11419 with two different bearing clearance values

6.6 Housing design

Three items on the PDS (as per Section 6.2) would affect the housing design: Item 3 which would require temperature control instrumentation to be incorporated into the housing, Item 4 which required easy replacement of the bearing shells and Item 8 which specified the bearing should run with a low volume of lubricant of around 50ml.

Cartridge heaters were specified to heat the housing to 80°C (the target set in Section 6.5) which corresponds to Item 3. The location of these are shown in Figure 6.6. To satisfy Item 4 a split housing was required so that the bearing shells could be inspected and removed without removing the shaft along with split shaft lip seals to retain the lubricant in the bearing housing. To ensure the two parts of the bearing housing were fastened into the same location each time a bearing shell was replaced dowels with an interference fit were employed. The dowel location was asymmetrical about the axis of the bearing to ensure the housing could not be installed the opposite way round, see Figure 6.6. Minimising the lubricant volume as per Item 8 would require

the housing to be as compact as possible. Compactness had the added benefit of reducing the size and weight of the bearing housing so that the parts are easier to handle which compliments Item 4. The final design for the bearing housing which satisfies the PDS is shown in Figures 6.6 and 6.7.

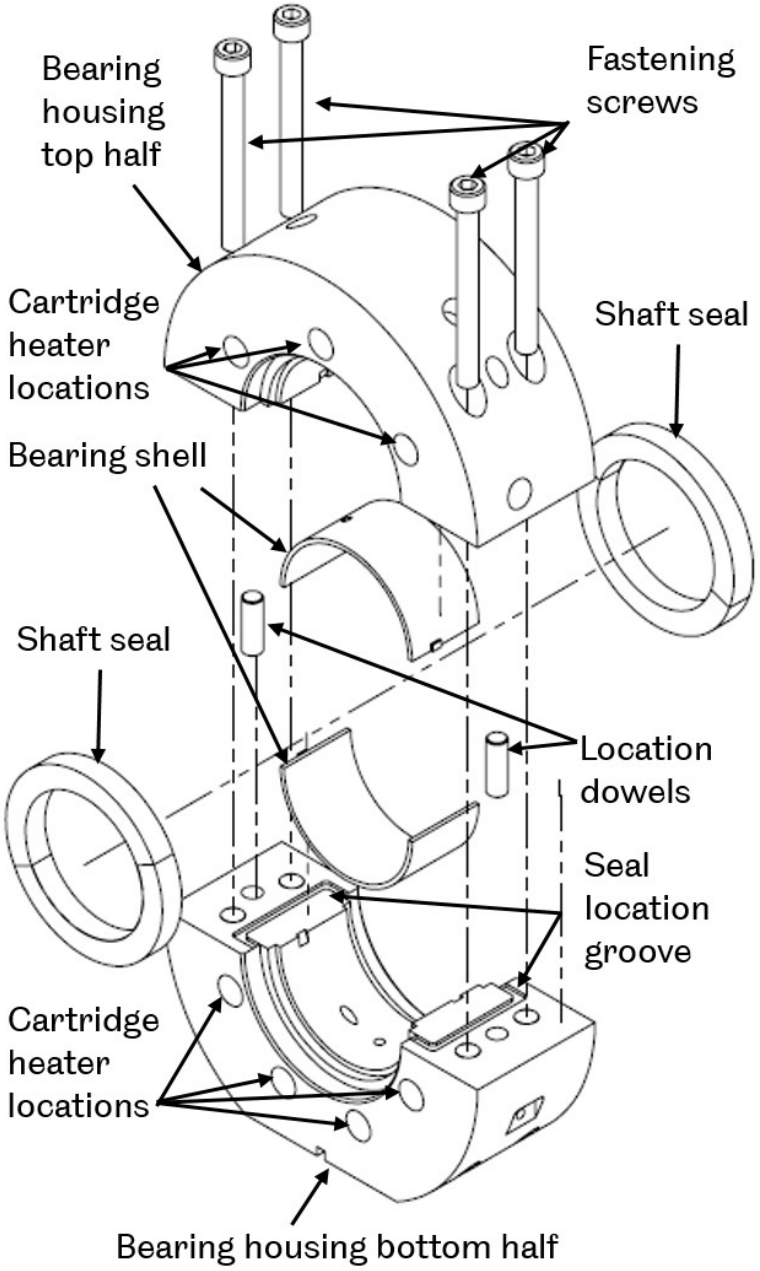

Figure 6.6: Exploded view of the bearing housing and component assembly

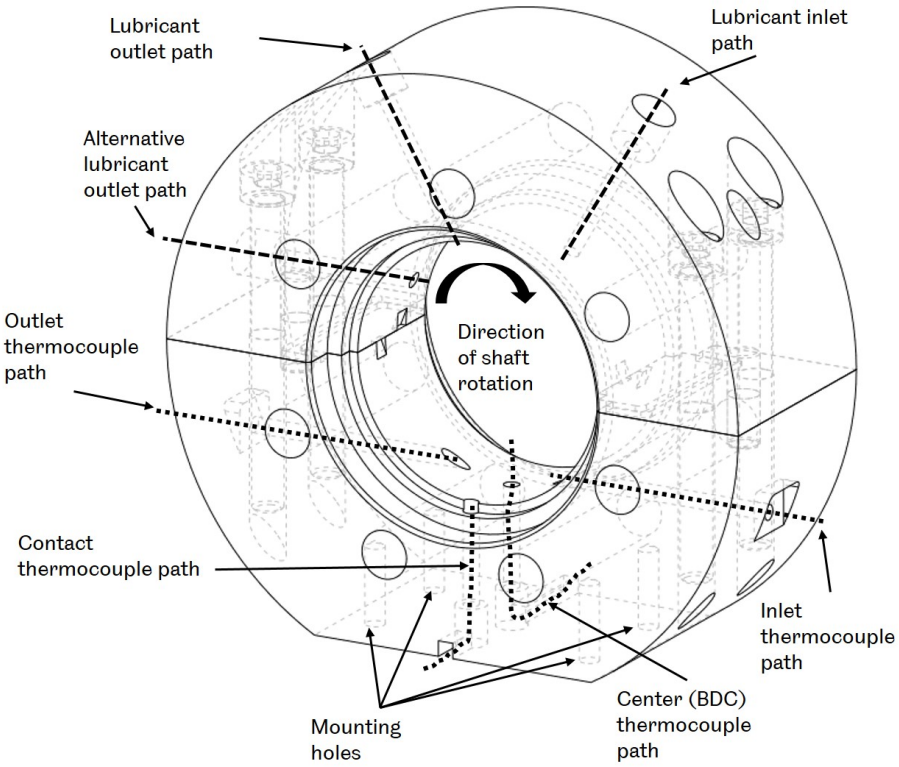

Figure 6.7: Annotated view of the bearing housing

The bearing housing was designed to be flooded with around 50ml of lubricant so that no lubricant circulation system was required. Despite this there are "inlet" and "outlet" sides due to the direction of rotation of the shaft which correspond to where the lubricant would be entrained into the lubricant film area (towards h_0 on Figure 6.8) which supports the bearing, and where the lubricant would be leaving it respectively. The inlet and outlet thermocouples are shown in Figure 6.7. The pathways labelled for lubricant were intended to be blocked once the bearing housing had been filled with the test lubricant but were included in the design to accommodate future experiments and a lubricant delivery module to satisfy Item 2 on the PDS (See Section 6.5).

The bearing housing was instrumented with four thermocouples which are labelled in Figure 6.7. The inlet thermocouple was used as a reference to control the output of the cartridge heaters and the other three for monitoring the lubricant performance. It was preferred because it was exposed directly to the lubricant film because the pathway shown on Figure 6.7 lines up with the existing lubricant hole in the bearing shell, shown in Figure 6.3.

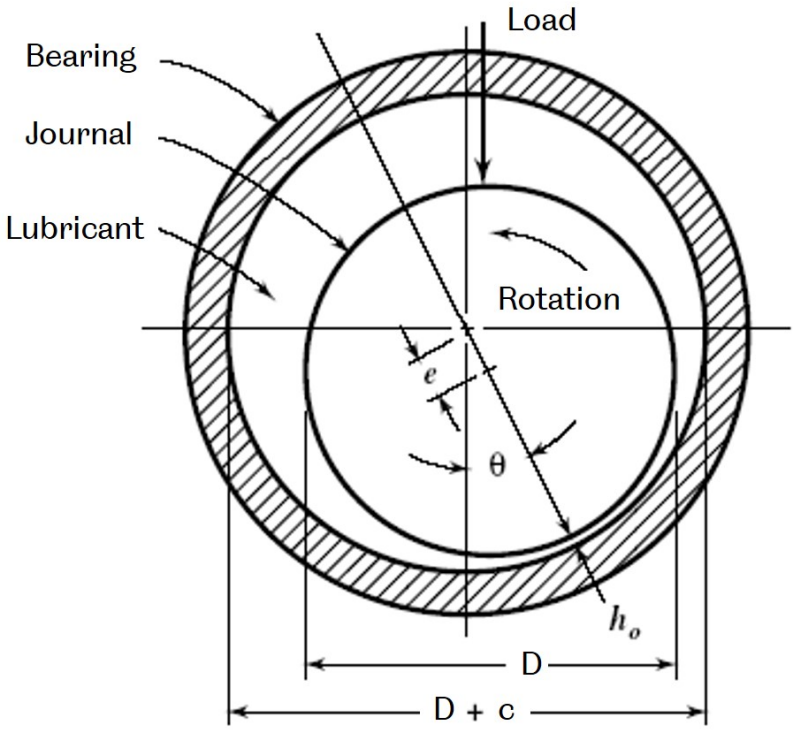

Figure 6.8: Cross-section of a journal bearing with exaggerated clearance for clarity

The contact thermocouple path was located in the highest pressure and temperature region of the lubricant film as closely as possible but without the end of the thermocouple disturbing the lubricant film formation. To do this it was offset from the central axis in the direction of the attitude angle, θ. The attitude angle increases with speed of rotation of the shaft and with decreasing load. DiMITRI would be required to take measurements from a full range of speeds and loads down to zero rotation speed where there would be no attitude angle. Therefore it was decided that the thermocouple hole would be offset so that the edge of the hole was inline with the centre of the bearing. This meant that the thermocouple could cover the minimum film area at the lowest speeds, but also cover a small area in the direction of increasing attitude angle. With this location, the attitude angle of the centre of the contact thermocouple location is 2°.

6.7 Shaft design

The shaft was to be loaded as a cantilever as per Item 7 on the PDS as is listed in Section 6.2. It would be supported by the test bearing and the roller support bearing and loaded on one end with a rod-end bearing as is illustrated in 6.1d. The load

which it was required to support was 75kN as is specified in Section 6.5. Given that this load was within the 100kN estimated maximum load on a hardened steel crank shaft a common shaft steel was selected. The specification chosen was AISI 6150 in its oil quenched and tempered at 540°C form because of its good machinability, high yield stress and high hardness.

The shaft was designed in conjunction with the bearing housing because the maximum stress in the shaft was highly dependent on its length. The more compact the bearing housing, the lower the stress in the shaft and the higher the factor of saftey (FOS). The spacing between the torque meter coupling, support bearing, bearing housing and rod-end also affected the length of the shaft and therefore the maximum stress. Throughout the design process, SOLIDWORKS simulation toolbox was used to conduct finite element analysis (FEA) on the shaft to minimise the stress and maximise the factor of safety of the shaft. The loads and supports modelled on the shaft are shown in Figure 6.9. The torque meter coupling was modelled as a fixed hinge, the support bearing as a roller support and the test bearing as a fixture. The fixture support was specified to allowe vertical movement of the shaft of 50microns which simulated the degree of freedom on the shaft given the test bearing radial clearance.

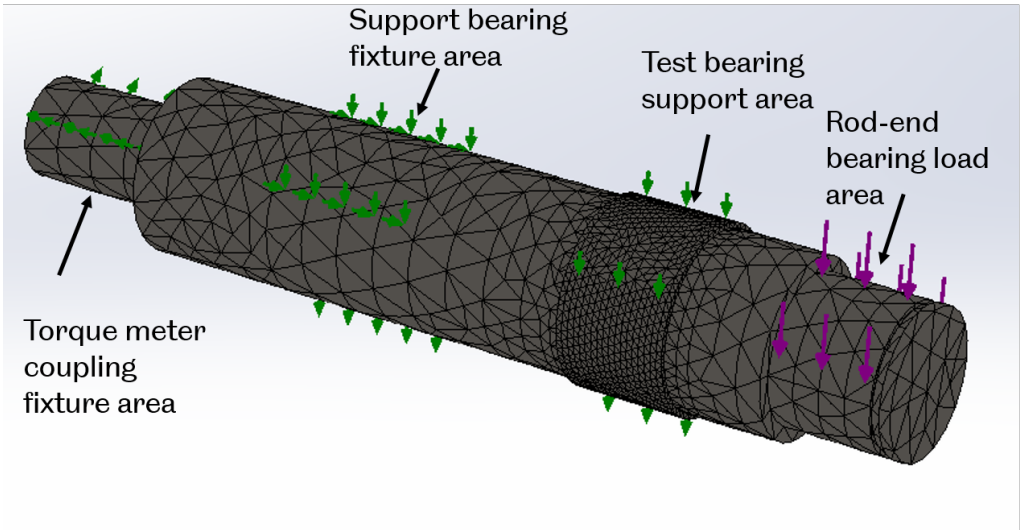

Figure 6.9: Shaft design showing loaded and supported areas with mesh

A mesh was generated on the shaft model and the final iteration of this is shown in Figure 6.9. Mesh independence was found by using a coarse mesh during the first iteration of the simulation and increasing mesh density until the maximum stress result converged to within 5% of the previous result. The regions of maximum stress

occurred in the test bearing support area can be seen in Figure 6.10b, hence this part has a more dense mesh than the rest of the model so that the processing time was optimised without compromising on the accuracy of the end result.

The displacement (Figure 6.10a) was modelled partly to check that the analysis was accurate in predicting the way that the shaft would be expected to deflect. This was in good agreement with the expectations of the author. This increased confidence in the stress analysis which predicted a FOS of 1.5 which is shown in Figure 6.10b.

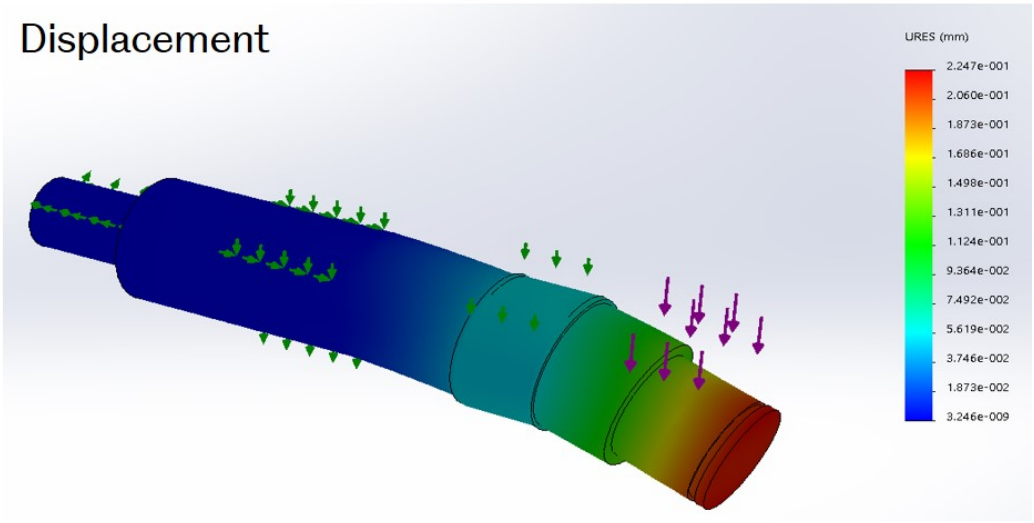

(a) Exaggerated diagram of shaft displacement under a maximum 75kN load

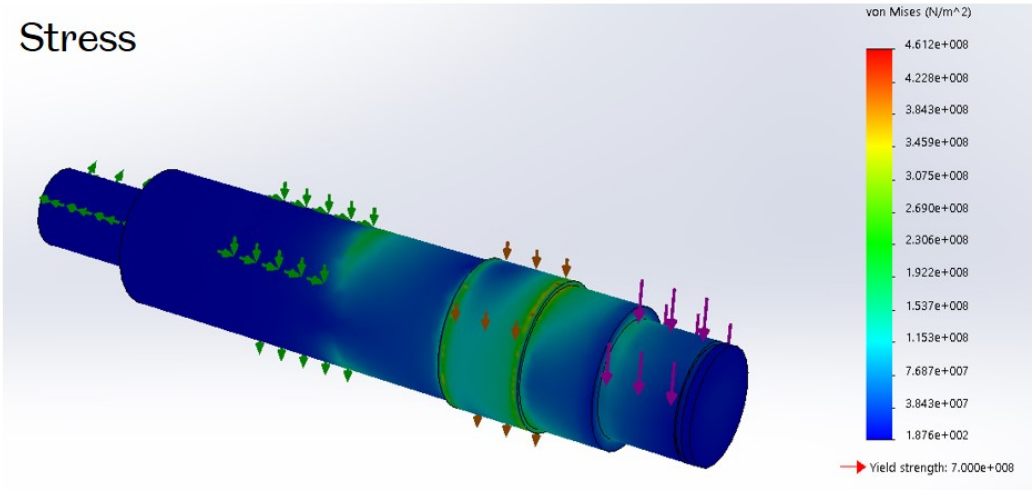

(b) Diagram of shaft stress under a maximum 75kN load

Figure 6.10: Predicted shaft displacement and stress generated using SOLIDWORKS Simulation FEA tool
Shaft design FEA under a 75kN maximum load]Shaft design FEA under a 75kN maximum load

Thermal expansion of the shaft was considered using Equation 6.1, where dl is the change in length of the shaft, L_0 is the original length of the shaft, α is the linear expansion coefficient and t_0 and t_1 are the initial and the final temperature respectively.

$$dl = L_0\alpha(t_1 - t_0) \tag{6.1}$$

The linear expansion coefficient of 12μm/m°C was assumed for the AISI 6150 (oil quenched and tempered at 540°C) shaft material from [78]. A temperature rise for an experiment was assumed to be from 15°C at room temperature to the 80°C set temperature of the rig. Under these conditions it was calculated that the shaft would expand in length by 0.3mm. The shaft would be constrained at the loaded end by the rod-end bearing and the support bearing would be specified to allow for thermal expansion. This meant that any linear expansion due to temperature increases would occur at the torque meter coupling. Therefore the torque meter coupling would be required to allow for at least 0.3mm of axial movement of the shaft.

6.8 Rig Assembly

All of the separate components were assembled onto a steel base plate which was designed to connect to the Schenck 250 test bed with machine screws. It would be lifted on to and off of this test bed using a crane via lifting eyes connected to the base. These features are shown in Figure 6.11. The assembly had to be simple enough to allow the rig to be fitted with future modules and it had to be easy to disassemble so that parts could be cleaned while avoiding having to conduct alignment checks after every reassembly. This was achieved by using a central locating key in the base plate from which the gearbox, support bearing and test bearing were all mounted onto the main base plate using their own individual base plates.

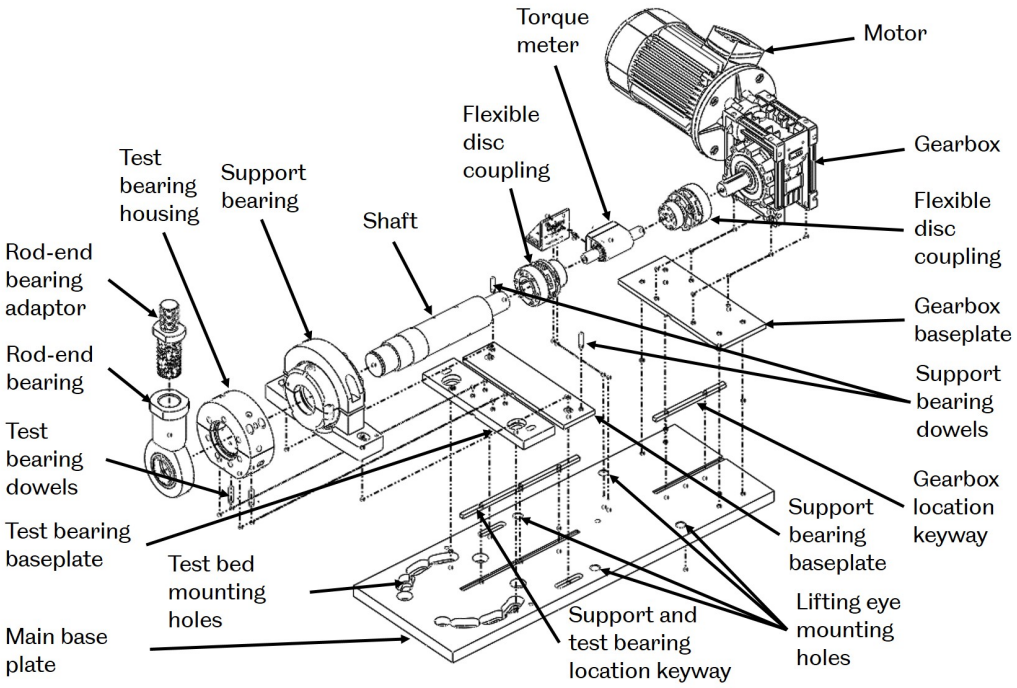

Figure 6.11: Exploded view of DiMITRI assembly

6.8.1 Alignment

An initial assembly of the components without connecting dowels was made in order to check the alignment between the test bearing shaft and gearbox shaft according to the tolerances of the torque meter couplings shown in Table 6.1. These were specified so that they could compensate for the thermal expansion of the shaft and any misalignment between the test bearing shaft and the gearbox shaft.

ROBA-DS Size 16 disc coupling (combined tolerance with two couplings)	**Tolerance**
Angular misalignment (°)	+/-0.7
Axial misalignment (mm)	+/-0.8
Radial misalignment (mm)	+/-2

Table 6.1: Torque meter coupling alignment tolerance

Figure 6.12 shows the method used to check the alignment. A dial gauge was used to measure the position of the test bearing shaft relative to the gearbox shaft which the dial gauge was mounted to. Both shafts were rotated clockwise and the misalignment was measured by reading the displacement of the dial gauge relative to a reference point at 0°. The displacement was measured at 90 °, 180°and 270°.

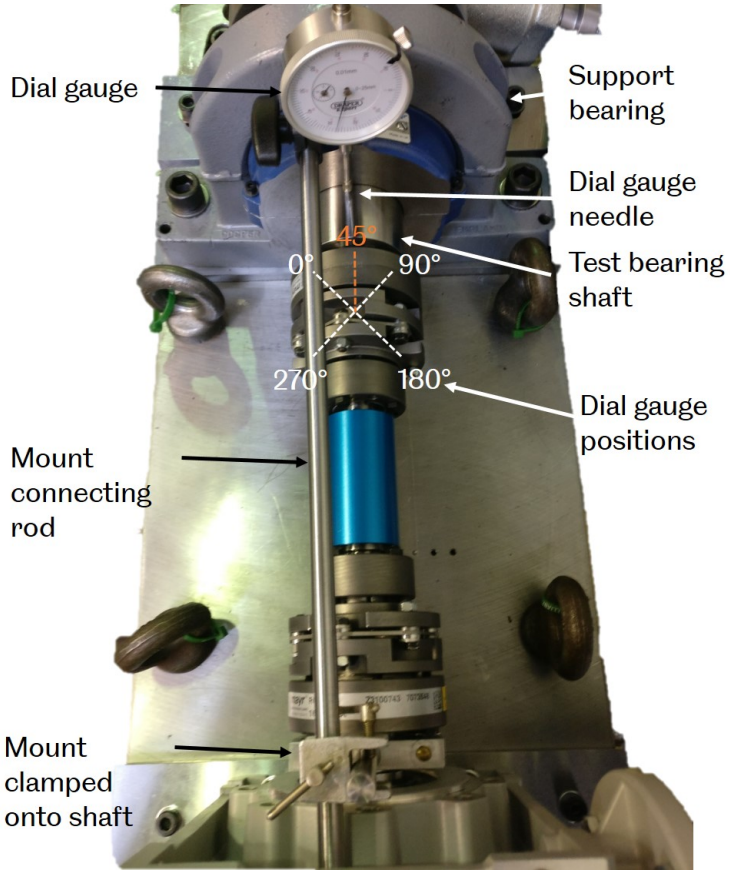

Figure 6.12: Dial gauge shown at approximately the 45°position on DiMITRI during alignment checks

Once the radial alignment was within the tolerance detailed in Table 6.1 the test bearing and test bearing baseplate were removed as a single assembly and the dowel holes were drilled so that they fixed the bearing housing in position relative to its base plate. The smaller tolerance for the dowel holes compared to the mounting screws (+0.006 to +0.015 mm compared to +0.3mm diameter for a standard M8 drilled hole) ensured that reassembly of the bearing housing would reduce the chance of misalignment between the housing and the shaft. The same method was used between the support bearing and the support bearing base plate. The dowels and base plate assemblies are labelled in Figure 6.11.

It became apparent that the radial and angular misalignment between the two shafts on DiMITRI varied depending on the load applied to the test bearing shaft. This was because the support bearing was not constrained as it was assumed it would be in the original design of the rig. This meant that additional measurements with the shaft under load were required to verify that the coupling could be kept within the misalignment tolerances during the experiments.

6.8.2 Misalignment measurement of the test bearing shaft

To measure the radial and angular misalignment caused by the deflection of the test shaft from the horizontal position under the loaded condition a laser displacement sensor was employed (model optoNCDT ILD1320-10). It was positioned above the end of the test bearing shaft which would be connected to the coupling as is shown in Figure 6.13. The distance measured by the sensor between the fixed laser head and the shaft surface (d on Figure 6.13) was used to work out an angular displacement (ψ on Figure 6.13) using trigonometry and Equation 6.2 and a measurement of the horizontal distance between the middle of the support bearing and the free end of the shaft (L on Figure 6.13). It was necessary to assume that the shafts were perfectly aligned when the locating dowels were fixed in place with no load.

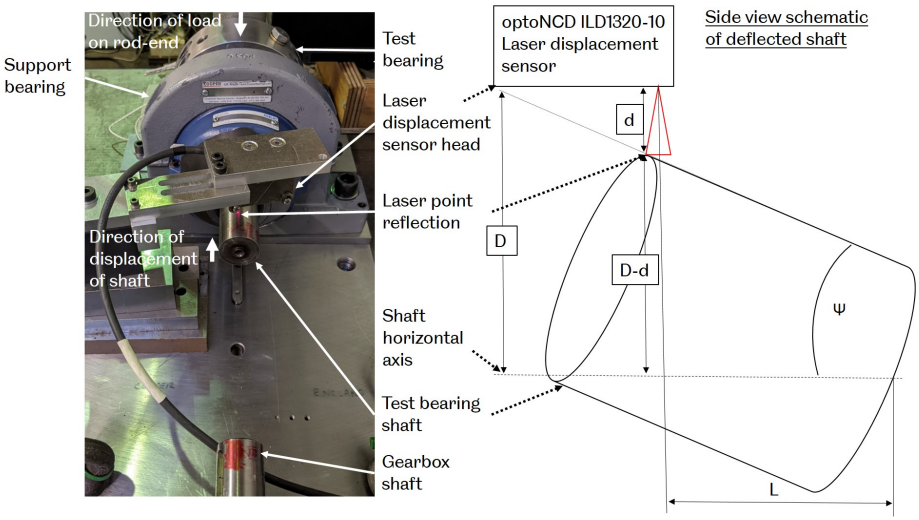

Figure 6.13: Laser displacement sensor set-up used to measure the change in height of the shaft end when under load

$$\psi = \tan^{-1} \frac{D-d}{L} \tag{6.2}$$

Each of the three types of misalignment could be assigned a percentage of the maximum tolerance specified in Table 6.1. The sum of the three percentages must be below 100 according to the manufacturer specifications of the coupling. At 20kN load on Figure 6.14 the displacement of the shaft was 0.44mm. Assuming this was similar to the actual radial misalignment value between the two shafts this was equal to 22% of the maximum 2mm tolerance. Given the 0.3mm axial misalignment from the thermal expansion of the shaft explained in Section 6.7 which is 37.5% of the maximum, the allowable angular misalignment is 40.5% or 0.28°. At 0.44mm displacement under a 20kN load the angular misalignment from the horizontal is 0.25°. Therefore the sum of the tolerances under 20kN load was 95%. Consequently to protect the couplings and the torque meter from damage the maximum permissible load was deemed to be 20kN.

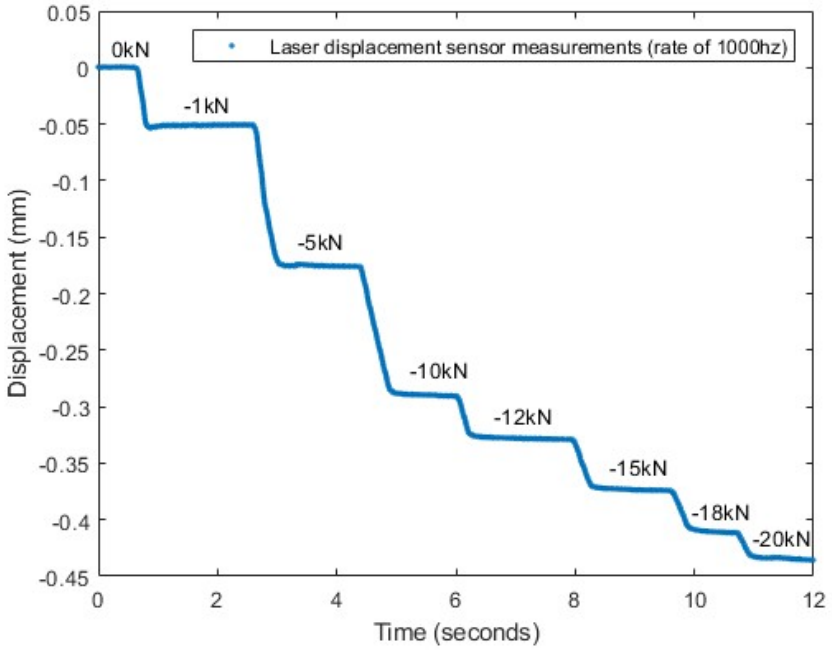

Figure 6.14: Measurement from laser displacement sensor at different loads as set up in Figure 6.13

6.8.3 Clearance measurement

The actual clearance in the bearing was measured by using Plastigauge clearance gauge. It was laid across the axial length of the journal surface which was subsequently assembled with the bearing shells and test bearing housing. Once the housing was fastened together the gauge was crushed between the shaft surface and the bearing shell which left a mark on the shaft. The bearing shell was then removed and the width of the mark left on the shaft was measured and the corresponding measurement was obtained. The mark that was left can be seen in Figure 6.15. The diametrical clearance measured was 0.90mm resulting in a radial clearance of 45 microns. This verified that the assembled rig was within the designed tolerance of 50 microns +/- 10 microns specified in Section 6.5.

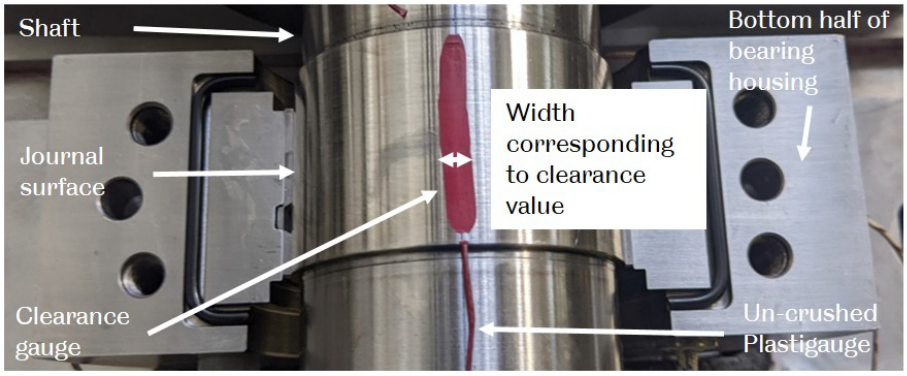

Figure 6.15: Red mark on bottom bearing shell left by the clearance gauge

6.9 Cartridge heater installation

A total of seven cartridge heaters were installed into the test bearing housing which were controlled by an Omega heater controller unit. These each had a maximum output of 250W resulting in the total value quoted in Table 6.2. The final specifications of all of the other instrumentation featured in DiMITRI as it was used in the experiments that follow in Chapter 7 and 8 are also shown in Table 6.2.

Parameter	**Range**	**Measurement device**	**Precision**	**Accuracy**
Shaft rpm	1-165rpm	Rotary encoder	-	+/- 0.35°per rev
Normal load on shaft	0-250kN	Load cell	+/-25N	+/- 0.25kN
Bearing housing BDC, Contact, inlet, outlet temp	-20-350°C	T-type thermocouple	+/- 0.002°C	+/- 1.0°C
Bearing frictional torque	0-100Nm	Non-contact rotary torque sensor	0.002Nm	+/- 0.1Nm
Cartridge heater power	0-1750 W	T-type thermocouple	+/- 0.002°C	+/- 1.0°C

Table 6.2: DiMITRI instrumentation specifications

6.10 Test rig design conclusions

The test rig satisfied Objective 3 of this thesis and would be used to satisfy Objective 4 by examining the friction of lubricants in the mixed regime at a Sommerfeld number range of 0.004 and above. To satisfy the PDS and material constraints the maximum load allowable was 75kN with a speed range of 0 to 165 revolutions per minute. Despite the load rating being reduced to 20kN after rig assembly and manufacture the rig would still meet the above specifications but over a reduced range of operating parameters. The cartridge heaters would allow the bearing housing to be heated to temperatures in excess of the steady state temperature of the oil in order to control the lubricant viscosity. Friction monitoring would be done using an inline torque meter. Thermocouples at the "inlet", "outlet", "BDC" and "contact" would monitor the temperature reached in the bearing. The load would be monitored using existing load cells on the Schenck 250 machine. The final design is included in Appendix B which includes all of the bespoke parts which were designed and manufactured by the author.

Chapter 7

Experimental methodology

7.1 Understanding the temperature viscosity relationship

The temperature viscosity relationship of the lubricants was important to understand since the viscosity of a lubricant directly relates to its film forming properties. The Sommerfeld number, the independent variable in a Stribeck curve, depends on lubricant viscosity. It was measured using the Stabinger viscometer described in section 5.1.1 for each of five lubricants: four of which are EALs and one of which is the Shell Melina mineral oil based lubricant. Further details of these lubricants have been described in the Table 5.4. Ten viscosity measurements were taken between 10°C and 100 °C for each lubricant with the exception of the Mobil SHC Aware EAL for which there were five measurements.

ASTM D341 is the standard method for modelling the viscosity-temperature relationship. Based on a standard model as per the following equations:

$$\log\log(Z) = A - B\log(t) \tag{7.1}$$

where:

$$Z = v + 0.7 + \exp(-1.47 - 1.84v - 0.51v^2) \tag{7.2}$$

and:

$$v = [Z-0.7] - \exp(-0.787 - 3.295[Z-0.7] + 0.6119[Z-0.7]^2 - 0.3193[Z-0.7]^3) \tag{7.3}$$

The standard model is based on two measurements of viscosity, normally taken at 100°C and 40 °C. A Z value for each temperature is calculated using Equation 7.2

and these values are substituted into Equation 7.1 to solve for A and B. To obtain a value for the viscosity at a particular temperature a value of Z at the temperature of interest is obtained with Equation 7.1 and substituted into Equation 7.3.

For this work it was convenient to measure the viscosity of each lubricant at more than two temperatures because most of the time invested into taking measurements was used to initially set up the viscometer for each lubricant. The multiple measurements that were taken allowed a bespoke exponential model to be fitted to the data. This method was more accurate than the ASTM D341 standard because it was based on a greater number of measurements. The bespoke models were fitted to the experimental results using MATLAB Curve Fitter application and were an exponential fit with two terms. This programme uses the non-linear least squares regression model to find an optimal exponential equation to fit the data. In this case a second order exponential equation was specified as the most appropriate model, see Equation 7.4.

$$v = a\exp(bt) + c\exp(dt) \tag{7.4}$$

where a, b, c and d are constants unique to each lubricant.

The bespoke models were most accurate compared to the ASTM D341 method for the EALs than for the Shell Melina lubricant below 20°C. For example, at 10°C the ASTM D341 extrapolation suggests the viscosity of SHC Aware EAL is 418 mm^2s^{-1} where as the viscometer measurement is 450 mm^2s^{-1}, which is a difference of around 7%. This is shown on Figure 7.1. The accuracy of the models for all of the other EALs is represented by the standard deviation of the measurements compared to each model. The bespoke model is generally more accurate at lower temperatures. As the temperature reaches 100°C ASTM D341 appears more accurate for both the EALs and the mineral oil. At 80°C the bespoke model is superior. Since the experiments will be conducted at 80 +/- 5°C the bespoke model was used for the calculation of the Sommerfeld number in the following results. Across the temperature range, Figure 7.1 shows that the ASTM D341 method was generally just as accurate as the bespoke method for the the Shell Melina but the same does not appear to be true for the EALs.

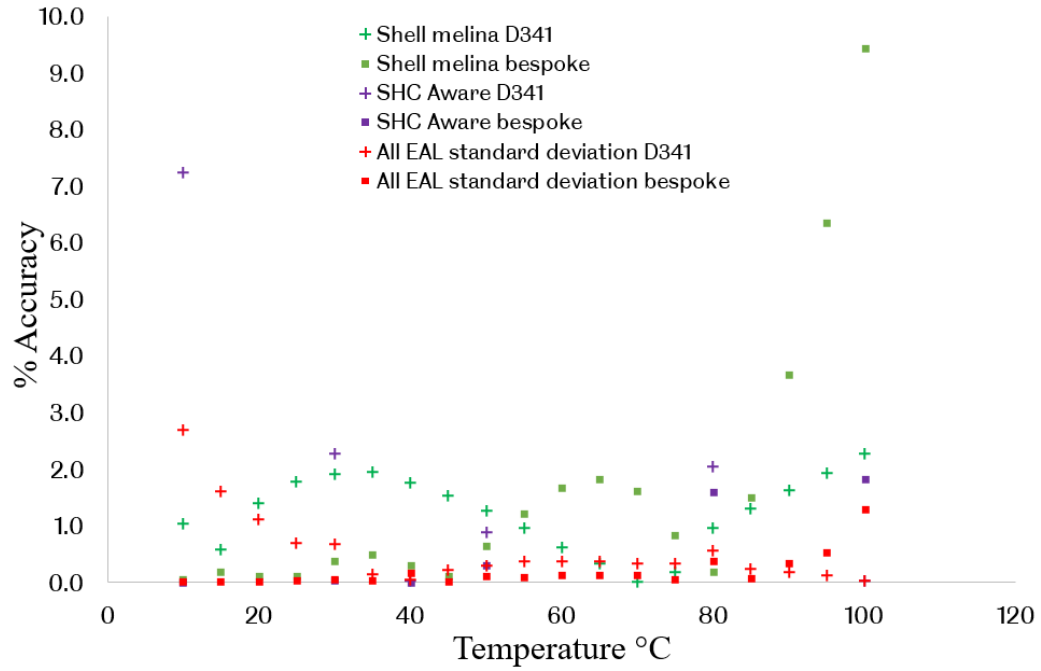

Figure 7.1: Comparison of viscosity model accuracy

The dynamic viscosity measured is shown in Figure 7.2. This clearly shows the increased viscosity of the Shell Melina mineral oil compared to the EALs at temperatures below 35°C and a decreased viscosity at temperatures of above 50°C. Mobil SHC Aware was an additional lubriant that was introduced for the experiments that were conducted using DiMITRI. Its viscosity is very similar to that of DE11419 above 50°C, but below this temperature it does not maintain this relationship due to the high VI. This lubricant appears to have the highest VI of all of the lubricants tested.

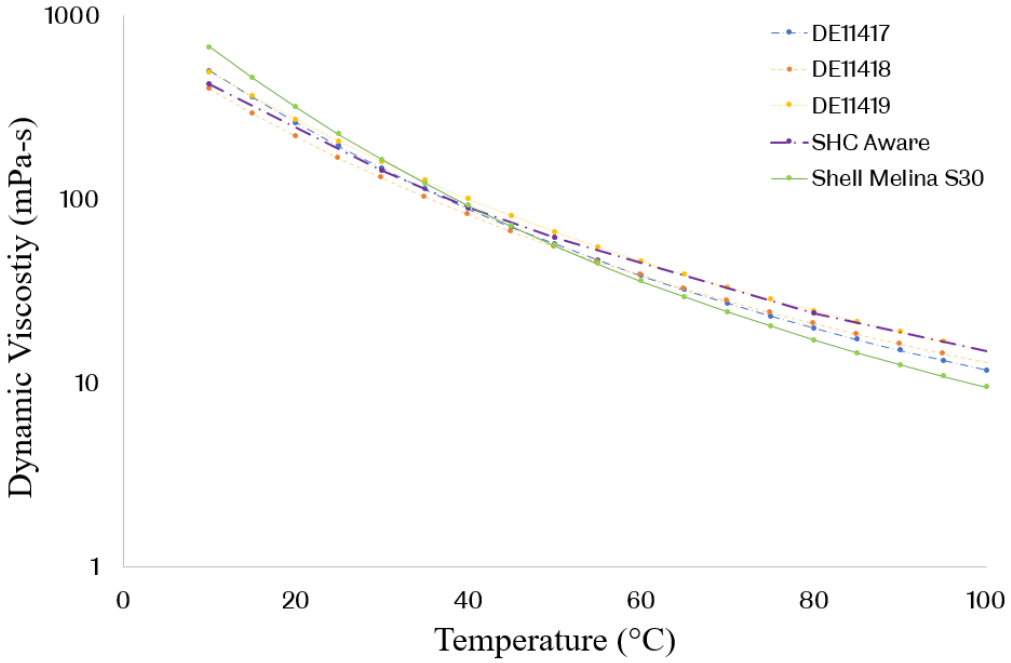

Figure 7.2: Viscosity temperature graph for all tested fresh lubricants

Oxidised oils were also tested and the viscosity temperature relationship of these is shown below in Figure 7.3. These were measured with the same method as the fresh oils but with fewer data points.

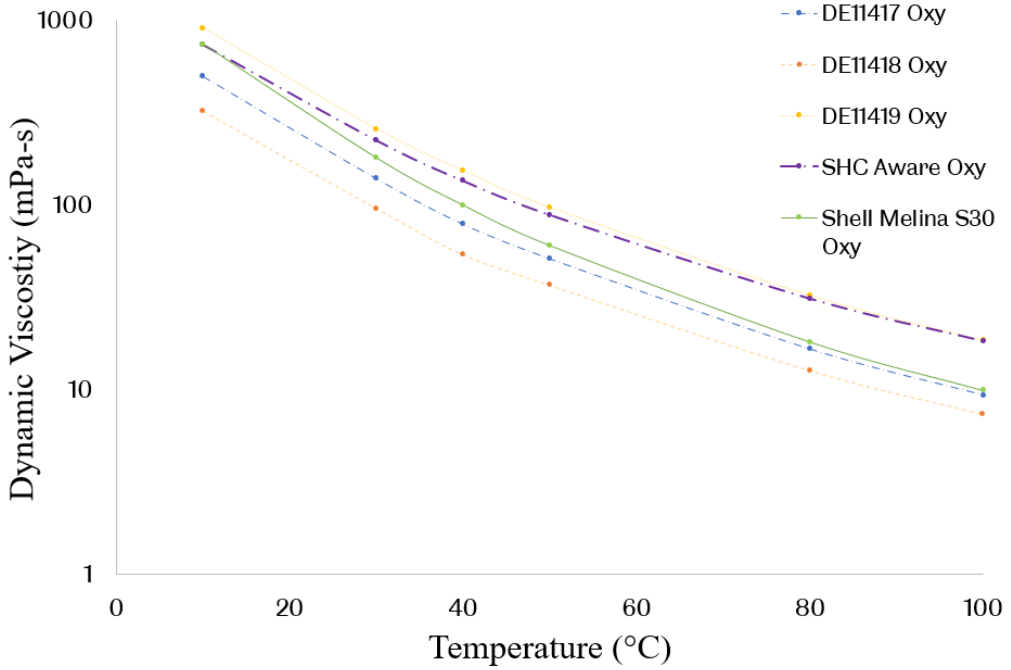

Figure 7.3: Viscosity temperature graph for all tested oxidised lubricants

7.2 Design of experiments (DOE)

While the learning experiments conducted with the Baxter rig gave the author a good idea about how the lubricants would perform in DiMITRI, differences between the two rigs meant that new learning experiments needed to be conducted before the novel experimental work in DiMITRI commenced. Commissioning tests were conducted during construction of DiMITRI to verify measurement equipment and theoretical predictions.

7.2.1 Load parameters

The maximum load permissible on the bearing was 20kN. During commissioning it was found that the wear was very severe above 15kN and the friction was high enough to cause seizure of the bearing at maximum speed. The target Sommerfeld number range was theoretically achievable with the minimum load on DiMITRI of 1kN. At 1kN load with the thickest oil at 80°C (DE11419) the Sommerfeld number range of interest between 0.004 and 0.01 would be achievable by running the rig between 0.6 and 20rpm. Given this short rpm range, the sensitivity of the So number to changes in the rpm would be at its highest and the precision of the measurements would be minimised. This is demonstrated by the 1kN line on Figure 7.4. To increase the sensitivity and maximise the precision of the measurements high loading was theoretically preferable. In practice the high temperatures generated in the rod-end bearing at loads over 10kN limited the number of tests that were achievable before it was too hot to operate reliably and safely. Consequently, Stribeck curves were generated for 1kN, 5kN, 10kN and 15kN with three replicates of each curve at each load, with the exception of 15kN where one measurement was taken because of the limitations in rod-end operating temperature. The 1kN Stribeck Curves were generated using a more gradual ramp (slower acceleration and deceleration) to maximise the number of friction measurements taken and therefore the accuracy. The Sommerfeld number range for each load condition is illustrated in Figure 7.4.

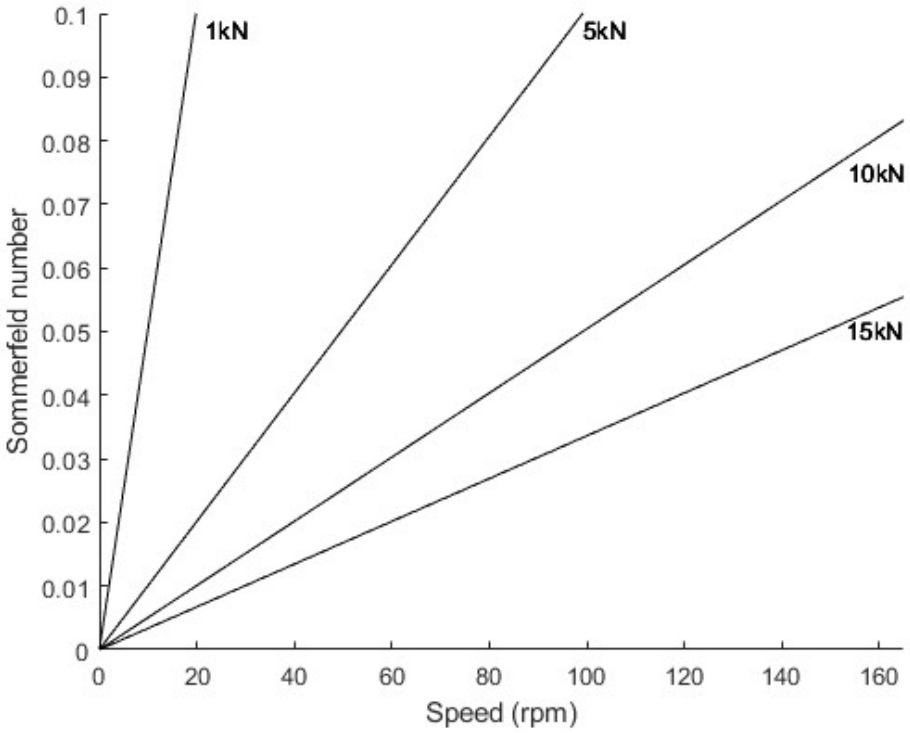

Figure 7.4: Sommerfeld number at different loads for DiMITRI at 80°C using DE11419

The distinct differences between DiMITRI and the Baxter rig meant the following three factors had to be considered:

1. Bearing shell wear
2. Heater control
3. Ancillary bearing friction (the support bearing and rod-end bearing which are part of the rig but not the subject of the experiment).

In the Baxter rig, bearing wear was minimal due to the tests falling into the hydrodynamic lubrication regime but this would not be the case for testing in the mixed lubrication regime in DiMITRI. Furthermore, it was not known how the active heating of the bearing housing would influence the temperature of the lubricant near the contact. Also, the ancillary support bearings, the rod-end bearing and the shaft seals would influence the friction measurement from the torque meter, so quantifying this was necessary to be able to isolate the friction caused by the lubricant.

7.2.2 Bearing shell wear

Bearing shell wear was a new variable factor which was not considered in the Baxter rig testing. This is mainly because the wear was not apparent after initial run-in of the bearing. In DiMITRI, where mixed lubrication was expected, as the bearing shell wears the friction would be influenced by the change in surface roughness, debris particles and an increase in bearing clearance. In service, under the mixed lubrication regime, the automotive journal bearing shells which are used in DiMITRI would quickly become worn to the point of being unusable. The severity of the wear using these bearings in combination with the test lubricants in DiMITRI was important to understand before designing the experiments. It was also necessary to decide how the bearing shell changes would be controlled so that the impact of this variable on the measurement of the lubricant friction was minimised. The options considered are shown in Table 7.1.

Option	**Advantages**	**Disadvantages**
1. Use the same bearings for all tests and monitor the wear.	Time efficient. Most comparable conditions provided wear is not severe.	Severe wear likely, causing debris and reduced comparability.
2. New bearing for each lubricant test.	Maximum comparability between test sets. Can compare anti-wear performance of each lubricant.	Run in phase will occur during testing.
3. Use a run-in bearing for each lubricant.	Repeatability of tests is maximised.	Most time consuming. Only relevant if wear during testing is not severe.

Table 7.1: Possible bearing shell operating methods

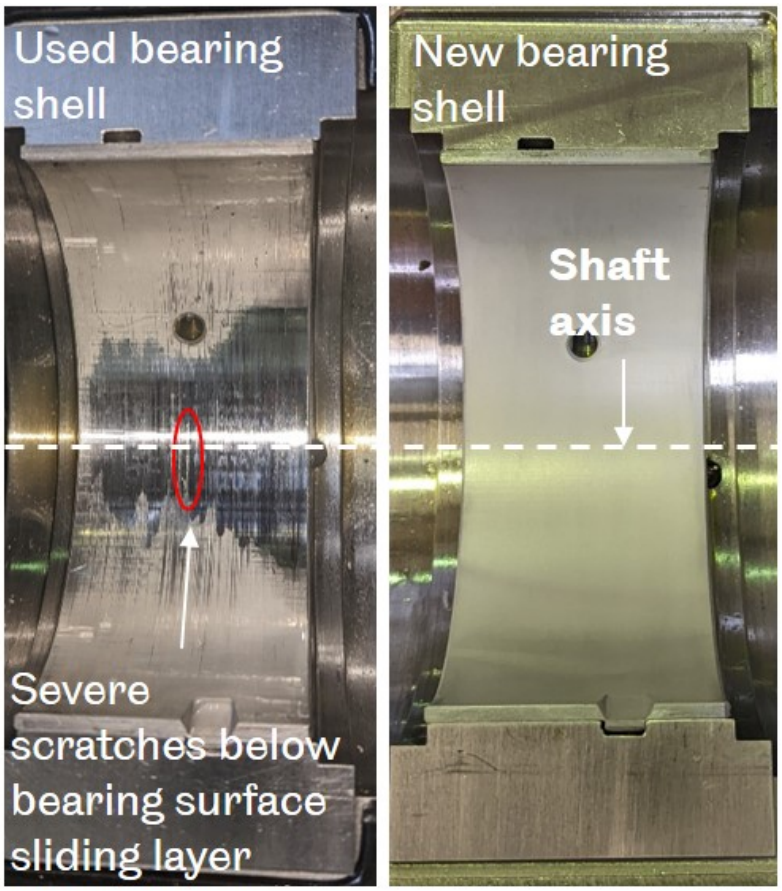

Figure 7.5: DiMITRI bearing shell number 1 (left), number 2 (right). Both bearings are imaged as they were before the learning experiments.

The used bearing in Figure 7.5 was photographed as it was found after it had been used during commissioning of the DiMITRI rig and had been used in a complete set of tests with Shell Melina S30 as the lubricant. This had been through a range of conditions from the highest to the lowest loads and the highest to the lowest speeds which DiMITRI was capable of. It was clearly worn past what would be considered serviceable wear. This is evident in Figure 7.5 where grooves can be seen showing that the top sliding layer of the bearing material had been worn away.

It was clear that option one in Table 7.1 was not favourable because of the severe wear evident in Figure 7.5. This is indicated by the scratches which are duller in appearance than the shinier "polished" area. The wear is similar to that seen in a real stern tube bearing such as in Figure 4.1 in Section 4.3.

Wear from the testing would cause cumulative damage which would alter the clearance and surface roughness of the bearing significantly. Option three was also not

feasible because the severe wear. The main theoretical advantage of starting with a run-in bearing would be a reduced variability due to wear particles disrupting the friction measurement. This would not be realised in reality because the wear rate was clearly significant regardless of whether the bearing was run-in. Option two would provide a consistent starting point (fresh bearing) meaning the bearing wear would be the most comparable between each set of tests (per lubricant) and therefore the fairest comparison between the lubricant performance. Furthermore, each test would theoretically begin with similar surface characteristics in the as new state.

7.2.3 Heater control

The temperature of 80°C which was specified in Section 6.5 was controlled using a heater controller equipped with automatic PID control of the heater output relative to a thermocouple reference temperature, see Figure 7.6. The unit was tuned by operating the rig in both a run up and a run down test under a light load. These conditions were selected because they were the most transient conditions. This was because the heat input rate into the lubricant would change with changing speed and because the lightest loads would reduce the heat input from bearing friction, meaning the heaters would require a higher output to maintain the relatively high set temperature.

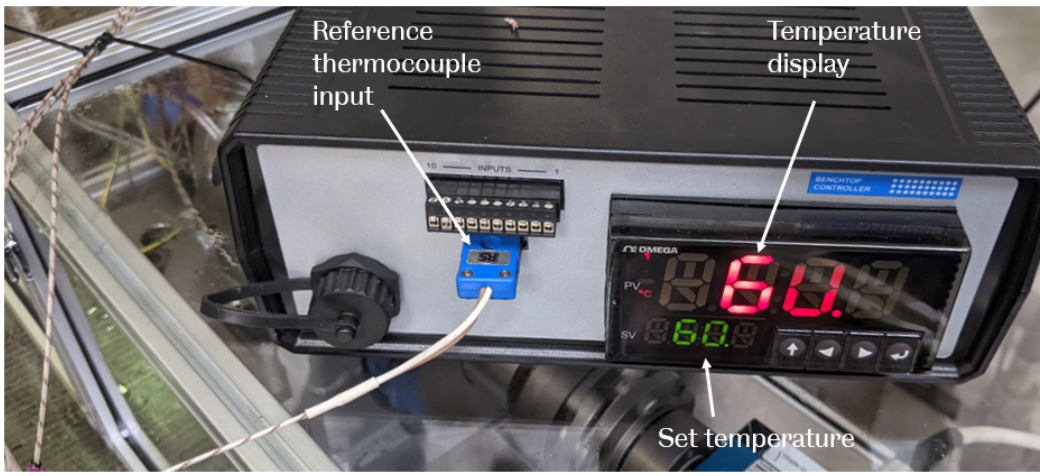

Figure 7.6: Photo of heater controller

Of the four thermocouples in the bearing housing the one which was used as the heater controller reference was the thermocouple nearest to where the lubricant was entrained into the bearing known as the “inlet thermocouple”. The“contact” thermocouple was so called because it was nearest to the minimum film thickness location out of any of

the other thermocouples. Its location is explained in more detail in Section 6.6. This was originally thought to be the most appropriate reference temperature because the friction measured at the transition between the mixed and the hydrodynamic regime would be most influenced by the temperature of the lubricant in this region. However, during commissioning it was found that the heater controller was not responsive enough to maintain a steady temperature as the bearing neared the mixed lubrication regime. This was because of the delay of the heat transfer from the heater into the bearing and through to the lubricant. Once the inlet thermocouple was used instead, this temperature change measured by the "contact" thermocouple could be observed and was considered a useful measurement in characterising the performance of the lubricants. An example shown in Figure 7.12 shows a distinct temperature drop of this thermocouple measurement which was not mirrored by thermocouples at different locations. This drop occurs as the bearing is slowing down from approximately 30rpm to 0rpm under a constant load of 5kN. The torque can be seen to be increasing which is caused by increased friction in the bearing as it slow which is characteristic of mixed lubrication. This is likely due to cavitation in the lubricant which insulates the thermocouple and reduces the heat transfer.

7.2.4 Ancillary Bearing Friction

The friction measurement from the torque meter on DiMITRI will include the friction generated in the support bearing, test bearing and rod-end bearing. To isolate the friction generated in the test bearing by the test lubricant the friction generated at the rod-end and the support bearing had to be understood separately.

The support bearing is a split roller bearing with a cage supporting the rollers. An estimate for the roller bearing "frictional torque" (torque required to overcome the bearing friction), T_f, was calculated based on a model using Equations 7.6 and 7.7 substituted into Equation 7.5 from [79], where T_0 and T_1 are the frictional torque dependent on bearing rpm and bearing normal load respectively.

$$T_f = T_0 + T_1 \tag{7.5}$$

$$T_0 = f_0(vn)^{2/3} \times d_m^3 \times 1 \times 10^{-7} \tag{7.6}$$

$$T_1 = f_1 F d_m \tag{7.7}$$

The change in frictional torque for all of the test conditions with DiMITRI are shown in Figures 7.7 and 7.8. The maximum frictional torque generated by the support

bearing was predicted to be approximately two orders of magnitude smaller than the overall measured friction. Changes in the frictional torque due to speed were even less significant to the point of negligibility, hence a single value for the frictional torque and coefficient of friction was carried forward into Table 7.2 for each load. This was based on the frictional torque and friction coefficient at 0rpm plus half of the range of values for each load line on Figures 7.7 and 7.8.

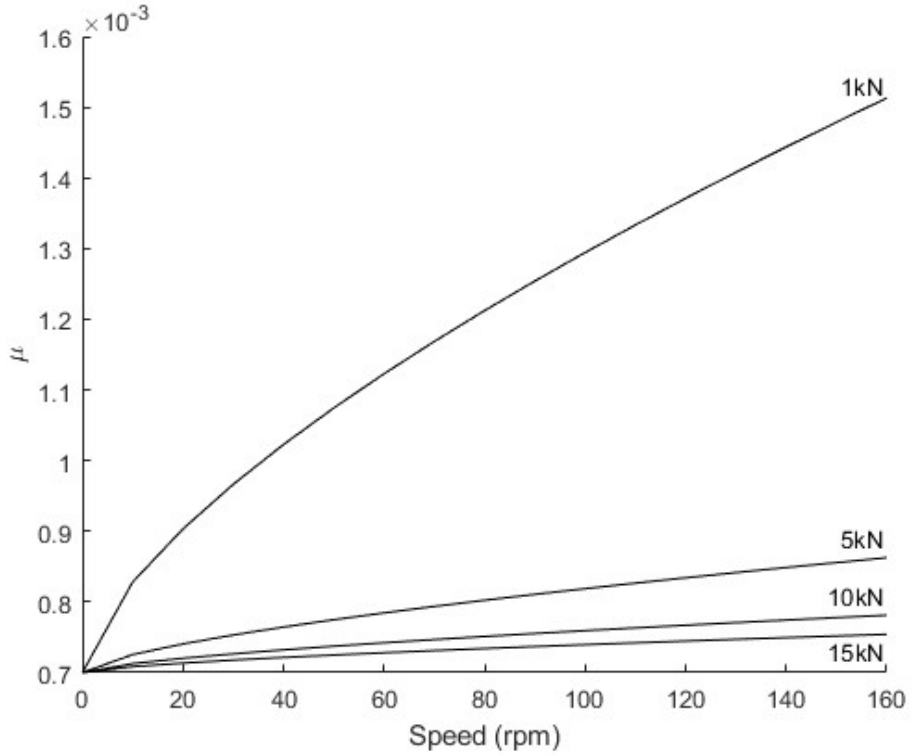

Figure 7.7: DiMITRI support bearing friction coefficient for all loads and speeds (note the y-axis scale)

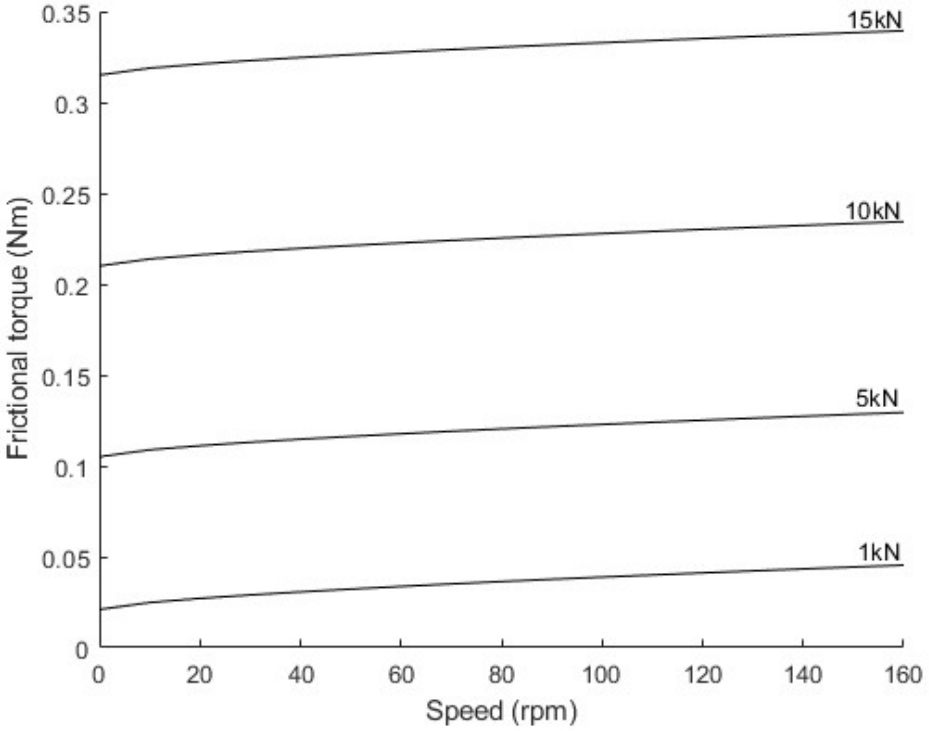

Figure 7.8: DiMITRI support bearing friction torque for all loads and speeds

The rod-end bearing friction was more significant because it is a sliding bearing as opposed to a roller bearing. For the steel-steel sliding pair with the recommended grease (Lithium soap base high pressure grease with extreme pressure additives), the manufacturer (Shaeffler) quoted a friction coefficient of between 0.08 and 0.22. This is dependent on load, speed and temperature. An increase in the temperature or load would result in a decrease in friction to a minimum according to the manufacturer specifications. The friction from sliding converges to a near constant friction coefficient for a relatively slow sliding speed. These relationships for the rod-end bearing are shown in Figure 7.9.

The rod-end bearing is primarily designed for articulation and partial rotation so the surface speed of the bearing on DiMITRI will be relatively high. It also reaches high temperatures in operation in DiMITRI of the of around 80°C which is high given the specified operating temperature range of -30°C to 130°C. Equation 5.4 based on the normal load and the diameter of the bearing was used to calculate the predicted frictional torque for each load which is quoted in Table 7.2.

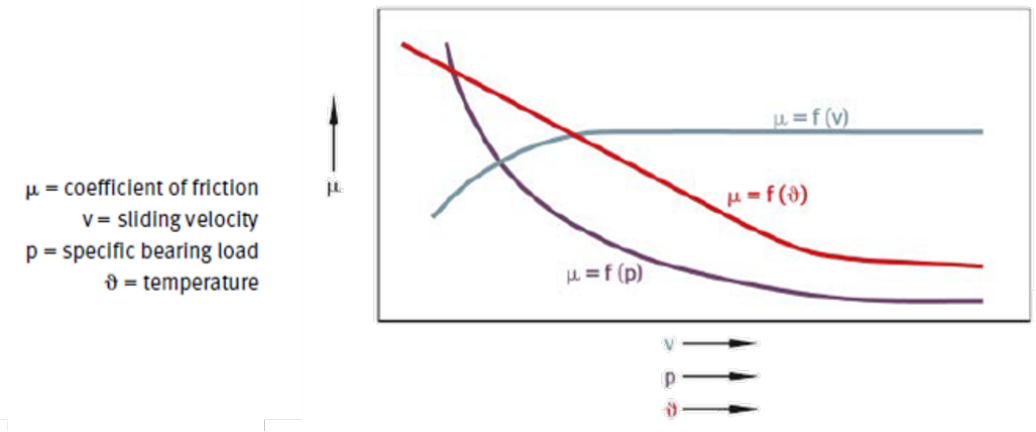

Figure 7.9: Rod-end bearing friction characteristic from Schaeffler manual [80]

Bearing	Load (kN)	Frictional Torque (Nm)	μ
Support bearing	1	0	0.0011
	5	0.1	0.0008
	10	0.2	0.0007
	15	0.3	0.0007
Rod-end bearing	1	2.0 - 5.5	0.08-0.22
	5	10 - 27.5	0.08-0.22
	10	20 - 55.0	0.08-0.22
	15	30 - 82.5	0.08-0.22

Table 7.2: Ancillary bearing friction contribution

Measurement of the ancillary bearing friction by isolating each bearing under the test conditions was considered. However it was not safe to load each bearing individually without risk of damaging the shaft or torque meter. The friction model and predictions used for the ancillary bearing were based on simple assumptions and the relative effect of the different test conditions in terms of temperature load and speed were better understood due to the models used. The absolute value of the test bearing friction is dependent on the accuracy of the predicted ancillary bearing friction, however the inflection point on the Stribeck curve is not dependent on this. A relative comparison between each lubricant was still possible even if the absolute value is not necessarily comparable with external data. Importantly the inflection point between mixed and hydrodynamic lubrication is not effected by the ancillary bearings. The rod-end bearing is permanently in a mixed/boundary lubrication regime by design and the roller support bearing is in the elastohydrodynamic regime with relativley steady friction for all conditions as is shown in Figure 7.7. Roller bearings in general do not operate over the inflection point as is explained by Nicholas et al. [81].

7.2.5 Test matrix

The test matrix for the fresh oil tests in DiMITRI was created based on the limitations found during commissioning and project time constraints. Stribeck curves characterising each of the five lubricants stated in Table 5.4 were obtained for each of the loads shown in Figure 7.4 across the full speed 0-165rpm speed range of the rig. A full set of tests was conducted for each lubricant before it was changed for the next lubricant which included a ramp up the shaft rotational speed to 165rpm and a ramp down to 0rpm under the load specified. For the 1kN tests the ramps were completed at a rate of 0.5rpm per second acceleration/deceleration and for all other tests this was 2.5rpm per second. For each set of lubricant tests the matrix was randomised with the exception of the 15kN test which was always conducted last because the rod-end bearing would overheat after this test. The order in which the lubricants was tested was also randomised. An example test matrix for Shell Melina S30 is shown in Table 7.3.

Lubricant	Load (kN)	Run up and run down
Shell Melina S30	5	Complete
	1	Complete
	10	Complete
	10	Complete
	1	Complete
	5	Complete
	1	Complete
	10	Complete
	5	Complete
	15	Run down only

Table 7.3: Example test matrix, randomised for each lubricant

7.3 Pressure-viscosity effect modelling

As was highlighted in the literature review, the pressure-viscosity coefficient of EALs has been under scrutiny and it has been suggested that this could lead to lubricant film collapse sooner than with mineral oil based lubricants. Given the 15kN maximum load tested in DiMITRI and the dimensions of the bearing, the projected pressure reaches a maximum of 7MPa. The maximum projected pressure expected from a stern tube bearing would be less than 1MPa, see Section 4.3. As discussed in the literature review, Chapter 4, in order for the damage to occur to the white metal layer the stress would need to exceed 40MPa.

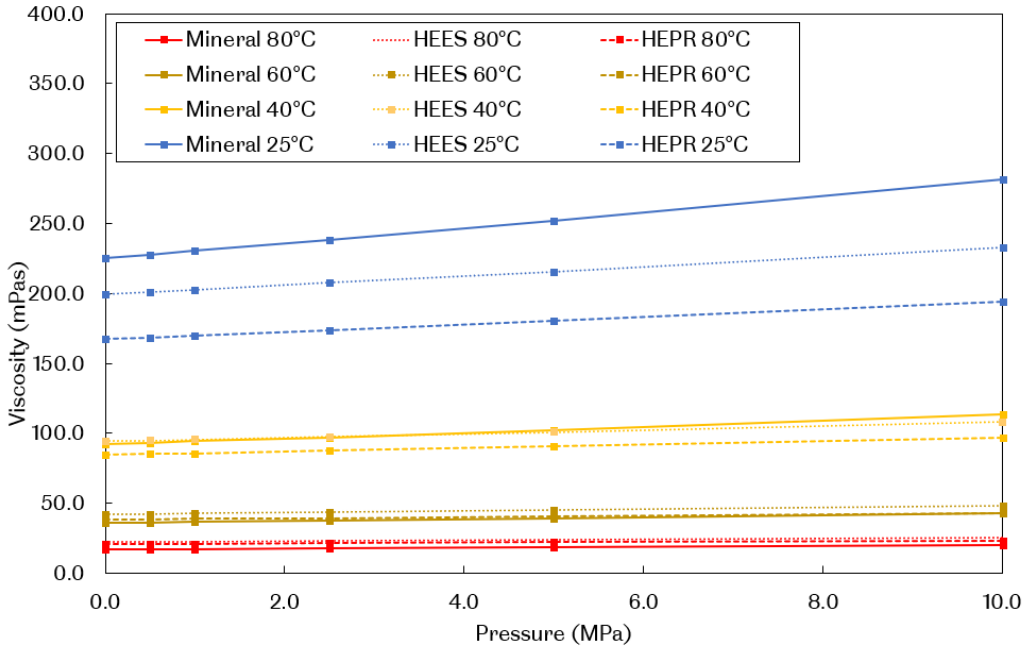

Figure 7.10: Effect of pressure-viscosity coefficient under stern tube conditions

Pressure-viscosity coefficients at the pressures and temperatures appropriate for stern tube applications can be seen in the literature [82–84] and the Barus equation, Equation 2.1, has been employed to quantify the change in viscosity expected. Its effect on lubricant film collapse by considering how it would effect the Sommerfeld number at the inflection point could then be understood. Figure 7.10 shows the viscosity change of three different lubricant categories which are used in stern tubes over a relevant pressure and temperature range.

The pressure-viscosity coefficients used for this work can be found in the work of Erik Höglund [83]. The value for the mineral oil based lubricant was quoted as an equal mix of naphthenic oil and paraffinic mineral oil. The HEES is the trimethylolpropane (TMP) ester and the HEPR is simply quoted as HEPR. This data was checked with similar data from other sources ([84],[82],[42]) and was in close agreement. The data from the single source was used to minimise errors from the use of slightly different measurement methods of different authors.

Figure 7.10 shows that at 60°C and above both the EAL types are thicker, regardless of the pressure. At 40°C HEPR is thinner than the other lubricant types and at 25°C the mineral oil lubricant would be thicker. The effect of pressure in the range expected is negligible at 40°C and above as the gradient of all lines are close to zero.

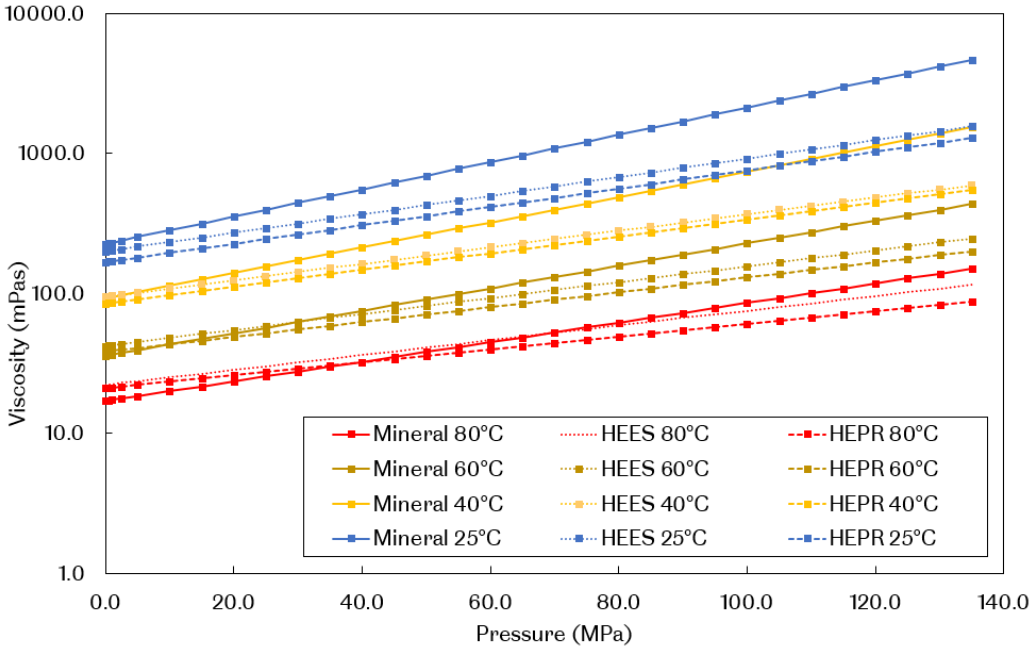

Figure 7.11: Effect of pressure-viscosity coefficient under stern tube conditions for a higher pressure range

At 25°C the mineral oil thickens the most significantly from 225mPas to 281mPas which is a 25% increase from 0 to 10MPa.

Below 40°C the lubricant viscosity is more dependent on pressure-viscosity coefficent especially for the mineral oil lubricant. By reading from Figure 7.10 it can be calculated that the HEES and HEPR lubricants would both increase in viscosity by 16% to the nearest 1% from 0 to 10MPa. If the viscosity of the lubricants was adjusted so that they were all the same under atmospheric pressure at 25°C the difference between the viscosity of the EALs and the viscosity of the mineral oil would be 9%.

Figure 7.11 shows that contact pressures of 70MPa and above would be required before the viscosity of mineral oils is higher than the EALs at all temperatures. The bearing material has a compressive strength of 40MPa so damage would occur before this point was reached if these pressures were apparent.

In terms of the Sommerfeld number inflection point on a Stribeck curve, a higher viscosity clearly means a higher Sommerfeld number at the inflection point. The effect of the 9% increase in viscosity is a worst case given that 10MPa is an order of magnitude higher than the expected stern tube lubricant pressure. However, assuming this could be the case it would result in a 9% difference in the Sommerfeld number

at the inflection point. Assuming that the rest of the variables such as load were constant the rotational speed at the inflection point would also be 9% higher.

The effect of the pressure-viscosity coefficient in the most extreme case, at low temperature and with 10MPa of pressure will be considered in the context of the results in Chapter 8, section 8.4.

7.4 Data processing methodology

During the commissioning of DiMITRI tests were conducted to check the data that was being collected. They were also used to determine the best method with which to process the results into useful graphics. National Instruments FlexLogger software was used to record all of the data inputs into Technical Data Management Streaming (TDMS) file formats which were then loaded into matlab where a bespoke processing script was developed and utilised.

For each test the TDMS file contained temperature readings from all four thermocouples taken at a rate of 1Hz. The sample rate from the encoder was 100Hz and the load and torque readings were measured at a rate of 1000Hz. All of the information that was recorded for each test is visualised on Figure 7.12 which was generated using LabView's built in TDMS file viewer function.

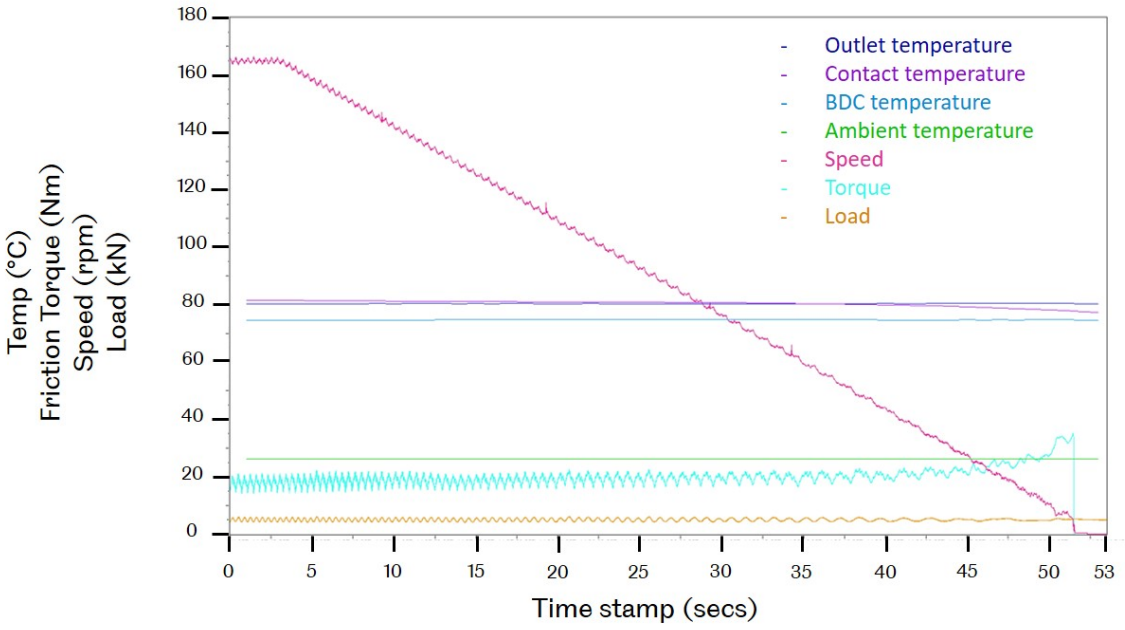

Figure 7.12: Example of tdms file data after each test. Example shown is a 5kN run-down test.

MATLAB was used to generate Stribeck curves from the torque, load and temperature data and to check the measurements for their general features and patterns. The torque and load measurements were used to calculate the value of μ for every data point. The Sommerfeld number calculation depended on the load, speed and temperature measurements. The temperature of the contact thermocouple was used to look up the value of the viscosity at each data point from the model in section 7.1. Given the bearing clearance of 0.90mm (0.45mm radial clearance) measured using the method explained in Section a value for Sommerfeld number was calculated for each frictional torque measurement which takes into account the measured load, speed and temperature at each point in time. A process flow diagram illustrates the procedure used in Figure 7.13.

The temperature plot (plot 2 on Figure 7.13) was checked to make sure the temperature was steadily controlled at 80°C for the outlet, contact and BDC thermocouples. It was also checked for temperature spikes or drops. An example is shown in Figure 7.14.

The temperature drop in Figure 7.14 was characteristic of this lubricant and the temperature control of all of the tests was maintained within 5°C of the 80°C target although some lubricants did not display a drop in temperature.

The torque plot (number 3 on Figure 7.13) shown in Figure 7.15 shows increased variation as the torque begins to rise. This rise is due to the rotation of the shaft slowing down, as is shown in the speed trace Figure 7.17, and moving into the mixed lubrication regime. The contact between the shaft and bearing surface causes torque spikes due to the energy required to deform and remove parts the bearing surface as it wears.

The load plot (number 4 on Figure 7.13) shown in Figure 7.16 displays the load measurement when the Schenk actuator was set to maintain a constant value of 1kN. The spike at the end in of the second test coincides with the bearing coming to a stop, which in this case caused a reaction force up into the rod-end which was attached to the load cell shown by the orange spike. It shows the load was kept with an accuracy of +/- 0.5kN. This is typical of all of the tests carried out.

The speed plot in Figure 7.17 (number 5 on Figure 7.13) shows the steady deceleration of the shaft before coming to a stop just before it reached zero rpm. This was typical as it had reached the limits of the maximum torque from the motor.

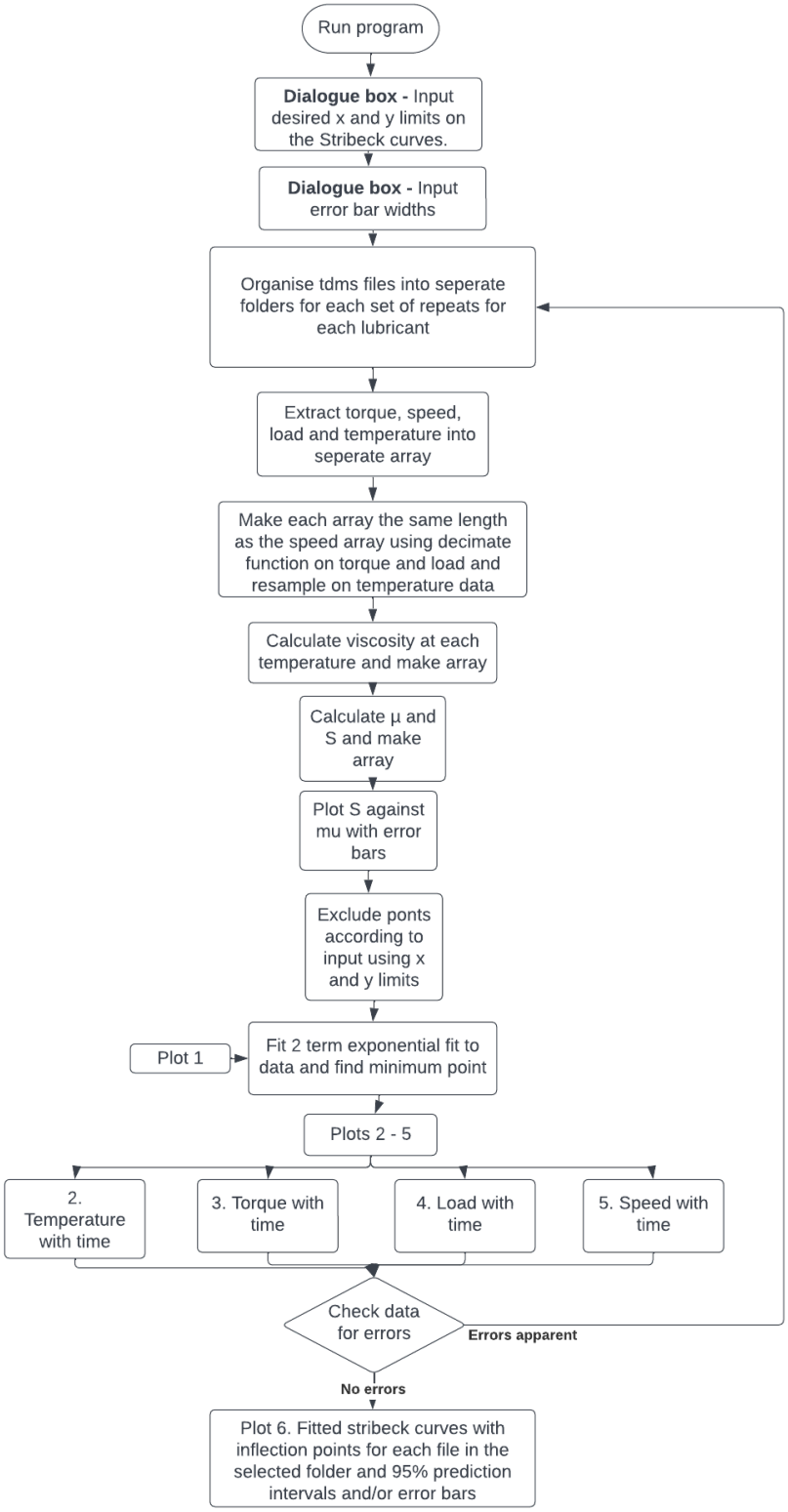

Figure 7.13: Stribeck curve generator process flow using MATLAB

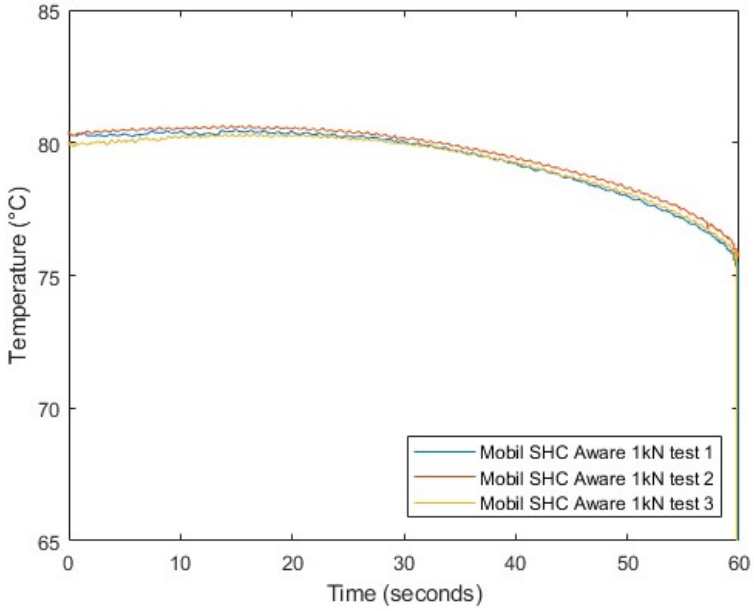

Figure 7.14: Example of temperature measurements after being processed with the MATLAB program in Figure 7.13

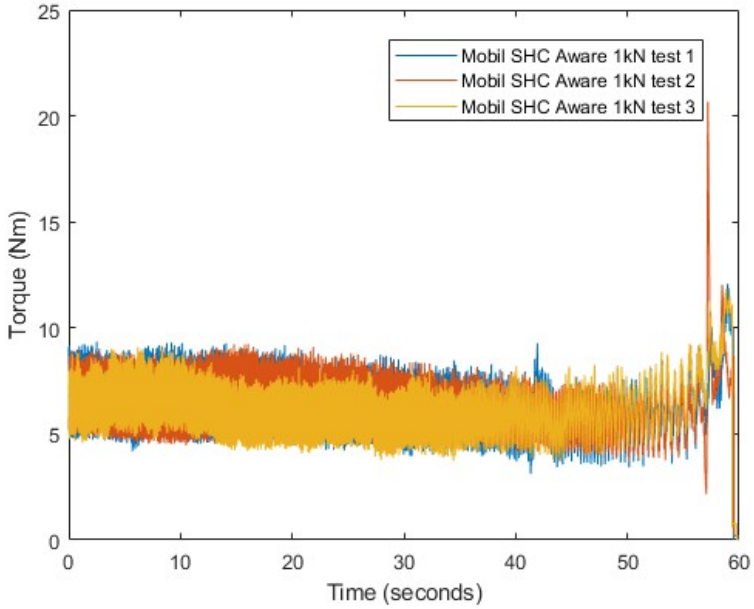

Figure 7.15: Example of torque measurements after being processed with the MATLAB program in Figure 7.13.

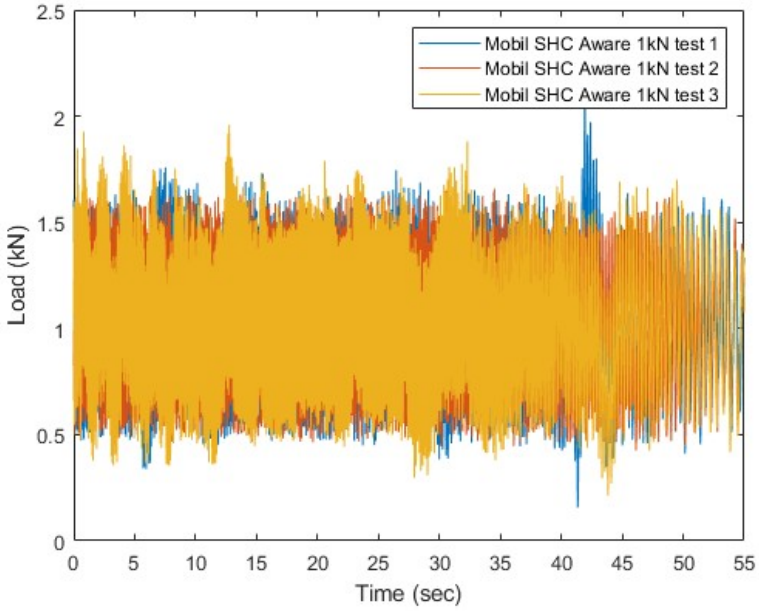

Figure 7.16: Example of load measurements after being processed with the MATLAB program in Figure 7.13

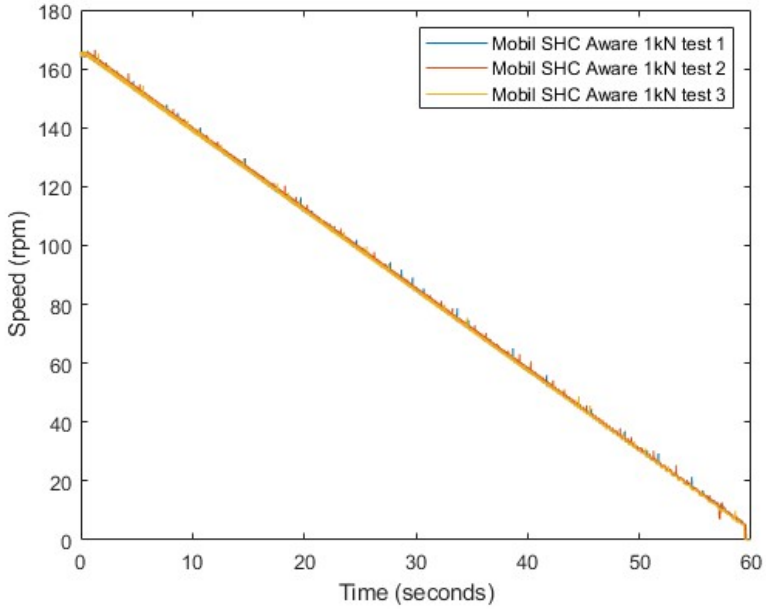

Figure 7.17: Example of speed measurements after being processed with the MATLAB program in Figure 7.13

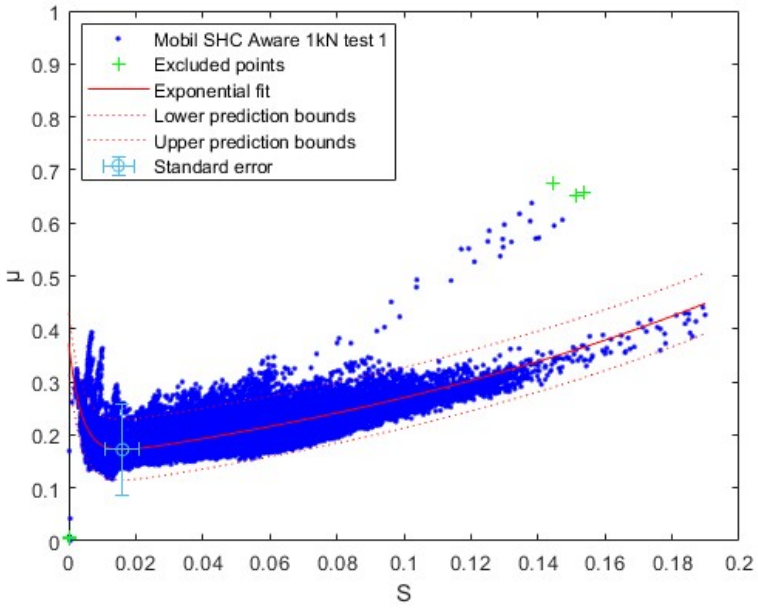

Figure 7.18: Example of Stribeck measurements after being processed with the MATLAB program in Figure 7.13

The Stribeck plot in Figure 7.18 (number 6 on Figure 7.13) shows all of the data which was calculated for each test. This was typical of all of the tests conducted. Where the outliers caused a considerable effect on the exponential fit, the threshold was adjusted and the points which are excluded from the calculation of the fit are highlighted in green.

After all of the data had been processed the most typical and least noisy example of each test was copied into a separate folder. The selected repeats were then used to represent each lubricant and generate plots which compared the performance of each lubricant against one another like those shown in Chapter 8. The friction coefficient values were not comparable with literature because it includes the friction of the ancillary bearings. However it was useful to compare the lubricants with one another because the ancillary bearings were under the same test conditions and were lubricated with separate lubricant, as recommended by the component manufacturers.

7.4.1 Error plotting

The errors for μ and S which are plotted in light blue on Figure 7.18, were calculated using the method for combining standard uncertainties from the instrument measurement accuracy (see Table 6.2 in section 6.5) used by Bell [74]. The error bars as can

be seen on all of the Stribeck curves in this document. These are separate from the 95% prediction bounds which are calculated using MATLAB curve plotter. These are the simultaneous observation bounds which show the boundary where 95% of future measurements would be predicted to lie, based on the current data set.

7.5 Measuring Wear

The wear on the bearing shell was expected to be severe from the tests conducted during rig commissioning. The shaft was not expected to wear significantly unless the bearing shell was completely worn through to the steel backing layer because of its much higher surface hardness. However, the surface of the shaft would be altered should soft metals from the bearing sliding layer adhere to it. Hence the roughness of the shaft was measured before any testing commenced and after after cleaning between lubricant changes. The instrument used was a Mitutoyo SJ-400 stylus-type contact profilometer as shown in Figure 7.19. It was used to measure the roughness of the shaft in both the axial and the radial direction at three different locations along the axis which are labelled in Figure 7.19. The stroke length of each measurement was 0.8mm and the stylus was of 12AAC731 (2 µm tip radius) type. The support bearing end (region 1), middle (region 2) and test bearing end (region 3) were each measured three times. Each time a measurement was taken the shaft was rotated an arbitrary amount so that the measurements were a sample of the whole journal surface. The test bearing end was expected to receive the most wear because of the cantilever loading towards that end of the shaft.

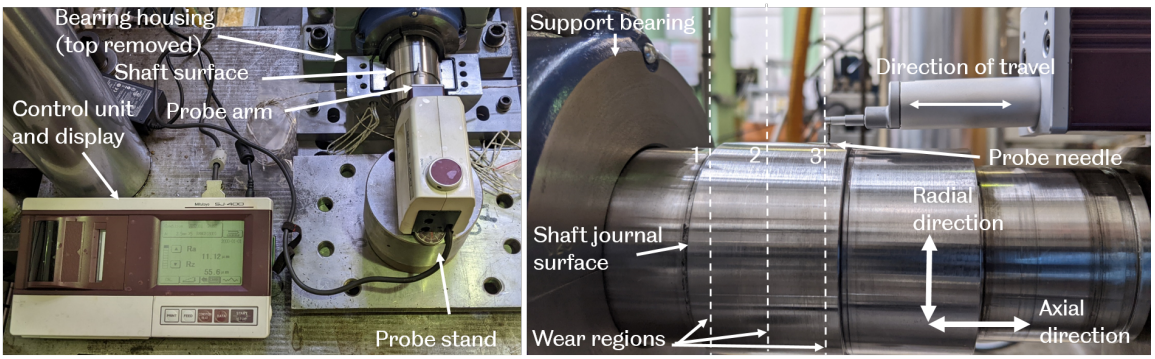

Figure 7.19: Photo of portable profilometer and set-up method

The bearing shell surface was measured using an Alicona Infinite Focus 3D measurement system (a 3D non-contact focus variation type profilometer) for each bearing

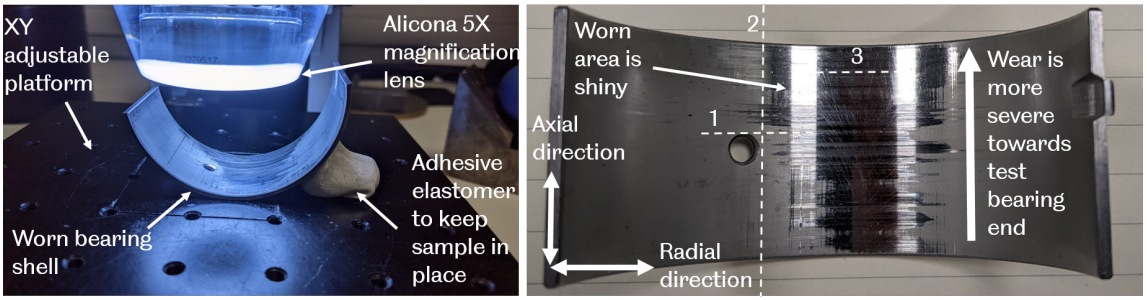

Figure 7.20: Photo of Alicona lens and set-up method

shell and measurements of the surface roughness in both the axial and radial direction were taken along the path of the numbered lines in Figure 7.20. This was done using the 2D profilometry module of the MeasureSuite v12.6.7. This information was to be used to compare the wear between each lubricant.

7.6 Oxidation of oils

As was highlighted in the literature review in Section 4.5, oxidised EALs had not so far been characterised under realistic operating conditions. Various methods of oxidation were researched and are discussed in section 2.3.2. Two of these different methods, using the RPVOT and the RSSOT machines were used on the lubricants for this research. This ensured that the variables of the test technique used were reduced and the results were more comprehensive, but also because it was of interest to compare the performance of the lubricants with each test. This was because the RPVOT test according to ISO standard D2272 required the presence of water so an additional mechanism of lubricant degradation in the form of hydrolysis was present. The testing using the RSSOT was conducted by the lubricant manufacturer. The RPVOT testing was conducted by the author and is explained in Section7.6.1.

7.6.1 RPVOT method

In an RPVOT machine the lubricant oxidises on a much quicker timescale than it would take in service because of a combination of the copper catalyst, pressurised pure oxygen atmosphere and high temperature. The oxidation induction time (OIT) is referred to as the time taken for the pressure in the sealed vessel to drop 25.4psi below the pressure reached after the oil in the vessel had reached 150°C. This is shown on the chart recorder usually as a sudden drop. Theoretically this is the point where the oxidation resistance or antioxidants in the lubricant have been used up. Modern

lubricants can have oxidation induction times in excess of 2000 minutes. As a result it is anticipated that the D2272 standard will be updated to include a pressure drop of 50psi to account for the improvements in modern lubricant oxidation resistance.

Each lubricant to be tested was tested as per the ISO standard D2272 [85]. A copper coil was prepared by wrapping 1.6mm diameter pure copper wire around a 42mm diameter pipe. It was weighed to ensure it was within the 55.6 +/-0.3gram specification and was scuffed with 100grit silicon carbide cloth. 50grams of lubricant was then added to the beaker, see figure 7.22. A small amount of distilled water is added to the lubricant and around the glass beaker in which it is contained and the glass beaker is inserted into the sealed carriage shown in 7.21. The sealed carriage was purged of air and charged with oxygen at room temperature to a pressure specified in the standard of 6.2bar. The vessel assembly is submerged into a silicon oil bath which is maintained at 150°C. A drive unit rotates the carriage at 100rpm and the vessel pressure measured by a gauge attached to a chart recorder so that the pressure drop over the duration of the test is documented as shown in Figure 7.23.

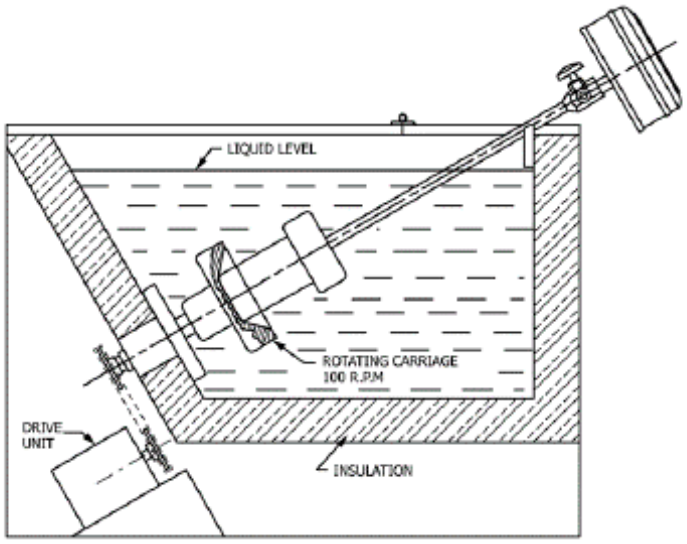

Figure 7.21: Rapid Pressure Vessel Oxidation Tester schematic from [85]

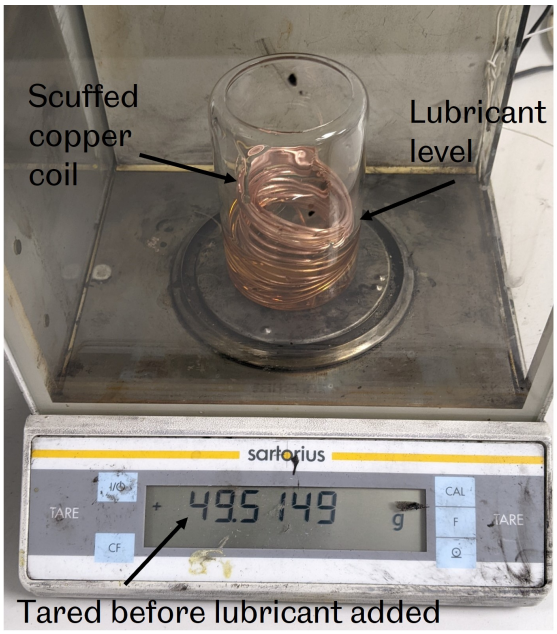

Figure 7.22: Copper coil submerged in lubricant ready to be inserted into the RPVOT chamber. Image shows 40.5grams of lubricant added to glass beaker and coil

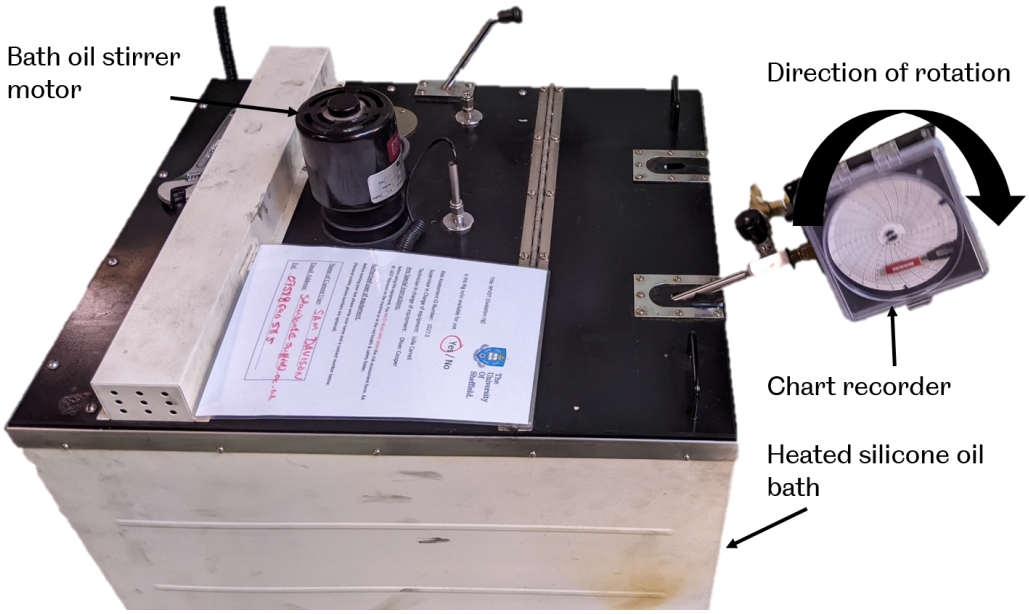

Figure 7.23: Rapid Pressure Vessel Oxidation Tester image

The trace labelled “A” on Figure 7.24 shows a typical reading from a D2272 test on a lubricant. The pressure builds up to a maximum within the first 10 minutes as the vessel reaches the bath temperature which causes the oxygen in the vessel to expand. After 210 minutes the pressure begins to drop before falling sharply. For this trace an OIT of 245 minutes would be recorded. For trace “B” this would also be around 245 minutes but a sudden drop is not apparent. This is a characteristic of some synthetic lubricants but a repeat would be taken to validate this result and verify that the gradual drop was not caused by an experimental error such as a vessel leak.

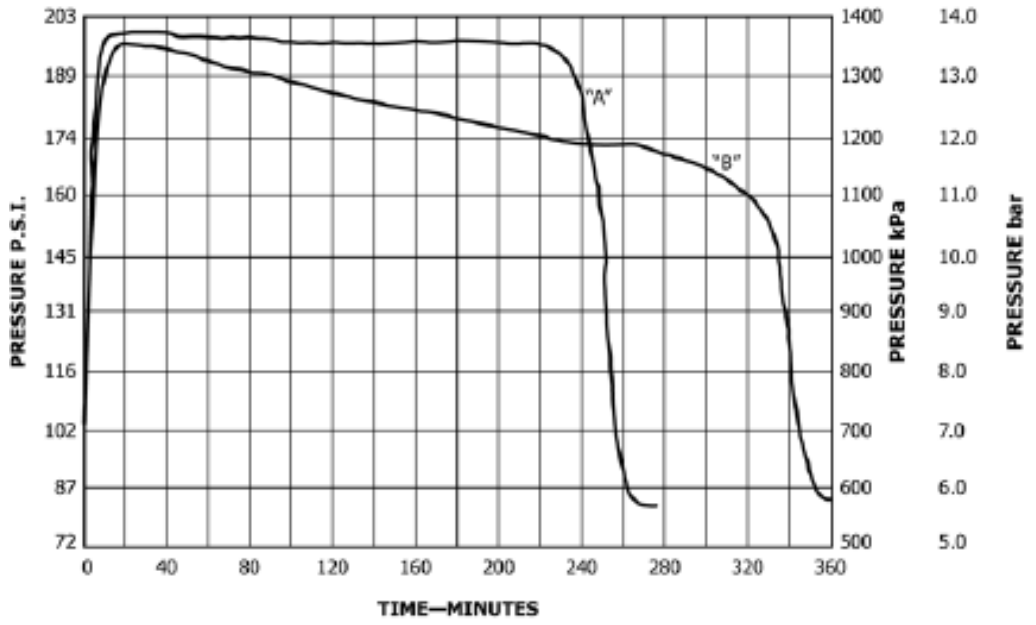

Figure 7.24: Example of RPVOT measurement trace from ASTM [85]

7.6.2 Using a tin catalyst in the RPVOT

Tin is the major component of the white metal, WJ2, which is used to line stern tube bearings as was discovered in the literature review, see Section 4.3. The oxidation tests were also conducted with tin as a catalyst as opposed to copper. This was done by using solder wire which was free from flux (antioxidant). The specification of the wire used is shown in table 7.4. Silver does not react to oxygen and the small amount of copper present was considered negligible in terms of comparing the pure copper catalyst to the solder catalyst.

Tin (%)	**Silver (%)**	**Copper (%)**
96.5	3	0.5

Table 7.4: Composition of solder used as a tin catalyst in RPVOT tests

The tin catalyst was prepared in the same way as the copper catalyst per D2272. The thickness of the solder was 1.2mm as oppose to 1.6mm so the surface area of the tin coil would be different if the same number of coils was used. Hence, the surface area of the tin coil was matched to that of the copper coils which are specified in the D2272 standard. This meant that 66 coils of solder were equivalent to the 24 coils of copper which was required by the standard.

Chapter 8

Results and analysis

The DiMITRI experiments were designed to improve on the Baxter rig experiments by answering the original hypotheses that the EAL performance at least matches that of the mineral oil based lubricants. It would do this by focussing the experiments in the mixed lubrication regime with friction measurements and not on film thickness. The trade-off between the stability and lubricity of the lubricants would be tested by using fresh and oxidised oils and comparing their friction performance in DiMITRI. The modified hypotheses are as follows:

1. EAL Stribeck curve inflection point occurs at a higher Sommerfeld number than that of mineral oil based lubricants in the mixed lubrication regime.
2. There will be a trade-off between EAL stability and lubricity in the mixed lubrication regime.
3. Oxidised lubricants will have lower lubricity and a higher Sommerfeld number at the Stribeck curve inflection point compared to their fresh counterparts.

8.1 Hypothesis 1 - Fresh oil Stribeck curves

As was explained in Section 7.4, Stribeck curves were fitted to the raw data using a two term exponential fit. The inflection point was identified by finding the minimum of the curve. This is the beginning of the mixed lubrication regime.

A comparison between all five fresh lubricants at each load is shown in Figure 8.1.

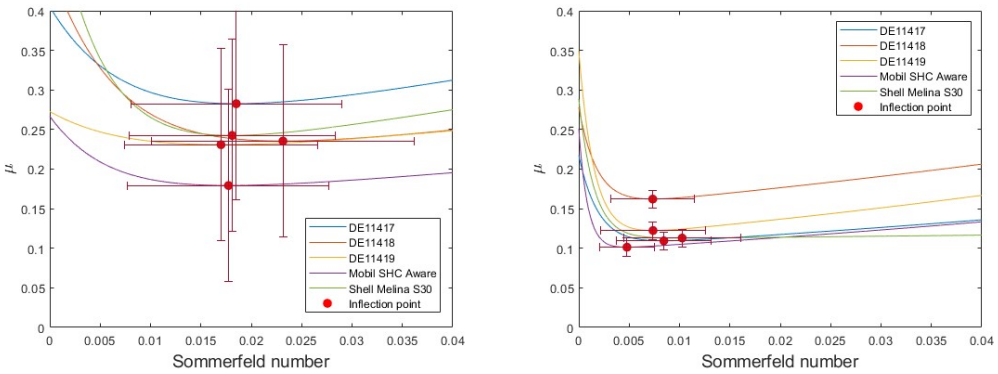

(a) 1kN (b) 5kN

(c) 10kN (d) 15kN

Figure 8.1: Fitted Stribeck curves collected during run down test for each lubricant, separate graph for each load. Red dot indicates the location of the minimum point on the curve which is the inflection point between the boundary and the hydrodynamic lubrication regimes

The Sommerfeld number of the inflection point was expected to be very similar regardless of the load, given that all the other test conditions were the same. Theoretically this should be true as the Sommerfeld number is non-dimensional and takes into account the main factors affecting bearing design and lubricant friction. Different loads were applied in order to find test conditions which optimised the experiment over the

Sommerfeld number range 0.004 to 0.01 specified in section 4.3 where real stern tube bearings can be known to operate.

As it appears in Figure 8.1 the Sommerfeld number at the inflection point decreases with increasing load. This difference is more pronounced in the 1kN tests which suggests that the slower deceleration rate which the 1kN tests were conducted at could be responsible for this. The fact that the 5, 10 and 15kN tests were all conducted at the same deceleration rate but the trend of decreasing Sommerfeld number with increasing load is still apparent but less pronounced implies it is not the only factor which has influenced this.

The reduction in sliding velocity at the inflection point with increasing load shows that the Sommerfeld number fails to take into a account all of the factors which effect the lubricant film that is generated. These results might suggest that the lubricant viscosity is much thinner in the contact than has been assumed. This could be due to local lubricant temperatures being much higher than was measured by the contact thermocouple resulting in a reduced viscosity. Equally there could be some other shear thinning effect with pressure. Factors such as the Eyring stress, heat capacity and thermal expansivity as suggested by Lord et al. [46] may not be negligible as discussed in Section 4.2.

Whether the missing factor can be accounted for or not, all of the lubricants have demonstrated similar performance. This is highlighted in Figures 8.2 and 8.3 where a 5kN test repeat from each lubricant is directly compared to a 5kN Shell Melina test. Overlap between the prediction bounds of each EAL Stribeck curve with the Shell Melina Stribeck curve as a benchmark can be seen. This demonstrates that the results are similar to the point where further measurements could favour any of the lubricants over another in terms of the inflection point and the friction.

In terms of hypothesis 1, the EALs tested have demonstrated very similar Sommerfeld numbers at the inflection point and in the 5kN case the EAL inflection points are lower than the mineral oil. Under 10kN and 15kN the mineral oil has the lowest Sommerfeld number, however this is well within the error bounds for the other lubricants. A statistically significant answer to the hypothesis is not feasible with the current number of repeats of each experiment.

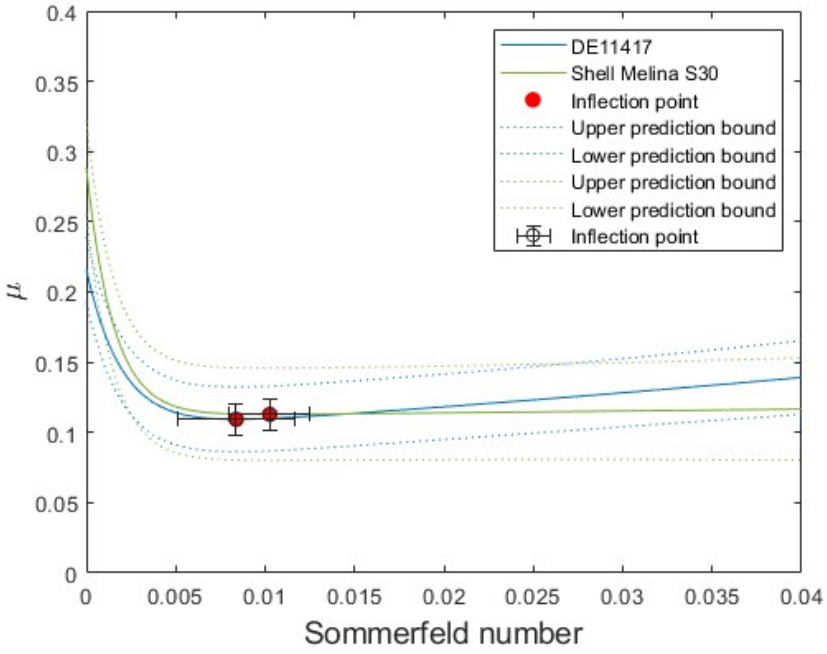

(a) DE11417 compared to Shell Melina

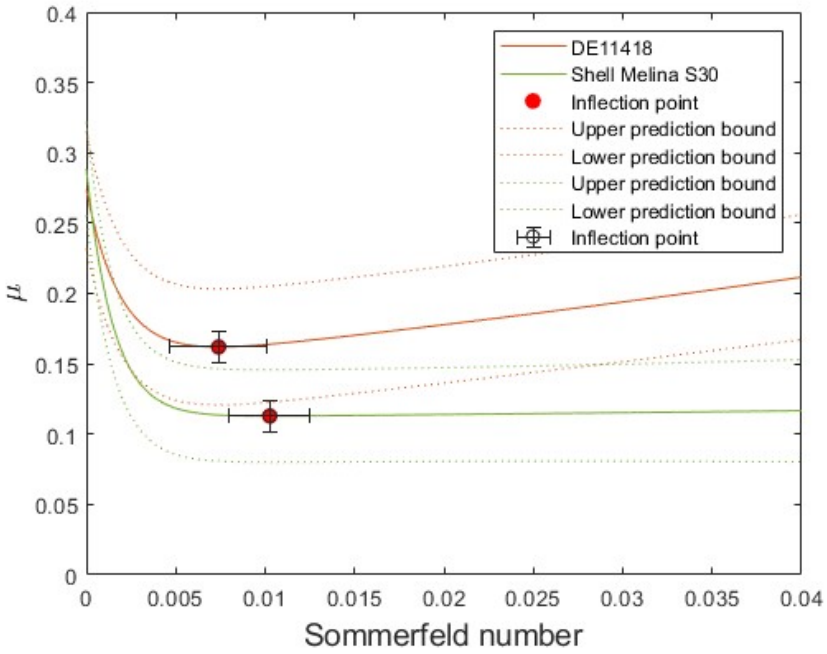

(b) DE11418 compared to Shell Melina

Figure 8.2: Direct comparison of mineral oil based lubricant and EAL Stribeck curves collected during run down test for each lubricant, the upper and lower prediction bounds for the curve fit are shown with each curve. 95% of measurements are predicted to fall within these boundaries based on the raw data.

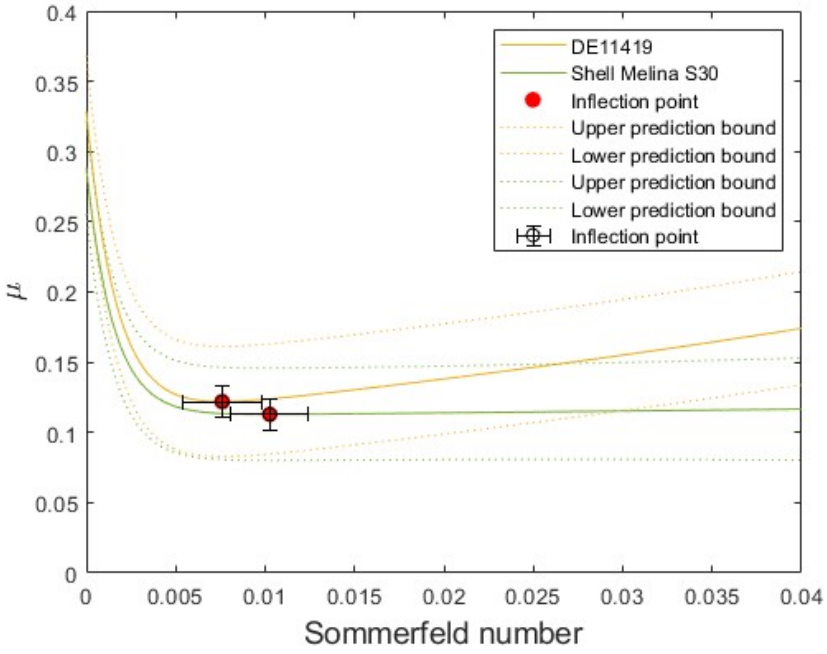

(a) DE11419 compared to Shell Melina

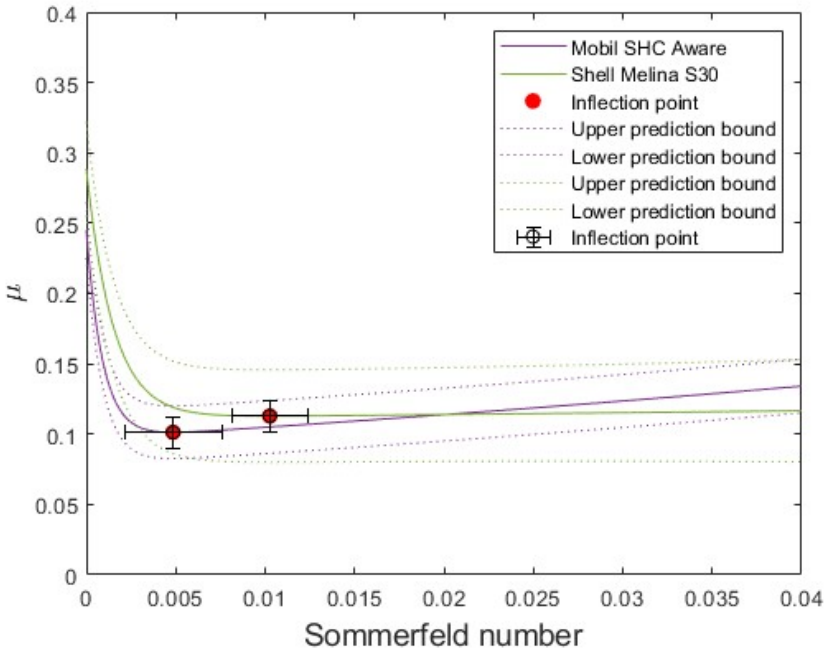

(b) Mobil SHC Aware compared to Shell Melina

Figure 8.3: Direct comparison of mineral oil based lubricant and EAL Stribeck curves collected during run down test for each lubricant, the upper and lower prediction bounds for the curve fit are shown with each curve. 95% of measurements are predicted to fall within these boundaries based on the raw data.

Mobil SHC Aware seems have the lowest friction at the inflection point at 1, 5 and 15kN. At 80°C this is the thickest oil according to Figure 7.2 which means that the relatively low friction is not due to bulk oil properties but the additives used in the lubricant such as friction modifiers. The results at 10kN however do not appear to fit with this trend.

The shape of the curves is similar for all lubricants under the lower loads, but under 10 and 15kN there is more variability. At 10kN for the DE11418 the friction rises sharply as Sommerfeld number increases after the inflection point, followed by Shell Melina. DE11417 and DE11419 appear to rise with a similar gradient to the lower loads whereas the Mobil SHC Aware appears flatter. Under 15kN of load all of the lubricants display the sharpest rise in friction after the inflection point (in the hydrodynamic regime) with Mobil SHC Aware being less affected than than the other lubricants.

On the 10kN and 15kN Stribeck curves in Figure 8.1 the error bars for the friction coefficient are omitted because they are within the inflection point marker boundaries. This was because the larger the load and torque measurements; the smaller the percentage error because the error is an absolute value based on the equipment specifications. They were calculated based on the accuracy of the torque meter and load cell instrumentation as explained in Section 7.4.1.

8.1.1 Hypothesis 1 conclusion

The hypothesis that the mineral oil based lubricant will produce a lower Sommerfeld number at the inflection point remains unproven. There is no clear evidence that the hypothesis holds true. Although the conclusiveness of the current study is limited by the number of repeats it remains unlikely that the results shown are an exception to the norm.

8.2 Hypothesis 2 - Stability trade-off

The oxidation stability of the lubricants has been assessed by exposing them to a standard oxidation test with an RPVOT as per ISO D2272 as is explained in Section 7.6.1 and also by the manufacturer with an RSSOT. It was then possible to rank them in order of the least to the most resistant to oxidation in the presence of water as a measure of their stability. The RSSOT method which is used by the manufacturer

of lubricants DE11417, DE11418 and DE11419 has also been conducted on all of the lubricants tested as mentioned in Section 7.6.

The OIT for both a 25psi and a 50psi drop in vessel pressure has been included in Figure 8.4 because the DE11417 lubricant did not show a sudden drop until 635 minutes into the test and the vessel pressure had already reduced past the usual 25.4psi drop without the sudden drop associated with OIT measurements. This was also because of the anticipated update to D2272 to specify the use of a 50psi. The sudden drop included both the 25.4psi and 50psi drop specification for all other lubricants.

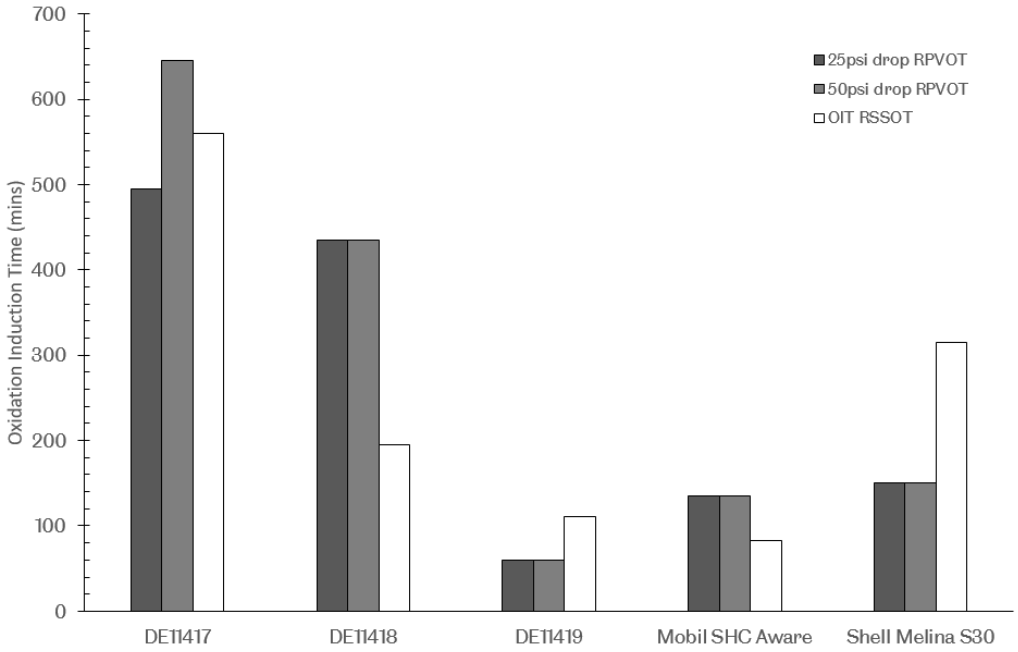

Figure 8.4: Oxidation induction time using the RPVOT as per ISO standard D2272 and a manufacturer RSSOT

DE11417, DE11418 and DE11419 demonstrated the stability (relative to each other) that was in agreement with what was expected by the manufacturer, see Table 5.4, with DE11417 being superior to DE11418 and DE11419 being the worst performer of the three. The ranking of all of the lubricants in terms of their stability from the two test methods is shown in Table 8.1 with a rank of 1 being the most stable and a rank of 5 being the least stable lubricant.

The two methods rank the lubricants in a different order, with DE11418 swapping places with Shell Melina and SHC and DE11419 also swapping places with each other.

Lubricant	OIT RPVOT 50PSI (mins)	Stability Rank	OIT RSSOT (mins)	Stability Rank
DE11417	645	1	560	1
DE11418	435	2	196	3
Shell Melina	150	3	316	2
SHC Aware	135	4	83	5
DE11419	60	5	110	4

Table 8.1: OIT of lubricant samples

This is thought to be due to the presence of water in the RPVOT method. As water is highly likely to be present in the stern tube application [86] the RPVOT test is the more appropriate ranking for stability hence this method has been used to age the lubricants in this in this work.

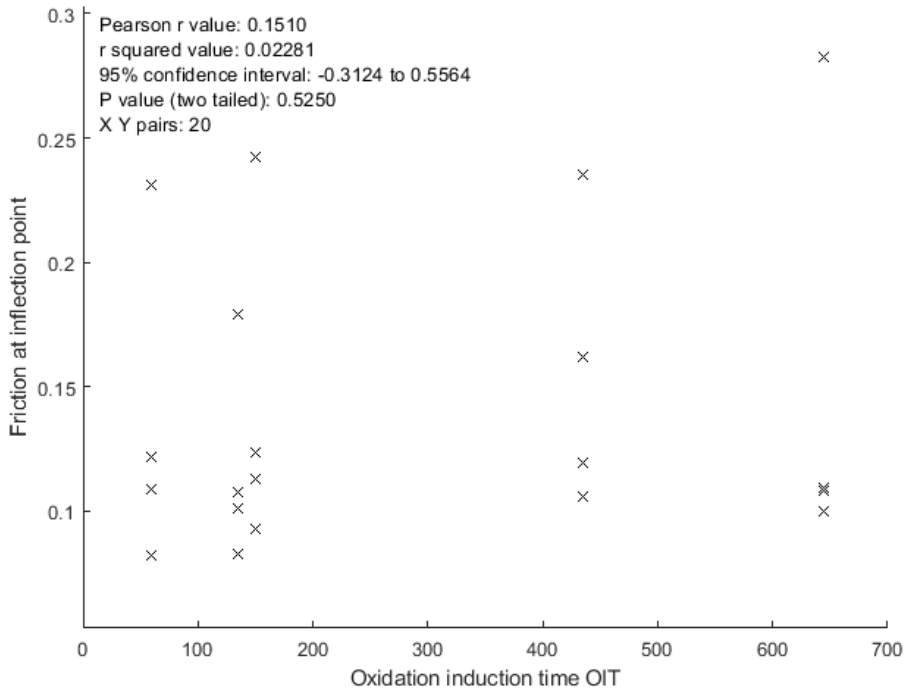

Figure 8.5: Correlation of OIT with friction in mixed lubrication regime

After defining the stability ranking of the lubricants as the OIT from the RPVOT test, the hypothesis that there is a trade-off with friction in the mixed lubrication regime could be tested. This was explored by plotting the friction at the inflection point against the OIT from the RPVOT method, as shown in Figure 8.5.

Each lubricant is represented by four points on the scatter chart, which are the friction at the inflection point for each load, or the points represented by the red dot on Figure 8.1. If the markers on Figure 8.5 from a particular lubricant were joined up they would form a vertical line up from the corresponding OIT for that lubricant. Twenty points make up the scatter plot: four points per lubricant (one per load case). A Pearson r value (correlation coefficient) was calculated using GraphPad Prism software. This assumes that the data follows a normal Gaussian distribution.

The r value of 0.151 shows a weak positive correlation between the lubricant stability and friction in the mixed regime, which suggests that the hypothesis could be true. The r-squared value is low which means that the variance in friction is not shared with the OIT. The P-value of 0.5 is also high which means that a statistically significant answer to the hypothesis is not achievable from this data.

8.2.1 Hypothesis 2 conclusion

The hypothesis that there is a trade-off between lubricant stability and friction has some truth demonstrated by a weak positive correlation between the stability and friction in the mixed lubrication regime. A larger experiment (in terms of the number of replicates and candidates) would be needed to increase confidence in this hypothesis.

8.3 Hypothesis 3 - Oxidised compared to fresh lubricant samples

The oxidised oils all show a shift upwards in the Sommerfeld number at the inflection point. This is demonstrated in Figure 8.6 where for the fresh lubricants the maximum Sommerfeld number is around 0.025 (DE11418) with the inflection point for the rest of the oils being around 0.02. For the oxidised lubricants the minimum inflection point is around 0.03 with DE11418 recording an inflection point of around 0.07.

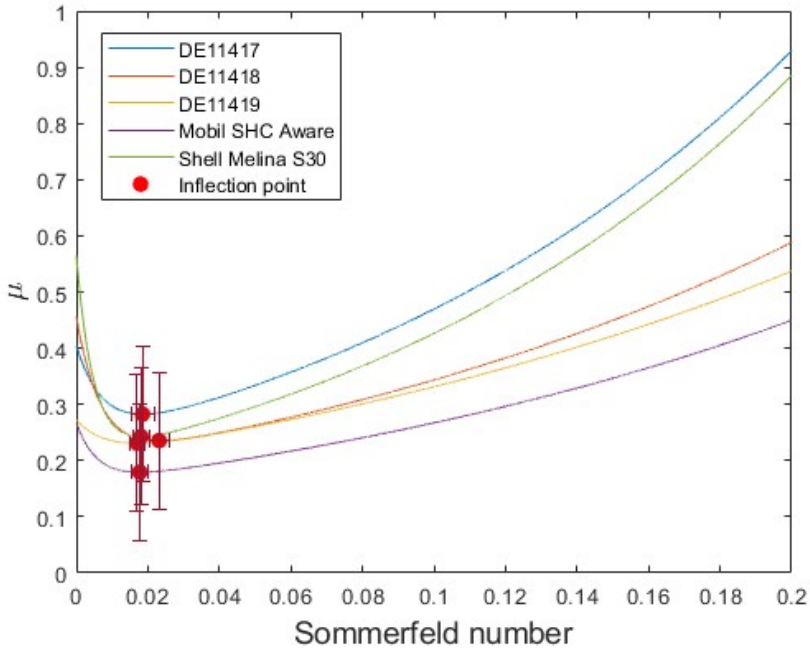

(a) 1kN Stribeck curve fresh

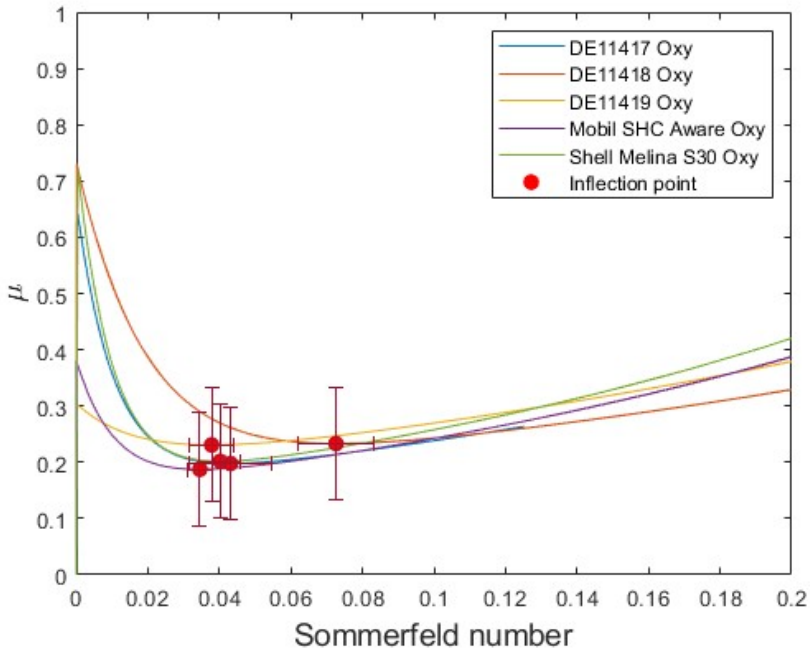

(b) 1kN Stribeck curve Oxidised

Figure 8.6: Direct comparison of Stribeck curves for fresh and oxidised lubricant under the same conditons at 1kN

The rise in friction in the hydrodynamic regime as the Sommerfeld number increases is higher for the fresh oils than for the oxidised lubricants generally. For example, the Shell Melina fresh lubricant results show a gradient of 4.6 between the friction coefficient range 0.1 to 0.2, but the oxidised lubricant has a gradient of 1.7 in the same range. This equates to a 63% decrease in gradient for the oxidised version of the same lubricant. For DE11417 and DE11418 this can be due to the fact that the viscosity of the fresh compared to the oxidised samples is higher (Table 8.2) which fits with the theory that a thicker lubricant will generate more internal friction. However, for DE11419 the opposite is apparent because the fresh samples are thinner and therefore would be expected to exhibit less friction in the hydrodynamic regime when compared to the oxidised DE11419. The friction with Mobil SHC Aware is largely unchanged despite an increase in viscosity once it was oxidised. The fresh Shell Melina S30 has higher friction in the hydrodynamic regime, but minimal change in viscosity with oxidation.

Viscosity at 80°C (mPas)		
Lubricant	Fresh sample	Oxidised sample
DE11417	20	16
DE11418	21	13
DE11419	25	32
Mobil SHC Aware	24	31
Shell Melina S30	17	18

Table 8.2: Dynamic viscosity measurements of all lubricant samples

In the mixed regime, the oxidised samples generally show a higher friction for the same Sommerfeld number when comparing (a) and (b) in Figure 8.6. The inflection point for the fresh lubricants on Figure 8.6a occurs at a Sommerfeld number of approximately 0.02 for all of the samples, at Sommerfeld numbers below this threshold the lubricants are in the mixed regime. At this threshold in Figure 8.6b all except DE11417 show a higher friction coefficient. This information is summarised in Table 8.3. A threshold of 0.005 is also shown for the 5kN tests. Up to a 67% increase is in friction in the mixed lubrication regime is apparent for the 1kN tests with oxidised samples. For the oxidised samples this friction increase is up to 69% for the Shell Melina as is shown in Table 8.3.

Lubricant sample	mean μ at Sommerfeld number of 0.02	% change	mean μ at Sommerfeld number of 0.005	% change
DE11417	0.28	NA	0.11	NA
DE11418	0.24	NA	0.17	NA
DE11419	0.23	NA	0.13	NA
SHC Aware	0.18	NA	0.10	NA
Shell Mel	0.24	NA	0.12	NA
DE11417 Oxy	0.25	-12	0.16	46
DE11418 Oxy	0.40	67	0.21	24
DE11419 Oxy	0.24	4	0.17	35
SHC Aware Oxy	0.27	52	0.13	30
Shell Mel Oxy	0.25	3	0.21	69

Table 8.3: Summary table of the mean friction in the mixed lubrication regime shown on Figures 8.6 and 8.7.

In the mixed regime, the oxidised samples also demonstrate characteristic curves depending on the lubricant in Figure 8.6. For instance on both graphs the DE11419 shows a shallower gradient than all of the other samples. Mobil SHC Aware demonstrates the lowest friction in the mixed regime for both fresh and oxidised samples and DE11418, DE11417 and Shell Melina have similar performance in the mixed regime for the fresh lubricants but DE11418 demonstrates higher friction when compared to these in the oxidised lubricant tests. This is linked to an increase in the Sommerfeld number of the inflection point demonstrated by DE11418 in Figure 8.6b, which shifts the Stribeck curve to the right. This shift could be attributed to the fact that this formulation will be less viscous under high shear rates present in the bearing. This lubricant is a mixture of a low viscosity PAO and a thicker ester (see Table 5.4) that is present in this formulation. PAO EAL formulations are known to be susceptible to shear thinning as was discussed in the literature review in Section 4.2.

The 5kN Stribeck curves in Figure 8.7 also highlight the relative (compared to the other samples) low friction of both Mobil SHC Aware samples. The other lubricant samples show similar gradients between them. The uncertainty in the inflection point for the oxidised samples is more extreme which is due to a higher variability in the repeat tests of each sample. Above 5kN a Stribeck curve for the oxidised lubricants could not be generated because there was no transition to the hydrodynamic regime. Hence only the 5kN and 1kN load cases are compared. The variability in results is because the bearing was operating at its hydrodynamic limit so the wear that was occurring under these conditions increased the variability.

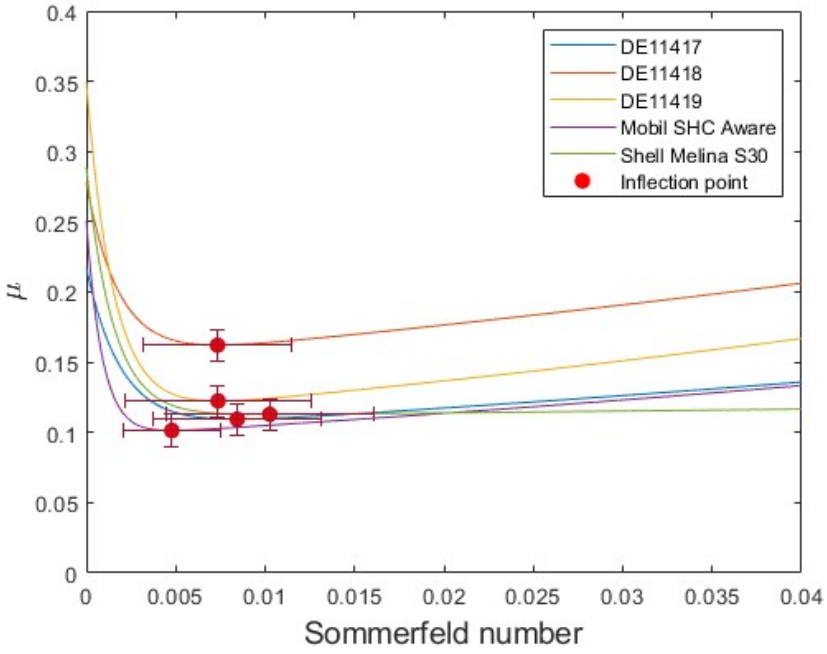

(a) 5kN Stribeck curve fresh

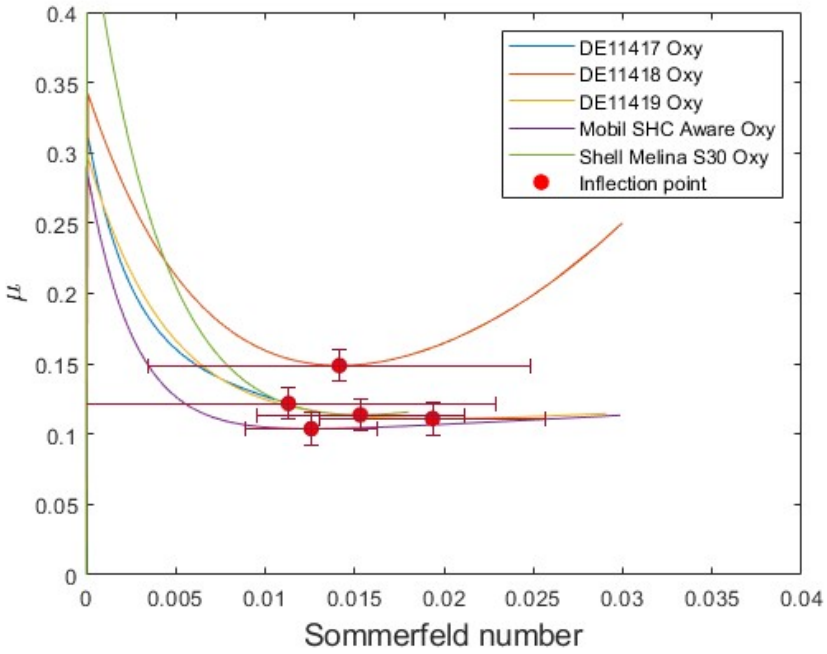

(b) 5kN Stribeck curve Oxidised

Figure 8.7: Direct comparison of Stribeck curves for fresh and oxidised lubricant under the same conditons at 5kN

8.3.1 Hypothesis 3 conclusion

The oxidised oils have shown higher friction with an increase of up to 69% in the mixed lubrication regime for the same Sommerfeld number (0.005) as is shown in Table 8.3. They have also demonstrated a higher Sommerfeld number at the inflection point. Both of these statements agree with the hypothesis.

8.4 Effect of the results in a marine stern tube context

In order to understand the significance of the results the Sommerfeld number at the inflection point was put into the context of a real stern tube bearing with realistic speeds, loads, temperatures and dimensions. This was also to address the shortfall identified in the literature which did not put the findings into the context of real stern tube operating parameters and dimensions. To achieve this the equation for calculating the Sommerfeld Number (Equation 2.3) was rearranged to make the journal speed in rpm the subject. Using the specifications of the stern tube bearing published by He et al. [55] (shown in Table 4.3) along with the viscosity measurements of the Shell Melina at 40°C, a value for the propeller shaft rpm at the infection point was calculated at maximum load. An equivalent propeller shaft rpm could be compared to the inflection point Sommerfeld number measured in DiMITRI to put the results from these studies into context. The propeller shaft rpm at the inflection point is labelled as the "Lift off RPM" on Figure 8.8 for the fresh lubricants and Figure 8.9 for the oxidised samples.

The results in Figures 8.8 and 8.9 are generated using the average inflection point for all of the repeats of each test. The error bars shown on each bar are the standard error calculated for each set of repeats for each test case as oppose to the uncertainty from the measurement error for the tests conducted using DiMITRI (see Section 7.4.1). For example, three repeats of DE11417 at 1kN load resulted in a standard error of +/- 0.0035 on the Sommerfeld number, indicated by the error bars on the first column on Figure 8.8. Some of the error bars are omitted and replaced with a '*' symbol to indicate that one repeat was recorded for this test case and hence the standard error for this test set could not be calculated.

The differences between each lubricant are easier to distinguish in Figures 8.8 and 8.9 compared to the Stribeck curves in Figures 8.1, 8.2, 8.3 and 8.7 but the differences are minor. There is agreement with the observation drawn from the Stribeck curves

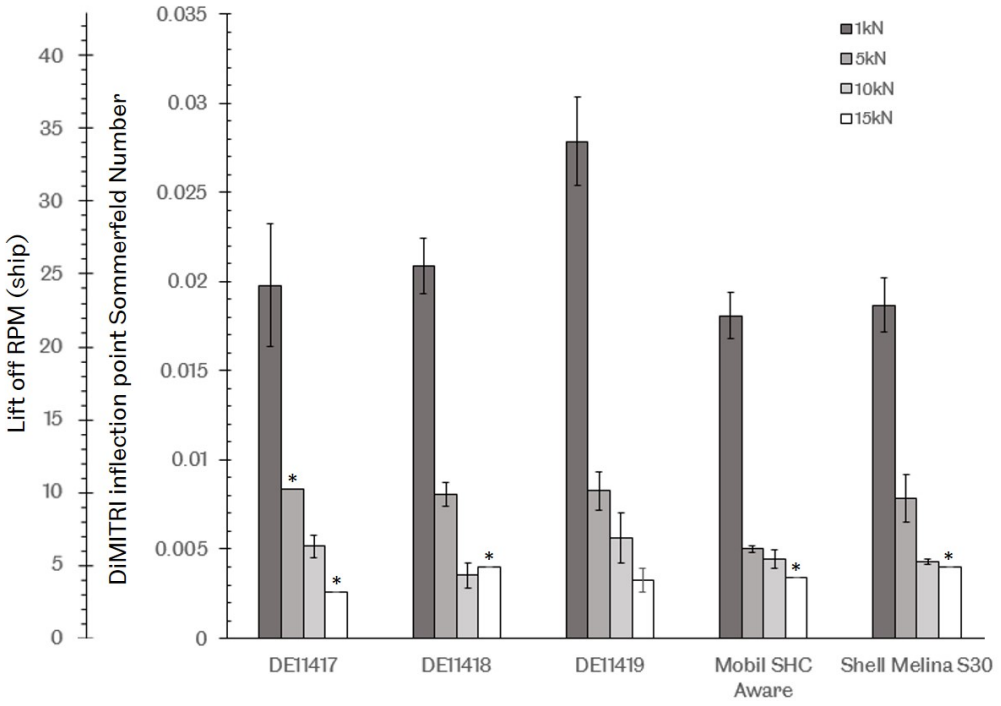

Figure 8.8: Inflection point of fresh samples with the equivalent marine stern tube rpm. $*$ indicate where error bars are omitted due to a limited number of repeats.

in section 8.1 that the Sommerfeld number at the inflection point is not independent of the load. However, the effect of increasing the load on reducing the inflection point seems to diminish and the value of the inflection point begins to converge at 10 and 15kN in Figure 8.8.

Bouyer et al. [87] observed that under misaligned conditions more significant changes in bearing performance occurred when the rotational speed or the load was low. This was characterised by an increased sensitivity of the oil flow rate through the bearing under low loads. The misalignment was similar to that found in DiMITRI when it us under load. The flow rate increased more significantly under lower loads suggesting that the hydrodynamic effects caused less resistance to misalignment. Higher misalignment has been theoretically shown to shift the inflection point to a higher Sommerfeld number [55, 88].

In the case of DiMITRI this does not seem to be the case because the inflection point decreases under the higher loads which would cause an increase in misalignment. The much larger Sommerfeld number of around 0.2 for the 1kN tests could be indicative that the inflection point is dependent on the rate of change of the Sommerfeld number, because these tests were conducted at a slower deceleration rate compared to all of

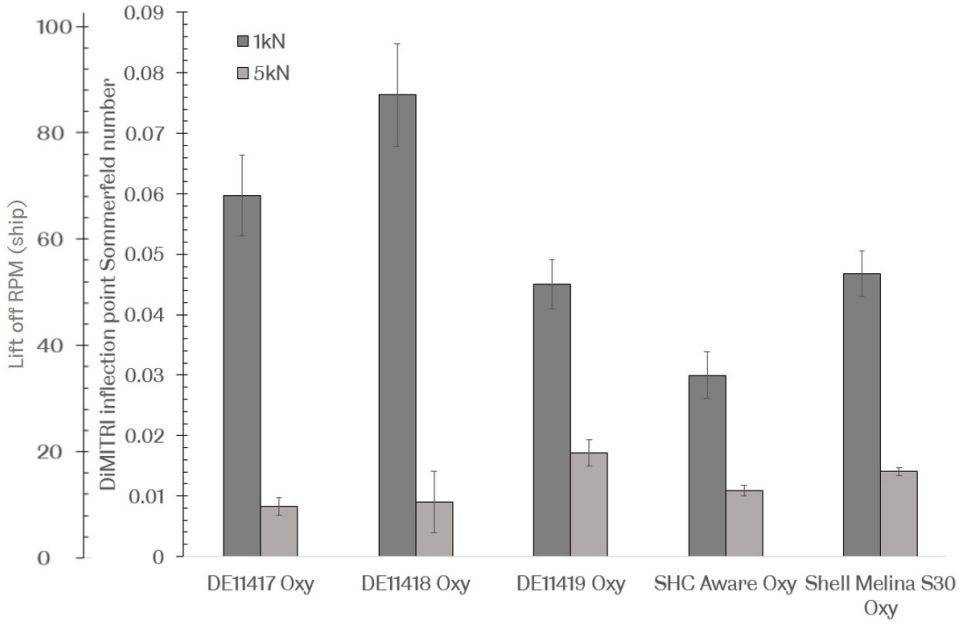

Figure 8.9: Inflection point of oxidised samples with the equivalent marine stern tube rpm.

the other tests. This was to maximise the sensitivity of measurements to changes in friction, as was explained in Section 7.2.1. Although an interesting phenomenon, further investigation into the effect of load on the Sommerfeld number at the inflection point was beyond the scope of this work and the aim of comparing the performance of the EALs was still possible since the test conditions were consistent for each lubricant.

The fresh lubricant sample results in Figure 8.8 show a lift off rpm range of 3 to 30rpm for all lubricants for the stern tube (Sommerfeld number 0.0035-0.024). In the context of a large marine stern tube like that specified by He et al. [55], this would be well within the dead slow ahead condition (used when manoeuvring in a harbour), which is typically below 30rpm [89]. The effect of the pressure-viscosity coefficient under the worst case conditions which were discussed in Section 7.3 was estimated to be up to 10MPa pressure in the contact. This would result in a 9% difference in the speed at the inflection point derived from the pressure-viscosity coefficient of the EALs. Therefore the modified range for the estimate of the lift-off rpm would be 3.3 to 33rpm to the nearest 0.1rpm. For the Shell Melina S30 the range predicted using Figure 8.8 would be 5-25rpm. Clearly even when put into the context of a real stern tube bearing the pressure-viscosity coefficient under the worst case scenario does not make a significant difference to the lift-off rpm of the bearing.

The oxidised lubricant sample results in Figure 8.9 show a lift-off range of 10 to

90rpm (Sommerfeld number 0.08-0.076). This suggests that the oxidised lubricants would be poor at generating a lubricant film and protecting the bearing from damage under conditions above the dead-slow operating speeds and up to a typical slow steaming rpm for a large container ship of around 90rpm [90]. The trend towards slow steaming has been linked to EAL lubricated bearing failures in industry news [91] and this finding provides a basis for this if the lubricants in question are aged.

8.5 Catalysts for oxidation

As mentioned in the literature review tin is the main material present in a typical oil lubricated stern tube bearing lining. Its potential to catalyse the oxidation of the EALs was investigated by using 96.5% tin based solder. The oxidation time after a 50psi drop was compared for the Shell Melina lubricant with Mobil SHC aware because they both had very similar OIT for the standard oxidation test using copper as a catalyst. These tests were conducted in the RPVOT according to ASTM standard D2272 as is described in Section 7.6.2. Figure 8.10 summarises the measurements that were taken.

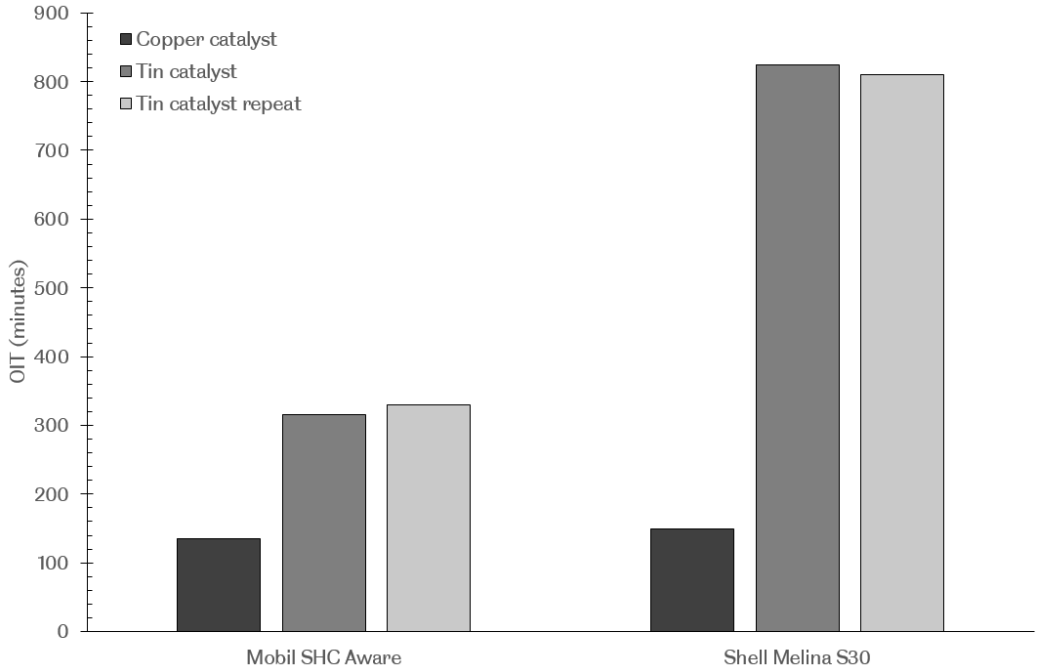

Figure 8.10: Oxidation induction time of mineral oil based lubricant compared to an EAL

Although tin is not a transition metal like copper it did catalyse the oxidation reactions with the EALs. This is demonstrated on Figure 8.10 which shows that the

Shell Melina is less sensitive to tin as an oxidation catalyst compared to Mobil SHC Aware EAL, because the performance of the two lubricants with copper as a catalyst was very similar, but was not with Tin. The reason for the increased sensitivity is unknown, but this finding suggests that inferior compatibility with tin may be a factor in the decreased service life of some EALs which has been blamed for stern tube bearing failures.

8.6 Shaft wear

Wear on the shaft and bearing shell was monitored throughout the experiments using the methods outlined in Section 7.5. Each measurement was taken after the test with lubricant with which it is labelled on Figures 8.11 and 8.12. The roughness of the shaft was not expected to change due to wear because it was much harder than the bearing shell. However it was necessary to identify if there was any effect on the roughness from soft bearing material adhering to the surface, because this would decrease the bearing clearance which has been assumed to be constant in the Sommerfeld number calculations. The measurements on the shaft from the surface profilometer are summarised in Figures 8.11 and 8.12. There are two sets of results for Shell Melina, as this lubricant was used as a benchmark to check the repeatability of the test rig.

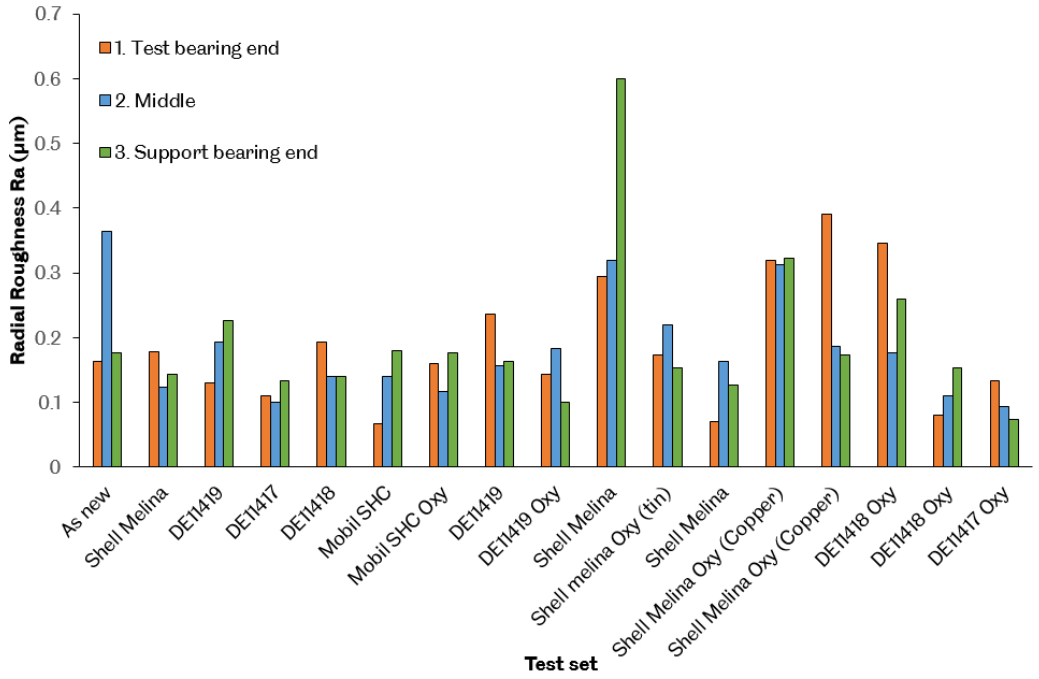

Figure 8.11: Roughness of shaft before each lubricant test set in the radial direction. Ra in μm

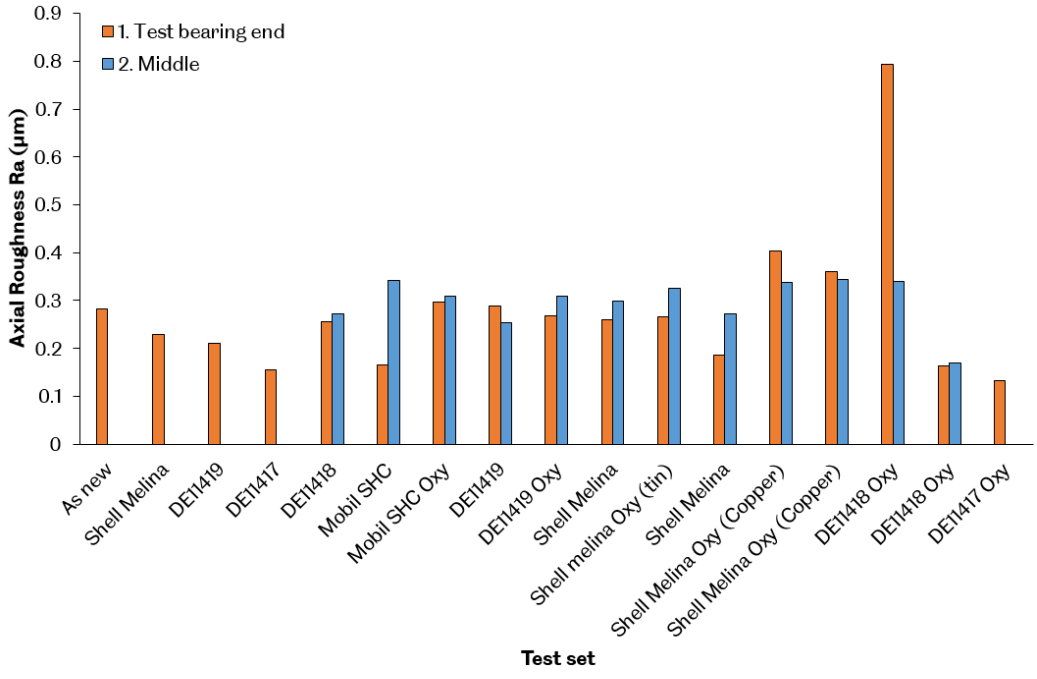

Figure 8.12: Roughness of shaft before each lubricant test set in the axial direction. Ra in μm

The roughness of the shaft in the radial direction just before the second Shell Melina

test set is over double the average roughness of 0.2Ra at the support bearing end for all of the tests sets prior to this. The roughness in the middle and at the test bearing end is also high relative to the test sets before this point. The reason for the increase in roughness was due to deposits left on the surface of the shaft. These were visible as a dull coating, which is pictured on the left in Figure 8.13.

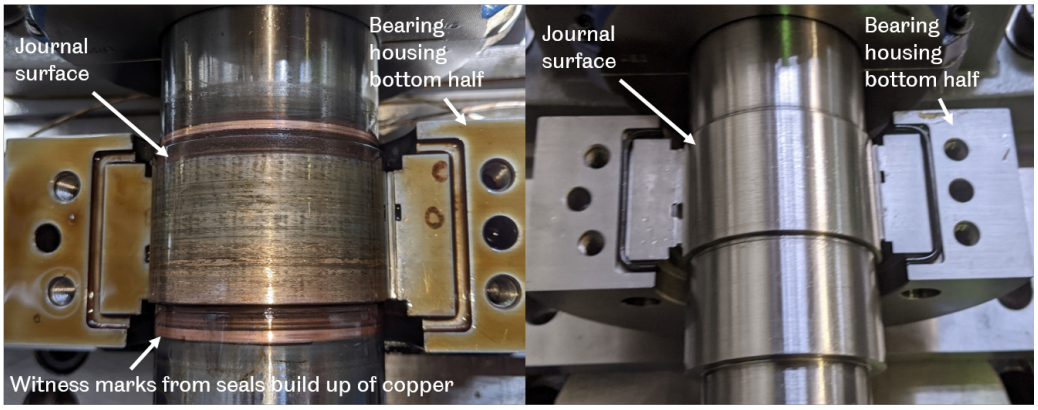

Figure 8.13: Appearance of shaft after a test with an oxidised lubricant (left) and with a fresh lubricant (right).

In Figure 8.13 copper deposits are clearly visible where the shaft seals are in contact with the shaft. The material deposited on the shaft surface is comparatively duller than this, although it does have a copper like colour. It is thought this could be mixed with the other metals in the soft layer of the bearing shell.

Silicone carbide grinding paper was used to bring the surface roughness of the shaft back to a consistent starting point before each test and to clean the shaft of the adhered soft metal. This process was done by hand along with the usual procedure of cleaning the shaft with n-Heptane solvent. All of the roughness measurements after the second Shell Melina test set were taken after this cleaning process had been carried out and the roughness of the subsequent tests are more similar to the norm. A third Shell Melina test set was taken in order to replace the second set of results.

8.7 Bearing shell wear

The bearing shell wear was evident with every lubricant. In Figure 8.14a each of the bottom bearing shells which was used in the experiments is photographed and annotated to indicate the lubricant with which it was tested. Each test set started with a new bearing shell on the bottom of the bearing housing like the one in Figure

8.14b which had a consistent dull surface finish across the whole bearing surface. The top bearing shell was the same for each experiment because no wear was apparent. This was expected because the direction of loading was always towards the bottom bearing shell.

Abrasive wear was apparent on the galvanic top layer (dull in appearance) which exposed the much more reflective nickel dam layer underneath. The abrasive wear was characterised by scratches in the direction of shaft rotation which are visible on the bearing surface in Figure 8.15. A feature which was common for all of the bearings was the general shape of the worn away layer which demonstrates that the damage was focused towards the loaded end as it is in an aft stern tube bearing.

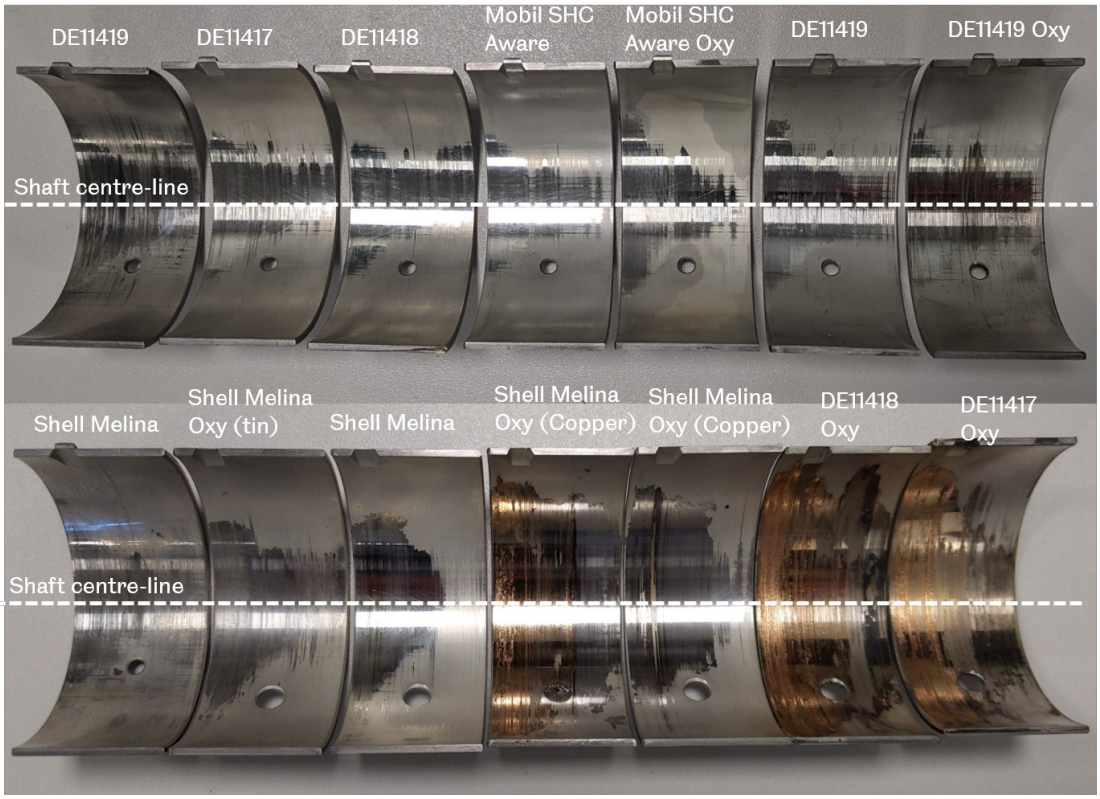

(a) Appearance of shaft bearing shells after the tests with the fresh lubricant

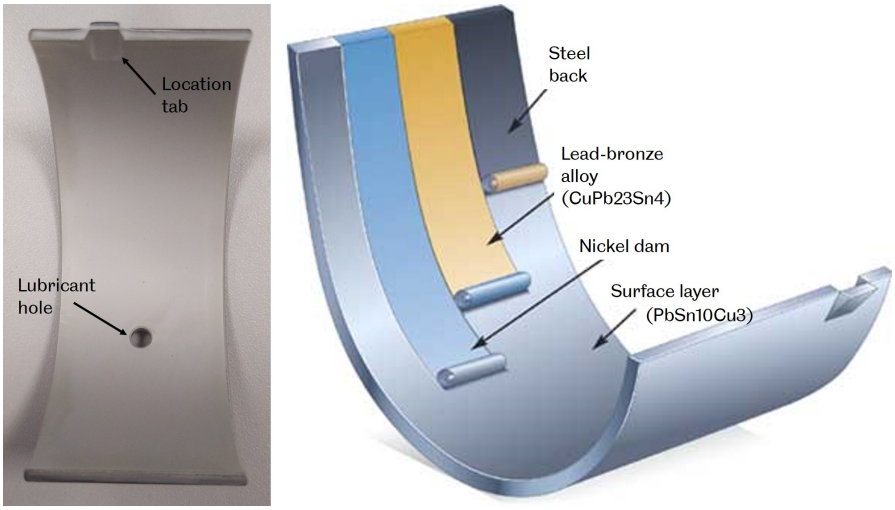

(b) New bearing shell

Figure 8.14: Worn and unworn bearing shells.

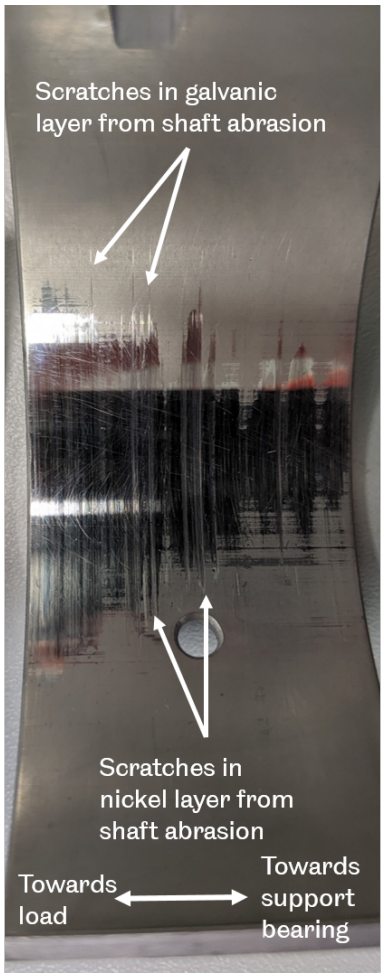

Figure 8.15: Individual worn bearing shell.

A further asymmetry about the centreline of the bearing in the direction of the shaft axis is evident in Figures 8.14 and 8.15. This is due to the direction of rotation of the shaft and the attitude angle, θ, that is generated. The attitude angle shown in Figure 6.8 demonstrates that the point of minimum film thickness, h_0, and the point where damage is most likely to occur is offset from the centre-line. For the oxidised lubricants more damage is apparent and copper deposits are visible as the orange coloured areas.

It appears the most apparent difference between the damaged bearing shells is between the shells which have been used with oxidised lubricants and those which have not. In order to compare the anti-wear properties of each lubricant it would be necessary to quantify the wear in the bearing shell by measuring the surfaces and comparing a property such as the volume of material removed. This is discussed in Chapter 9 as future work.

Chapter 9

Conclusions

This chapter begins by reviewing the objectives that were set out in Section 1.3. It then summarises the main findings of the work and states the novelty of before exploring future work which has been inspired by this thesis.

9.1 Review of the objectives

9.1.1 Objective 1

The first objective of this work was to review the field of bio-lubricant tribology and to identify an application where research considering the fundamental engineering science and understanding of its role in the design of hardware was lacking. It found that the marine sector was under represented in the research despite it being a large part of the overall bio-lubricants market and a key area where environmental considerations are paramount. The research area was further specified when it was clear that the greatest impact (in terms of the environment and current industry issues) was from the application of bio-lubricants in ship stern tubes.

This objective was completed successfully and it influenced the formulation of the aim of this Thesis: to assess the feasibility of bio-lubricants lubricants in marine stern tubes in terms of their tribology.

9.1.2 Objective 2

The second objective involved conducting learning experiments to assess the performance characteristics of different EALs. It was also directly supported by industrial

collaborators who provided commercial stern tube lubricant products. The hypothesis (proposed in Section 5.2) that the EAL performance would match that of the mineral oil based lubricants in terms of their frictional properties and film thickness was partially confirmed because the experiments were limited by the ability of the Baxter rig to operate in the mixed lubrication regime. The conclusion to the second hypothesis was also limited by the operating parameters of the rig because the results obtained were within the hydrodynamic regime only.

The fulfilment of this objective highlighted the need for a bespoke test platform to comprehensively meet the aim of this thesis. It also shifted the focus away from film thickness measurements and towards friction measurements because the performance of EALs under the hydrodynamic regime where film thickness was more relevant was very similar.

9.1.3 Objective 3

A test rig was designed that was capable of testing the lubricants at a component level using commercial bearing shells with an instrumented housing. The apparatus, which included cartridge heaters and thermocouples, allowed realistic operating conditions to be explored with the design which was loaded like a miniaturised stern tube bearing. Inclusion of a torque meter enabled friction measurements to be recorded and Stribeck curves were generated which were useful for characterising the performance of the EALs under extreme operating conditions such as those in the mixed lubrication regime.

Designing a test rig to investigate the performance of EALs under extreme operating conditions was achieved with the development of DiMITRI in Chapter 6. This rig was capable of testing a journal bearing component with realistic geometry and loading scenario. It was also able to replicate lower Sommerfeld number operation than existing rigs, while using a small volume of lubricant. The temperature control capability was also bespoke.

9.1.4 Objective 4

Objective 4 was to use the test rig to make comparisons at a range of different lubrication regimes from the boundary/mixed to full hydrodynamic level. The comparisons made in Section 8.2 indicated that the EAL lubricity could be reduced in the most highly stable formulations with a degree of uncertainty. It was also found that the

oxidised lubricants generated more friction (up to 69% increased friction coefficient) in the mixed lubrication regime and a higher Sommerfeld number (in the range 0.08-0.076 compared to 0.0035-0.024) at the inflection point.

It can be concluded that there is no evidence that the mineral oil based lubricant would necessarily produce a lower inflection point between the hydrodynamic and mixed lubrication regimes in terms of the Sommerfeld number in the operating range for a stern tube aft bearing of 0.004 - 0.01. In the case of a PAO based EAL a mineral oil based lubricant may produce a lower Sommerfeld number if it is oxidised.

9.2 Main findings

The findings were put into context using the Sommerfeld number to identify equivalent operating parameters in a real stern tube to those which were used in the experiments. This found that the fresh lubricants would perform in the hydrodynamic regime for most realistic operating conditions but oxidised lubricants might fail to operate in this regime at slow steaming conditions. The pressure-viscosity coefficient would not have a significant effect on the performance of the lubricants when compared to mineral oil based equivalents.

Different methods of ageing the EAL samples were trialled and two different catalysts which were relevant to the materials found in stern tube bearings were compared. It was found that high levels of tin present in marine stern tubes may have an affect on the oxidation time of EALs when compared to their mineral oil equivalents.

Finally the wear of the bearing shell components used in the experiments validated that the high friction measurements for the oxidised lubricants were caused by lubricant film break down and contact between the shaft and bearing shell and the wear that occurred was coherent with a journal bearing which was misaligned due to cantilever loading.

9.2.1 Novelty

The work outlined in this thesis is Novel in the following ways:

- DiMITRI test rig. The author is unaware of any test rigs which would operate in the Sommerfeld number range appropriate for investigating the mixed lubrication regime at the component level realism of a journal bearing tribological contact. It is also unique in achieving this with a low volume of lubricant. The modular design which allows it to be operated using a standard servo-hydraulic machine is different to all other journal bearing test rigs.
- To date there is limited experimental characterisation of the performance of oxidised EALs, but no studies have so far attempted to use aged EALs in a complete journal bearing and assess the wear.
- None of the studies which assess the performance of EALs for use in stern tubes have related the results to real operating conditions on board a large marine vessel.
- The use of and effect of tin as a catalyst to age EALs has not been explored before.

9.2.2 Advice to industry

A case study of a stern tube bearing failure which has been blamed on EALs is needed to gain a better insight into the perspective of ship operators and industry in order to inform future investigation. The work in this thesis has gone some way to putting the results into context but that context is inferred and not necessarily informed by direct industry experience. An example if this is the recommendation of both emulsifying and non-emulsifying lubricants EALs for use in stern tubes by lubricant manufacturers. Practically, which is best depends on the lubricant circulation system in different ships and whether they feature a lubricant/water separation system. Despite this, manufacturers tend to only recommend one or the other for use in stern tubes. A case study would shed some light as to why there is an inconsistency into which of emulsifying or non-emulsifying lubricants are most suitable.

DiMITRI also has the potential to aid in the characterisation of wind turbine bearing lubricants especially as they move towards tilting pad journal bearing designs. The cantilever loading is also a feature of wind turbine main drive shafts and dynamic loading of up to 10Hz can be applied to DiMITRI using the Schenck 250 machine.

Operational problems which are outside of the scope of this thesis could be a contributing factor to the recent increase in stern tube bearing failures. For example, in the literature review it was found that lubricant is normally heated in stern tube systems. Stern tubes are also not normally inspected until a temperature rise alarm is detected which is often too late to prevent damage because any lubricant film break does not necessarily occur near the location of the temperature probes. It was also found in the literature review (Section 4.2) that EALs have greater specific heat capacity so any temperature spike would not be detected as quickly when compared to mineral oil lubricants.

9.2.3 Limitations and future work

Although lubricant tested represent a cross-section of the products which are available on the market, the sample size is not large enough for statistically significant conclusions. Therefore, further repeats of each of the test cases in conducted using DiMITRI would increase the confidence in the conclusion that EALs are not inherently floored for use in marine stern tubes. Testing a broader range of lubricants, both EALs and mineral oil types, would increase the amount of empirical data available to end users and lubricant manufactures to enable specific characteristics of certain structures and formulations and how these relate to the lubricant performance in marine stern tubes. The number of EAL lubricants available on the market for stern tubes is unknown and a precise number would need to be confirmed before any statistically significant experiments could be designed, however this is likely to be less than 100. In which case the number of samples needed for a statistically significant conclusion would need to be relatively large [92] (more than half of the population) and likely impractical given time constraints on laboratory equipment (in the case of DiMITRI this is the Schenck 250). A possible method of increasing the range of lubricants tested whilst minimising the time required to conduct the experiments would be to maximise the number of samples tested at a specimen level and develop a simple screening test before investing the time in testing the worst performing lubricants in DiMITRI against a benchmark lubricant.

A main limitation to the conclusion of this work that a PAO based lubricant may produce a lower Sommerfeld number if it is oxidised is that the degree of oxidation which is required to trigger this change us unknown. The acid number is a method which could be used to indicate the level of oxidation of a lubricant and should be measured in future work. It would also be appropriate to repeat the experiments in

the RPVOT ageing tests because each lubricant test was replicated once and therefore the conclusion drawn in hypothesis 2 in Section 8.2.1 has a low degree of statistical confidence.

Also highlighted in the literature review was the fact that the additives in EALs will be needed in greater quantities because of their lower polarity. Since EALs have not been developed as extensively as mineral oil based lubricants there are also fewer anti-wear additives available.

An intriguing feature of the experiments was a hysteresis in the Stribeck curves when comparing the run-up and run-down tests. It is thought that this could be because of oscillation in the bearing rotation. Oscillation is known to cause friction hysteresis depending on whether the bearing has accelerated or decelerated towards a fixed speed as is investigated in the work of Lu et al. [93]. Further investigation into this phenomenon was outside of the scope of this work, but is a potential limitation of DiMITRI.

A further source of intrigue was the fact that the Sommerfeld number of the inflection point in Chapter 8 was dependent on the load applied on the bearing. If the Sommerfeld number is truly non-dimensional it was expected that this number should be independent of the load. Further investigation is needed to identify the route cause. It is thought that there is another variable which the Sommerfeld number does not include and was significant enough in these experiments that should be accounted for in future when non-dimensionalising the results.

9.2.4 Improvements to DiMITRI

DiMITRI could be improved by replacing the relatively high friction (compared to the test bearing) plain rod-end bearing with a roller and spherical type rod-end bearing like the one shown in Figure 9.1. This would reduce the parasitic friction on the rig and make it easier to get a more meaningful value of the coefficient of friction for each lubricant. This was explored during the course of the rig design but the solution found in this initial iteration of DiMITRI was selected because of the high loading expected. In reality the original specification for the maximum load was too high and much lower loads of 20kN and below were the most useful. Hence a roller type rod-end bearing is in fact feasible.

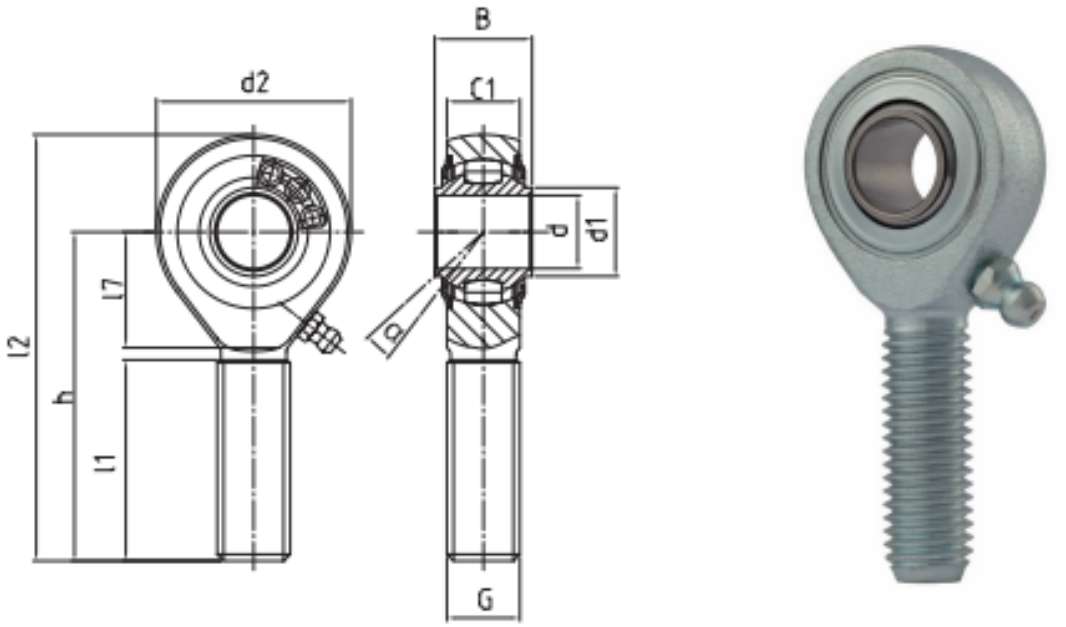

Figure 9.1: Rod-end with roller spherical bearing as opposed to a plain spherical bearing from [94].

A further improvement would be to replace the support bearing with a bearing that does not have a self-aligning function. This would mean that the friction generated by the rod-end bearing and support bearing under load could be measured without the risk of damaging the torque meter from misalignment due to shaft deflection. This would mean it could be taken into account and subtracted from the measured friction.

Cooling of the test bearing would enhance the capabilities of the rig by increasing its Sommerfeld number range. This could be incorporated into the existing test bearing housing by removing the cartridge heaters and using the channels within which they were housed to circulate a cooling liquid through them. An advantage of the compact design of the bearing housing means that the an environment chamber for heating or cooling is a realistic option to incorporate into DiMITRI.

The comparison of the catalysts for oxidation in Section 8.5 suggested that EALs might be more sensitive to oxidation in the presence of tin compared to mineral oil based lubricants. A future study which includes further repeats of this with multiple mineral oil based lubricants would be required to investigate this.

9.3 Publications arising

- Sam Davison, Tom Slatter, Julia Carrell "Experimental Comparison of EALs for Marine Vessel Stern Tubes". Presentation delivered at the 75th Annual Meeting and Exhibition Society of Tribologists and Lubrication Engineers, 2021.
- Sam Davison, Tom Slatter, Rob Dwyer-Joyce, Julia Carrell "Feasibility of Biolubricants Under Mixed Lubrication Conditions". Presentation delivered at the 76th Annual Meeting and Exhibition Society of Tribologists and Lubrication Engineers, 2022.

References

[1] J. C. Bart, E. Gucciardi, and S. Cavallaro, *Biolubricants: Science and technology*. Woodhead Publishing Limited, 2013.

[2] Inkwood Research, "Global Lubricants Market — Trends, Share, Size, Analysis." [Online]. Available: https://inkwoodresearch.com/reports/lubricants-market/

[3] Grand View Research, "Biolubricants Market Size Worth $2.92 Billion By 2024." [Online]. Available: https://www.grandviewresearch.com/press-release/bio-lubricants-market

[4] BSI, "PD CEN-TR 16227-2011–[2022-08-08–02-07-56 PM].pdf," 2011.

[5] MarketsandMarkets Research Private Ltd., "Bio-lubricants Market Global Forecast to 2025 — MarketsandMarkets." [Online]. Available: https://www.marketsandmarkets.com/Market-Reports/biolubricants-market-17431466.html

[6] Fortunebusinessinsights, "Bio lubricants Market Size, Share — Global Report, 2020-2027." [Online]. Available: https://www.fortunebusinessinsights.com/bio-lubricants-market-104654

[7] C. Copeland, "CRS Report for Congress EPA's Vessel General Permit: Background and Issues," 2013. [Online]. Available: www.crs.govR42142.c11173008

[8] Unctad, "REVIEW OF MARITIME TRANSPORT 2013," 2013.

[9] International Maritime Organization, "MEPC 58/INF.22-2," Tech. Rep. [Online]. Available: www.thordonbearings.com

[10] C. E. Vest, "SPECIAL TOPIC LUBRICATION OF SPACECRAFT MECHANISMS," *fohns Hopkins APL Technical Digest*, vol. 14, 1993.

[11] G. W. Stachowiak and A. W. Batchelor, *Engineering tribology*, 3rd ed. Boston, MA: Butterworth-Heinemann, 2013. [Online]. Available:

https://books.google.com/books?hl=en&lr=&id=_wVoTz1pDlwC&oi=fnd&pg=PR1&dq=E-
N G I N E E R I N G T R I B O L O G Y&f=false

[12] S. Q. A. Rizvi, *A Comprehensive Review of Lubricant Chemistry, Technology, Selection, and Design*, 2009.

[13] "Annual book of ASTM standards." West Conshohocken, PA, 2002.

[14] M. Torbacke, Å. K. Rudolphi, and E. Kassfeldt, *Lubricants: Introduction to Properties and Performance*. Wiley Blackwell, may 2014, vol. 9781118799.

[15] S. R. J. F. D. R. Totten George E., "10.0 Petroleum-Derived Hydrocarbon Base Oils," in *Fuels and Lubricants Handbook - Technology, Properties, Performance, and Testing (2nd Edition): (MNL 37-2nd-EB)*. ASTM International, 2019, p. 274. [Online]. Available: https://app.knovel.com/web/view/khtml/show.v/rcid:kpFLHTPP01/cid:kt012WU508/viewe
lubricants-handbook/url_slug:petroleum-derived-hydrocarbon?&b-toc-cid=kpFLHTPP01&b-toc-root-slug=fuels-lubricants-handbook&b-toc-title=Fuels and L

[16] L. R. Rudnick, *Synthetics, mineral oils, and bio-based lubricants: chemistry and technology*. CRC Press, feb 2013.

[17] A. Pettersson, "High-performance base fluids for environmentally adapted lubricants," *Tribology International*, vol. 40, pp. 638–645, 2007. [Online]. Available: www.elsevier.com/locate/triboint

[18] A. H. Lichtenstein, "Fats and Oils," in *Encyclopedia of Human Nutrition*. Academic Press, jan 2013, vol. 2-4, pp. 201–208.

[19] U.S. Army Corps of Engineers, *Engineering and Design, Lubricants and Hydraulic Fluids*. Washington DC: U.S Army Corps for Engineers, 1999.

[20] Grand View Research, "Lubricants Market Size, Share and Trends — Industry Report, 2019-2025," 2019. [Online]. Available: https://www.grandviewresearch.com/industry-analysis/lubricants-market

[21] UNEP/GPA, "The State of the Marine Environment: Trends and processes. UNEP/GPA. The Hague ISBN 92-807-2708-7," *Technical Report*, pp. 1 – 52, 2006.

[22] J. Wang, C. R. Jia, C. K. Wong, and P. K. Wong, "CHARACTERIZATION OF POLYCYCLIC AROMATIC HYDROCARBONS CREATED IN LUBRICATING OILS," 2000.

[23] M. A. Q. Khan, S. M. Al-Ghais, and S. Al-Marri, "Environmental contamination petroleum hydrocarbons in fish from the Arabian Gulf," *Archives of Environmental Contamination and Toxicology*, vol. 29, pp. 517–522, 1995. [Online]. Available: http://dx.doi.org/10.1007/BF00208382

[24] D. Schmidt Etkin, "Worldwide Analysis of In-Port Vessel Operational Lubricant Discharges and Leakages," Tech. Rep.

[25] Vickers Oil, "Hydrox bio range."

[26] US Environmental Protect, "Phase I Final Rule and Technical Development Document of Uniform National Discharge Standards (UNDS) Stern Tube Seals and Underwater Bearing Lubrication : Nature of Discharge," 1999.

[27] Riviera Newsletters, "Riviera Maritime Media - Opinion - Why are stern tube bearings failing?" 2018. [Online]. Available: https://www.rivieramm.com/opinion/why-are-stern-tube-bearings-failing-23762

[28] E. H. Nervold and Ø. Å. Alnes, "Ensuring satisfactory aft stern tube bearing lubrication performance - DNV GL," 2019. [Online]. Available: https://www.dnvgl.com/expert-story/maritime-impact/Ensuring-satisfactory-aft-stern-tube-bearing-lubrication-performance.html

[29] R. Mulder, "The good and the bad of EALs," *The Motorship*, pp. 32,33, aug 2018. [Online]. Available: https://www.motorship.com/news101/fuels-and-oils/the-good-and-the-bad-of-eals

[30] U. E. P. Agency, "National Pollution Discharge Elimination System (NPDES)," 2017. [Online]. Available: https://www.epa.gov/npdes/vessels-vgp

[31] BSI, "BS EN ISO 6743-4-2015–[2022-08-08–02-19-47 PM].pdf," 2015.

[32] L. Roldo, I. Komar, and N. Vulić, "Design and materials selection for environmentally friendly ship propulsion system," *Strojniski Vestnik/Journal of Mechanical Engineering*, vol. 59, no. 1, pp. 25–31, 2013.

[33] X. Zhang, Z. Yin, D. Jiang, G. Gao, Y. Wang, and X. Wang, "Load carrying capacity of misaligned hydrodynamic water-lubricated plain journal bearings

with rigid bush materials," *Tribology International*, vol. 99, pp. 1–13, 2016. [Online]. Available: http://dx.doi.org/10.1016/j.triboint.2016.02.038

[34] Fathom Maritime Intelligence, "Technical Considerations," *Choosing optimum lubricant solution for your operation by Fathom Maritime Intelligence*, p. 34, 2014. [Online]. Available: https://issuu.com/fathomshipping/docs/focus_-_choosing_optimum_lubricant_

[35] T. M. Serra, D. R. De Mendona, J. P. Da Silva, M. R. Meneghetti, and S. M. Plentz Meneghetti, "Comparison of soybean oil and castor oil methanolysis in the presence of tin(IV) complexes," *Fuel*, vol. 90, no. 6, pp. 2203–2206, jun 2011.

[36] T. Rühle and M. Fies, "Eco Requirements for Lubricant Additives," in *Lubricant additives : Chemistry and applications*, 2017, pp. 597–619.

[37] J. F. Carpenter, "Biodegradability and toxicity of polyalphaolefin base stocks," *Journal of synthetic lubrication*, vol. 12, no. 1, pp. 13–20, 1995.

[38] R. Mcdonald, "PICKING THE RIGHT ENVIRONMENTALLY ACCEPTABLE LUBRICANT (EAL): MEETING ENVIRONMENTAL REGULATIONS, MAXIMIZ ING PERFORMANCE."

[39] J. Carrell, R. Lewis, and T. Slatter, "Elastomer solubility and stress relaxation in bio-lubricants," *Tribology International*, vol. 141, 2020.

[40] F. X. Borras, M. B. de Rooij, and D. J. Schipper, "Rheological and wetting properties of Environmentally Acceptable Lubricants (EALs) for application in stern tube seals," *Lubricants*, vol. 6, no. 4, nov 2018.

[41] A. Pettersson and O. Andersson, "PROPERTIES OF BASE FLUIDS FOR ENVIRONMENTALLY ADAPTED LUBRICANTS," 2002.

[42] A. Yano, E. Iwawaki, M. Mihara, and S. Yoshihara, "Study on the Load Carrying Capacity of Sliding Bearing Lubricated by Synthetic Ester Oils," vol. 5, pp. 377–389, 2015.

[43] A. Pettersson, J. Lord, and E. Kassfeldt, "Film formation capability of environmentally adapted base fluids," in *Proceedings of the ASME/STLE international joint tribology conference : October 24 - 27, 2004, Long Beach, California, USA*, Luleå University of Technology, Machine Elements. American Society of Mechanical Engineers, 2004, pp. 379–385.

[44] R. Bayat and A. Lehtovaara, "EHL/mixed transition of fully formulated environmentally acceptable gear oils," *Tribology International*, vol. 146, no. December 2019, p. 106158, 2020. [Online]. Available: https://doi.org/10.1016/j.triboint.2020.106158

[45] Fathom Maritime Intelligence, "Why it pays to understand lubricant issues," *Choosing optimum lubricant solution for your operation*, p. 4, 2014. [Online]. Available: https://issuu.com/fathomshipping/docs/focus_-_choosing_optimum_lubricant_

[46] J. Lord and R. Larsson, "Effects of slide-roll ratio and lubricant properties on elastohydrodynamic lubrication film thickness and traction," *Proceedings of the Institution of Mechanical Engineers, Part J: Journal of Engineering Tribology*, vol. 215, no. 3, pp. 301–308, 2001.

[47] S. R. J. F. D. R. Totten George E., "13.6.2 Lubrication," p. 527, 2019. [Online]. Available: https://app.knovel.com/hotlink/khtml/id:kt012WU9C3/fuels-lubricants-handbook/lubrication

[48] ——, "13.6.3 Environmental Acceptability," p. 528, 2019. [Online]. Available: https://app.knovel.com/hotlink/khtml/id:kt012WU9D7/fuels-lubricants-handbook/environmental-acceptability

[49] ——, "ASTM Standards," p. 529, 2019. [Online]. Available: https://app.knovel.com/hotlink/khtml/id:kt012WU9F8/fuels-lubricants-handbook/synthetic–astm-standards

[50] R. d. M. Castro, E. I. M. Curi, L. F. F. Inácio, and A. d. S. Rocha, "Analysis of the tribological performances of biodegradable hydraulic oils HEES and HEPR in the sliding of Cu–Zn/WC–CoCr alloys using the Stribeck curve," *Journal of the Brazilian Society of Mechanical Sciences and Engineering*, vol. 42, no. 1, pp. 1–20, 2020. [Online]. Available: https://doi.org/10.1007/s40430-019-2080-5

[51] Germanischer Lloyd, "Guidelines for Sea Trials of Motor Vessels," Tech. Rep., 2012.

[52] MAN Primserv, "Slow steaming," Copenhagen, Tech. Rep., 2012.

[53] Wartsila, "Technology review," Tech. Rep., 2001.

[54] I. Komar, N. Vulić, and L. Roldo, "Hydrodynamic and elastohydrodynamic lubrication model to verify the performance of marine propulsion shafting," *Transactions of Famena*, vol. 37, no. 1, pp. 15–27, 2013.

[55] T. He, D. Zou, X. Lu, Y. Guo, Z. Wang, and W. Li, "Mixed-lubrication analysis of marine stern tube bearing considering bending deformation of stern shaft and cavitation," *Tribology International*, vol. 73, pp. 108–116, may 2014.

[56] Y. Tachi, S. Ishihara, K. Tamura, T. Goshima, and A. J. McEvily, "Predicting sliding wear behaviour of a tin-based white metal under varying pressure and speed conditions," *Proceedings of the Institution of Mechanical Engineers, Part J: Journal of Engineering Tribology*, vol. 219, no. 6, pp. 451–457, 2005.

[57] DNV GL, "Safeguard shaft seals and propeller shaft bearings – avoid costly failures," jan 2022. [Online]. Available: https://www.dnv.com/news/safeguard-shaft-seals-and-propeller-shaft-bearings-avoid-costly-failures-215171

[58] B. Weintz, "Sterntube Bearing And Propeller Tailshaft Inspections," *Workshop Insider*, pp. 1–7, sep 2021. [Online]. Available: https://workshopinsider.com/sterntube-bearing-tailshaft-inspections/

[59] X. Lu and M. M. Khonsari, "On the lift-off speed in journal bearings," *Tribology Letters*, vol. 20, no. 3-4, pp. 299–305, 2005.

[60] A. F. Cristea, J. Bouyer, M. Fillon, and M. D. Pascovici, "Transient Pressure and Temperature Field Measurements in a Lightly Loaded Circumferential Groove Journal Bearing from Startup to Steady-State Thermal Stabilization," *Tribology Transactions*, vol. 60, no. 6, pp. 988–1010, 2017. [Online]. Available: https://doi.org/10.1080/10402004.2016.1241330

[61] X. Zhang, Z. Yin, and Q. Dong, "An experimental study of axial misalignment effect on seizure load of journal bearings," *Tribology International*, vol. 131, no. July 2018, pp. 476–487, 2019. [Online]. Available: https://doi.org/10.1016/j.triboint.2018.11.014

[62] S. Beamish, X. Li, H. Brunskill, A. Hunter, and R. Dwyer-Joyce, "Circumferential film thickness measurement in journal bearings via the ultrasonic technique," *Tribology International*, vol. 148, p. 106295, aug 2020.

[63] S. Beamish and R. S. Dwyer-Joyce, "Experimental Measurements of Oil Films in a Dynamically Loaded Journal Bearing," *Tribology Trans-*

actions, vol. 65, no. 6, pp. 1022–1040, 2022. [Online]. Available: https://doi.org/10.1080/10402004.2022.2106926

[64] W. Litwin and C. Dymarski, "Experimental research on water-lubricated marine stern tube bearings in conditions of improper lubrication and cooling causing rapid bush wear," *Tribology International*, vol. 95, pp. 449–455, mar 2016.

[65] W. Litwin, "Influence of surface roughness topography on properties of water-lubricated polymer bearings: Experimental research," *Tribology Transactions*, vol. 54, no. 3, pp. 351–361, 2011.

[66] W. Litwin and A. Olszewski, "Water-lubricated sintered bronze journal bearings-Theoretical and experimental research," *Tribology Transactions*, vol. 57, no. 1, pp. 114–122, 2013.

[67] W. Litwin, A. Olszewski, and M. Wodtke, "Influence of Shaft Misalignment on Water Lubricated Turbine Sliding Bearings with Various Bush Modules of Elasticity," *Key Engineering Materials*, vol. 490, pp. 128–134, 2012.

[68] J. Kowalski, L. Wojciech, D. Piatek, and D. Cuper-Przybylska, "Assessing the potential replacement of mineral oil with envirnomentally acceptable lubricants in a stern tube bearing: an experimental analysis of bearing performance.pdf," *Polish Maritime Research 4*, vol. 28, no. 112, pp. 160–166, 2021.

[69] S. Beamish, "Oil Film Thickness Measurements in Journal Bearings under Normal, Severe & Dynamic Loading Conditions using Ultrasound," Ph.D. dissertation, University of Sheffield, 2021.

[70] T. Reddyhoff, S. Kasolang, R. S. Dwyer-Joyce, and B. W. Drinkwater, "The Phase Shift of an Ultrasonic Pulse at an Oil Layer and Determination of Film Thickness," *Proceedings of the Institution of Mechanical Engineers, Part J: Journal of Engineering Tribology*, vol. 219, no. 6, pp. 387–400, jun 2005. [Online]. Available: http://journals.sagepub.com/doi/10.1243/135065005X34044

[71] American Bureau of Shipping, "ABS-led Research Identifies Key Recommendations for Evaluating Environmentally Acceptable Lubricants (EALs)." [Online]. Available: https://ww2.eagle.org/en/news/press-room/abs-led-research-identifies-key-recommendations-for-evaluating-environmentally-acceptable-lubricants-eals.html

[72] C. Dipl-Ing, G. Gurr, A. G. Lloyd, P. Dr-Ing, and H. Rulfs, "Influence of transient operating conditions on propeller shaft bearings," *Journal of Marine Engineering & Technology*, vol. 7, no. 2, pp. 3–11, 2008. [Online]. Available: http://www.tandfonline.com/action/journalInformation?journalCode=tmar20

[73] X. Li, "TDMS FMS Data Read and Analyse v1.1.2 All Rev," 2019.

[74] S. Bell, "Good Practice Guide No. 11 - The Beginner's Guide to Guide to Uncertainty of Measurement," p. 41, 2001.

[75] Robert Scott, "Journal Bearings and Their Lubrication," jul 2005. [Online]. Available: https://www.machinerylubrication.com/Read/779/journal-bearing-lubrication

[76] P. Eilts, C. P. Stoeber-Schmidt, and R. Wolf, "Investigation of extreme mean effective and maximum cylinder pressures in a passenger car diesel engine," *SAE Technical Papers*, vol. 2, 2013.

[77] S. Pashneh-Tala, A. Malins, R. Lewis, G. Heppell, and E. Rodriguez-falcon, *The Little Book of Design . 1 st Edition*, 2011.

[78] Ansys, "Granta EduPack 2021 R2," 2021.

[79] Schaeffler Technologies AG & KG Co., *Schaeffler - Technical Pocket Guide*, 2014.

[80] Shaeffler, "Plain bearings," p. 69.

[81] G. Nicholas, B. P. Clarke, and R. S. Dwyer-Joyce, "Detection of lubrication state in a field operational wind turbine gearbox bearing using ultrasonic reflectometry," *Lubricants*, vol. 9, no. 1, pp. 1–22, 2021.

[82] G. Biresaw and G. B. Bantchev, "Pressure viscosity coefficient of vegetable oils," *Tribology Letters*, vol. 49, no. 3, pp. 501–512, 2013.

[83] E. Höglund, "Influence of lubricant properties on elastohydrodynamic lubrication," *Wear*, vol. 232, no. 2, pp. 176–184, 1999.

[84] A. Pettersson, "Tribological characterization of environmentally adapted ester based fluids," *Tribology International*, vol. 36, pp. 815–820, 2003. [Online]. Available: www.elsevier.com/locate/triboint

[85] ASTM International, "Standard Test Method for Oxidation Stability of Steam Turbine Oils by Rotating," 2022.

[86] Vickers Oil, "Emulsifiable v Non-emulsifiable Sterntube Lubricants," Tech. Rep., 2018.

[87] J. Bouyer and M. Fillon, "An experimental analysis of misalignment effects on hydrodynamic plain journal bearing performances," *Journal of Tribology*, vol. 124, no. 2, pp. 313–319, 2002.

[88] X. Song, W. Wu, and S. Yuan, "Mixed-lubrication analysis of misaligned journal bearing considering turbulence and cavitation," *AIP Advances*, vol. 12, no. 1, 2022. [Online]. Available: https://doi.org/10.1063/5.0074896

[89] M. Kaushik, "How Marine Propulsion Engine of the Ship is Protected?" 2019. [Online]. Available: https://www.marineinsight.com/main-engine/how-marine-propulsion-engine-of-the-ship-is-protected/

[90] M. Sanguri, "How to Test Ship's Main Engine for Slow Steaming?" 2019. [Online]. Available: https://www.marineinsight.com/main-engine/how-to-test-ships-main-engine-for-slow-steaming/

[91] J. Snyder, "Riviera - News Content Hub - Minimising stern tube failures starts with the right EAL," aug 2020. [Online]. Available: https://www.rivieramm.com/news-content-hub/news-content-hub/minimising-stern-tube-failures-starts-with-the-right-eal-60560

[92] J. Martínez-Mesa, D. A. González-Chica, J. L. Bastos, R. R. Bonamigo, and R. P. Duquia, "Sample size: how many participants do I need in my research?" *Anais brasileiros de dermatologia*, vol. 89, no. 4, pp. 609–615, 2014.

[93] X. Lu and M. M. Khonsari, "An Experimental Study of Oil-Lubricated Journal Bearings Undergoing Oscillatory Motion," *Journal of Tribology*, vol. 130, no. 2, pp. 1–7, apr 2008. [Online]. Available: https://asmedigitalcollection.asme.org/tribology/article/doi/10.1115/1.2908907/458423/An-Experimental-Study-of-OilLubricated-Journal

[94] RS Components Ltd., "BRTM 30-00-501 — Durbal Forged Steel Rod End, 30mm Bore, 145mm Long, Metric Thread Standard, Male Connection Gender — RS." [Online]. Available: https://uk.rs-online.com/web/p/rod-ends/1850080

Appendices

Appendix A

DiMITRI product design specification

1 Introduction and Scope

This document outlines the specification for a test rig which aims to characterise the performance of different lubricants in a marine stern tube journal bearing. The rig will be capable of testing the lubricants in the mixed/boundary lubrication regime. A motor will be used to spin the shaft and a load will be applied on the end of the shaft with a servo hydraulic testing machine which will allow dynamic loads up to 250kN.

2 Changes to Previous version

Version	Date changed	Change details
01	30/03/20	Initial version
02	20/04/20	Modified so shaft is not replaceable/moveable along its axis. This was unrealistic given budgetary and time constraints. Removed dynamic loading requirement.
03	25/10/20	Updated budget due to funding award. Updated to include approximate bearing diameter. Added scaling design feature.
04	05/11/20	Replaced item 3 with requirement for heating or cooling.

3 Technical Specification

1.1 Test rig bearing parameters

Parameter	Spec	Reason
Sommerfeld number	0.004-0.01	This seems to be the operating range of stern tube bearings including the most extreme conditions. This is based on the parameters provided by DNV and by Brookesbell. Other test rigs have operated at a minimum

		magnitude of 0.006 with EALs in the boundary regime.
Clearance ratio	0.0018-0.005	This will be similar to stern tube bearings which have a comparatively large clearance ratio when compared to automotive journal bearings.
Bearing temperature	<200°C based on flash temperature. Probably lower still based on viscosity of lubricant. Need to check what sort of temperatures I will need to achieve other parameters given the shaft diameter.	Will be adjusted up with cartridge heaters to allow the Sommerfeld number to be lower because speed is likely to be higher. Rather the speed at which the optimum torque from the motor will occur to get some good measurements and running through the boundary condition will ideally be higher than a few rpm. Best way to achieve higher seizure speeds is to heat the oil, but still need to keep the same sommerfeld number range.
Bearing Diameter	50mm	Baxter rig and rig in paper by Yano et al (2015) was 100mm. my rig needs to be smaller to be able to be lifted off and on the Schenck machine easily so an appropriate scale is half the size. Therefore bearing diameter around 50mm is appropriate.
Shaft diameter	Decided use diameter recommended for bearing in a crankshaft. This is likely to be on the small side of the clearance ratio that I might desire. If it is preferable, the shaft can be machined smaller in sections.	
Lambda ratio	Will be determined by what a stern tube bearing lambda ratio tends to be. Also by film thickness expected once the shaft and bearing components have been selected. For mixed lubrication regime want a small lambda ratio. Because buying off the shelf components the lambda ratio will be dictated most likely. Possibility of using laser etching (MTC).	

1.2 Design criteria

Design objectives

a) Cost
   Considers the cost of the parts and labour to produce the rig. A low cost solution will score highly.
b) Manufacturing complexity
   Considers the complexity of the parts to be manufactured which influences the cost and time involved with the rig build. Off-the-shelf parts will reduce the manufacturing complexity and the reduce the time required to build the rig. A reduced complexity will score highly.
c) Closeness to real conditions
   Considers the conditions under which the lubricants will be subject to and whether they are likely to meet the design spec and how close they are to real operating conditions.
d) Adaptability
   The degree to which the rig will be compatible with a variety of lubricants and how large the range of operating parameters are likely to be. If the rig is likely to have a large operating range across speed, load and lubrication regimes it will score highly.
e) Modularity
   Potential for conducting tests on other bearings by swapping out components. Reduced complexity of disassembly and reassembly will scorehighly.

Objective hierarchy

	A	B	C	D	E	Total	Rank
A	-	1	1	1	1	4	1
B	0	-	0	1	1	2	3
C	0	1	-	1	1	3	2
D	0	0	0	-	1	1	4
E	0	0	0	0	-	0	5

2 Design features

1. Capable of generating sommerfeld numbers close to real ship.
2. Modular design to allow different bearings to be installed.
3. Some form of temperature control – heating or cooling.
4. Removable bearing shells that don't require movement of the shaft in order for them to be replaced.
5. Scaled approximately half the size of Baxter rig to ensure it was portable and fitted within the dimensions of the Schenck 250 test bed.
6. All surfaces in contact with oil should be compatible to be cleaned with solvents and degreasers. Surfaces will be accessible to be wiped clean and where access is not possible, minimal dismantling of the rig will be required.
7. Misaligned bearing/cantilever loaded as per a propeller shaft.
8. The lubricant volume required for the oil circulation system will be minimised.

3 Packaging and size

The shaft must be mounted on the platform for an existing servo-hydraulic tester in the Lea laboratory. The footprint space available for the shaft, test and support bearings is shown in Figure 1 and Figure 2.

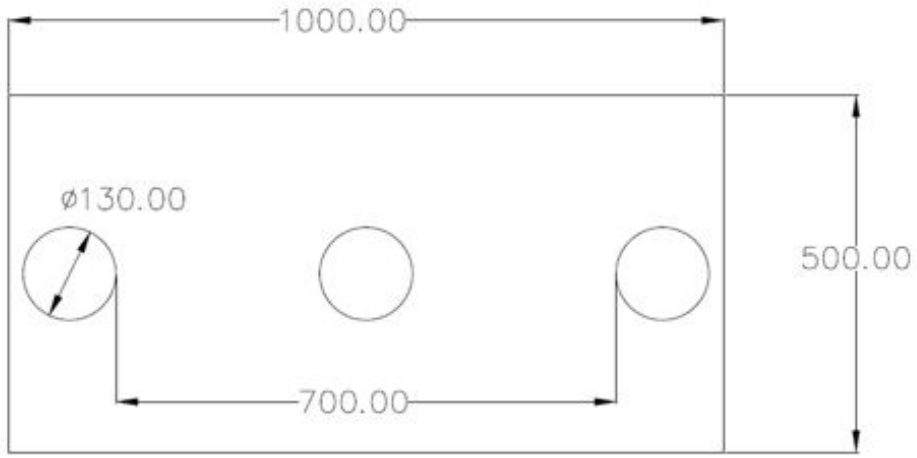

Figure 1 - Dimensions of mounting area on Schenck machine.

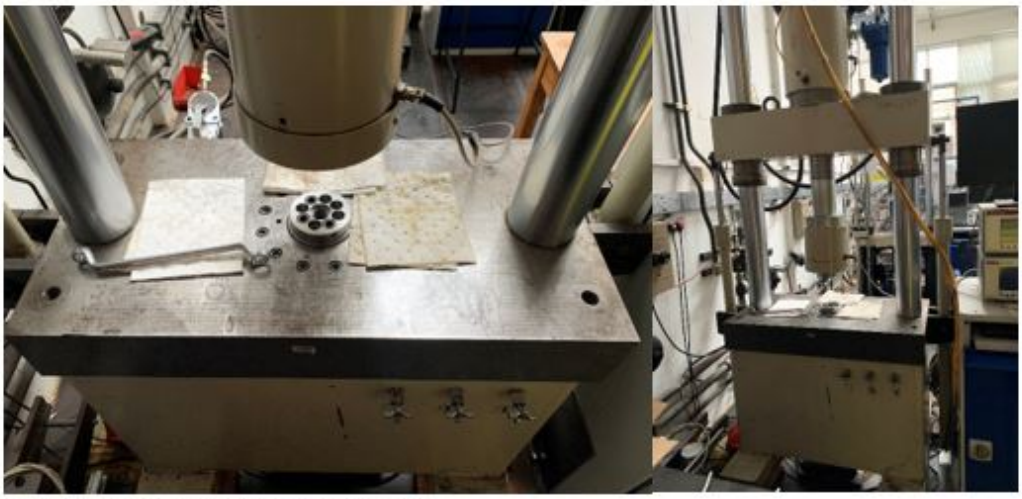

Figure 2 - Test bed mounting area on Schenck machine

4 Cost

The budget for the purchase of components and raw materials is: £5000.

Appendix B

DiMITRI assembly drawing

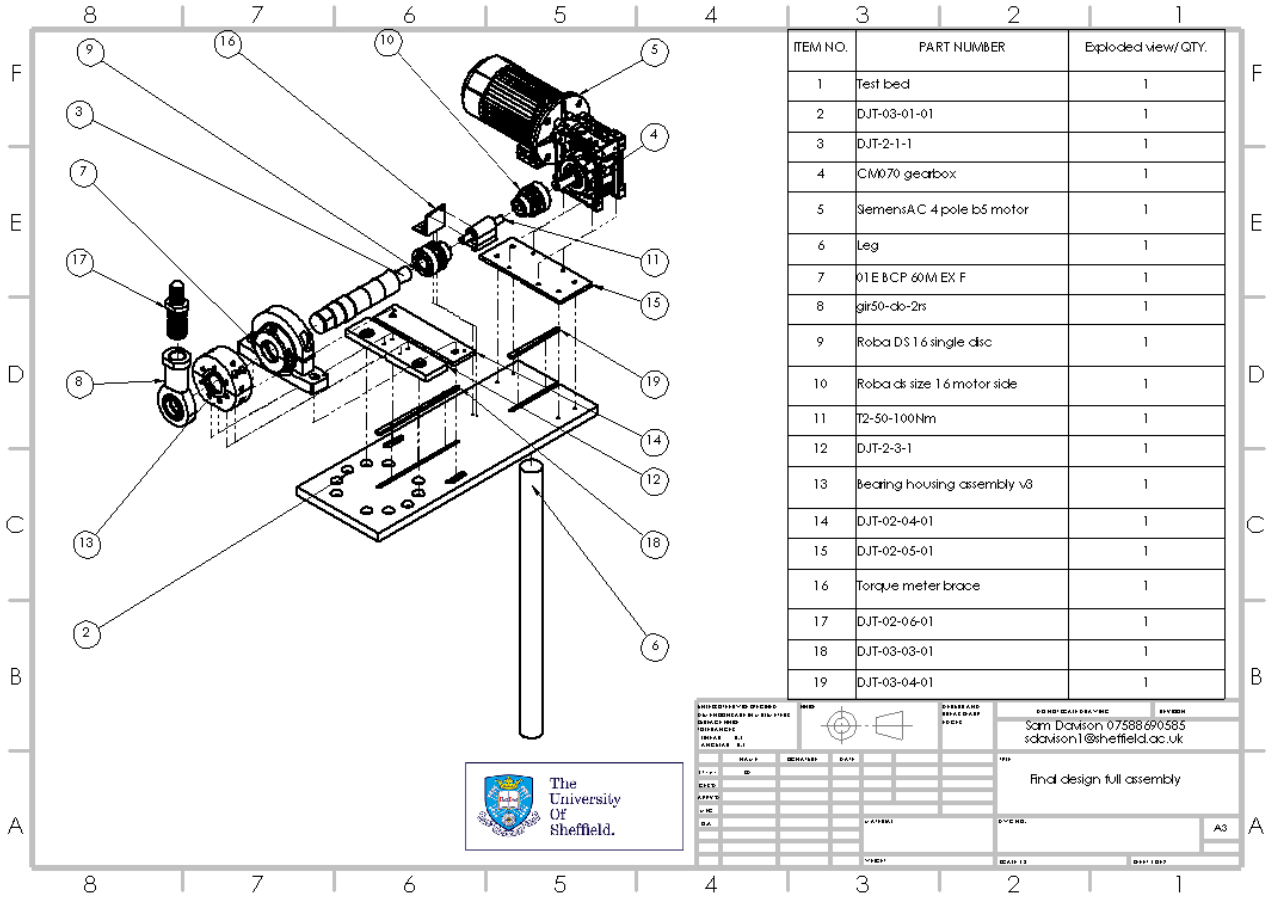

ITEM NO.	PART NUMBER	Exploded view/ QTY.
1	Test bed	1
2	DJT-03-01-01	1
3	DJT-2-1-1	1
4	CMV070 gearbox	1
5	SiemensAC 4 pole b5 motor	1
6	Leg	1
7	01E BCP 60M EX F	1
8	gir50-do-2rs	1
9	Roba DS 16 single disc	1
10	Roba ds size 16 motor side	1
11	T2-50-100Nm	1
12	DJT-2-3-1	1
13	Bearing housing assembly v3	1
14	DJT-02-04-01	1
15	DJT-02-05-01	1
16	Torque meter brace	1
17	DJT-02-06-01	1
18	DJT-03-03-01	1
19	DJT-03-04-01	1

The University Of Sheffield.

Sam Davison 07588690585
samdavison1@sheffield.ac.uk

Final design full assembly

A3